## Exploring pantothenate energy-coupling factor (ECF) transporters as a novel antibiotic target

### **Dissertation**

zur Erlangung des Grades
des Doktors der Naturwissenschaften
der Naturwissenschaftlich-Technischen Fakultät
der Universität des Saarlandes

von

M.Sc. Atanaz Shams

Saarbrücken

September 2025

Tag des Kolloquiums: 10.09.2025

**Dekan:** Prof. Dr.-Ing. Dirk Bähre

**Berichterstatter:** Prof. Dr. Anna K. H. Hirsch

Prof. Dr. Alexandra K. Kiemer

**Akad. Mitglied:** Dr. Brigitta Loretz

Die vorliegende Arbeit wurde von Juni 2021 bis Februar 2025 unter Anleitung von Frau Prof. Dr. Anna K. H. Hirsch in der Fachrichtung Pharmazie der Naturwissenschaftlich-Technischen Fakultät der Universität des Saarlandes, sowie am Helmholtz-Institut für Pharmazeutische Forschung Saarland (HIPS) in der Abteilung Drug Design and Optimization (DDOP) angefertigt.

When asked about his definition of happiness, Alfred Hitchcock once remarked:

"A clear horizon, nothing to worry about on your plate. Only things that are creative, and not destructive. That's within yourself, within me. I can't bear quarreling; I can't bear feelings between people. I think hatred is wasted energy. It's all non-productive. I'm very sensitive. A sharp word said by, say, a person who has a temper, if they're close for me, hurts me for days. I know we're only human, we do go in for these various emotions, call them negative emotions, but when all these are removed and you can look forward and the road is clear ahead, and now you're going to create something. I think that's as happy as I would ever want to be."

### - Alfred Hitchcock

### Acknowledgments

First and foremost, I want to express my deepest gratitude to myself for standing strong through all these years, navigating the challenges of moving from my home country to here. Despite the many obstacles, I have not only faced them head-on but have also learned from them, transforming each one into a valuable life experience. I also owe a special thanks to my beloved mother, Dr. med. Mastaneh Mirkamali, whose unwavering support and encouragement have been my foundation throughout my life and studies. Her belief in me has been a driving force, making all the difference.

I have had the distinct privilege of completing both my master's thesis and PhD at the Helmholtz Institute for Pharmaceutical Research Saarland, in collaboration with Saarland University. This transformative experience has profoundly shaped me, both personally and professionally, under the expert supervision of Professor Dr. Anna K. H. Hirsch. I am deeply grateful to Professor Hirsch for providing me with the invaluable opportunity to be part of her exceptional team. Her trust in me has been pivotal in allowing me to pursue my passion, broaden my knowledge, and elevate the quality of my work. The insightful feedback, unwavering support, and constant encouragement she has offered have been fundamental to my growth and development throughout this journey.

I would also like to express my sincere gratitude to Dr. Jörg Haupenthal, my research supervisor, for his continuous guidance and support throughout this research. His care and attention to detail have been a steady source of inspiration.

My deepest appreciation also goes to Prof. Dr. Kiemer. I am truly thankful for the patience and understanding she has shown during my thesis committee meetings, offering me thoughtful insights that have enriched my work.

I would like to thank Dr. Eleonora Diamanti, Dr. Mostafa Hamed, and Dr. Walid A. M. Elgaher for their valuable advice and unwavering support. Their time, kindness, and expertise have been crucial in helping me refine my research.

A special note of gratitude goes to Prof. Dr. Dirk J. Slotboom for offering me the incredible opportunity to spend six months in the Membrane Enzymology group at the Groningen Biomolecular Sciences and Biotechnology Institute (GBB) and the Zernike Institute for Advanced Materials. I am deeply thankful for the warmth, kindness, and hospitality of his team, especially Aleksei, Kaori, Solene, Ksenia, Michele, Zaid, Jose, Iris, Mark, Miyer, Anna, Lyan, Jelmer, and many others. Their camaraderie made my experience truly unforgettable.

I would also like to thank all the DDOP, AVID, and CBCH members, especially the ECF group: Spyros, Eleonora, Mostafa, Virgyl, Ioulia, and Justine. It has been a true pleasure to collaborate with each of you.

Additionally, I am grateful to the technicians of the laboratory of the Department of Drug Design and Optimization at HIPS, Simone, Jeannine, Selina, Jannine, and Tabea, as well as the secretaries Bahareh and Nicole, for their continued support and assistance.

Finally, my heartfelt thanks go to my beloved friends: Mostafa, Nazila, Romina, Shahrzad, Roya, Marie, Yingwen, Maryam, Tina, Mohammad, Justine, Jack, Sepideh, Arghavan, Shakila, Afroz, Fatemeh, Sepand, Hamid, and Jonas. Your presence and unwavering encouragement have been a constant source of strength and motivation.

### **Summary**

Antimicrobial resistance is a major global health threat, driven by the overuse and misuse of antimicrobial in clinical and agricultural settings. Resistant bacteria evade antibiotics through various mechanisms, including enzymatic degradation, structural modifications, efflux pumps, and reduced membrane permeability. The rise of multidrug-resistant pathogens such as *Escherichia coli*, *Klebsiella pneumoniae*, and *Acinetobacter baumannii* necessitates novel therapeutic strategies, including antimicrobial stewardship, alternative treatments, and advanced diagnostic tools.

Vitamins play a crucial role in both human health and bacterial survival. Bacteria, much like humans, either synthesize vitamins or acquire them from their surroundings. The ATP-binding cassette (ABC) and energy-coupling factor (ECF) transporters facilitate vitamin uptake in bacteria, with ECF-FolT2 and ECF-PanT transporting folate and pantothenate, respectively. Understanding these transport mechanisms presents opportunities for developing antimicrobial agents targeting bacterial vitamin dependency.

This study explores the biochemical and structural properties of ECF transporters, their role in bacterial metabolism, and their potential as drug targets. By elucidating the molecular mechanisms of vitamin transport, this research contributes to the development of innovative therapeutic strategies to combat antimicrobial resistance.

### Zusammenfassung

Die antimikrobielle Resistenz ist eine bedeutende globale Gesundheitsbedrohung, die durch den übermäßigen und unsachgemäßen Einsatz von antimikrobiellen Wirkstoffen begünstigt wird. Einsatz von Antibiotika in klinischen und landwirtschaftlichen Bereichen vorangetrieben wird. Resistente Bakterien umgehen Antibiotika durch verschiedene Mechanismen, darunter enzymatischer Abbau, strukturelle Modifikationen, Effluxpumpen und verringerte Membranpermeabilität. Das Aufkommen multiresistenter Erreger wie Escherichia coli, Klebsiella pneumoniae und Acinetobacter baumannii erfordert neue therapeutische Strategien, darunter ein umsichtiges Antibiotikamanagement, alternative Behandlungen und fortschrittliche Diagnosetools.

Vitamine spielen eine entscheidende Rolle sowohl für die menschliche Gesundheit als auch für das Überleben von Bakterien. Bakterien, ähnlich wie der Mensch, synthetisieren entweder Vitamine oder nehmen sie aus ihrer Umgebung auf. Die ATP-bindenden Kassettentransporter (ABC) und die energiegekoppelten Faktortransporter (ECF) erleichtern die Vitaminaufnahme in Bakterien, wobei ECF-FolT2 und ECF-PanT speziell Folat bzw. Pantothenat transportieren. Das Verständnis dieser Transportmechanismen bietet Möglichkeiten zur Entwicklung antimikrobieller Wirkstoffe, die auf die Vitaminabhängigkeit von Bakterien abzielen.

Diese Studie untersucht die biochemischen und strukturellen Eigenschaften von ECF-Transportern, ihre Rolle im bakteriellen Stoffwechsel und ihr Potenzial als medikamentöse Zielstrukturen. Durch die Aufklärung der molekularen Mechanismen des Vitamintransports trägt diese Forschung zur Entwicklung innovativer therapeutischer Strategien zur Bekämpfung der Antimikrobielle Resistenz bei.

### **Publications Included in This Thesis**

### Publication A:

Shams A.; Bousis S.; Diamanti E.; Elgaher W. A. M.; Zeimetz L.; Haupenthal J.; Slotboom Dirk J.; Hirsch Anna K. H. Expression and characterization of pantothenate energy-coupling factor transporters as an anti-infective drug target. *Protein Sci* **2024**. DOI: 10.1002/pro.5195

### Publication B:

Exapicheidou I. A.  $\perp$ ; Shams A.  $\perp$ ; Ibrahim H.; Tsarenko A.; Backenköhler M.; Hamed M.; Diamanti E.; Volkamer A.; Slotboom Dirk J.; Hirsch Anna K. H: Hit optimization by dynamic combinatorial chemistry on *Streptococcus pneumoniae* energy-coupling factor transporter ECF-PanT. *Chem. Commun* **2024**. DOI: 10.1039/D3CC04738E

1 these authors contributed equally

### **Publication C**:

<u>Shams A.</u>; Zeimetz L., Haupenthal J.; Bousis S.; Hirsch Anna K. H: Investigation of the rescue effect of energy coupling factor inhibitors against roseoflavin toxicity in *Streptococcus pneumoniae*. The manuscript and experimental protocol are currently in preparation.

### **Publications of the Author Which Are Not Included in This Thesis**

Drost M.; Diamanti E.; Fuhrmann K.; Goes A.; <u>Shams A.</u>; Haupenthal J.; Koch M.; Hirsch A. K. H.; Fuhrmann G: Bacteriomimetic Liposomes Improve Antibiotic Activity of a Novel Energy-Coupling Factor Transporter Inhibitor. *Pharmaceutics* **2021**. DOI: 10.3390/pharmaceutics14010004

Diamanti E.; Souza Paulo C. T.; Setyawati I.; Bousis S.; Monjas L.; Swier Lotteke J.Y.M.; Shams A.; Tsarenko A.; Stanek Weronika K.; Jäger M.; Marrink Siewert J.; Dirk J. Slotboom.; Hirsch Anna K. H.; Identification of inhibitors targeting the energy coupling factor (ECF) transporters. *Commun. Biol.* **2023**. DOI: 10.1038/s42003-023-05555-x

Diamanti E.; Cremers A.; Yue L.; Exapicheidou I.; Gibson P.; Shams A.; Martin L.; Becker R.; Setyawati I.; Zeimetz L.; Haupenthal J.; Witschel M.; Slotboom D.; Hamed M. M.; Veening J.-W.; Hirsch A. K. H.; Structure–activity relationship study of an inhibitor targeting Energy-Coupling Factor (ECF) transporters, a novel antimicrobial target in *Streptococcus pneumoniae*. *J. Med. Chem.* **2025**, *submitted*, *under revision*.

Exapicheidou I.; Tsarenko A.; Zeller L.; Baumann C.; Shams A.; Hoffmann P.; Yue L.; Kany A.; Herrmann J.; Slotboom D.; Müller R.; Hamed M. M.; Diamanti E.; Hirsch A. K. H.; Hit-to-Lead optimization of energy-coupling factor (ECF) transporters inhibitors as novel anti-infectives. *J. Med. Chem.* **2025**, *submitted, under revision*.

### **Contribution Report**

<u>Publication A</u>: The author planned all the experiments and performed the expression and purification of various protein homologs. She also carried out sequence alignment, TSA for stability determination, and evaluated the results using size exclusion chromatography (SEC). The assessment of ECF inhibitors was done through proteoliposome uptake assays, SPR, and *Galleria mellonella in vivo* assays. Furthermore, she wrote the manuscript.

<u>Publication B</u>: The author expressed and purified the ECF-PanT protein and conducted functional assays, including a bacterial uptake assay using *Lactobacillus casei* at HIPS and a proteoliposome uptake assay at Groningen University. She optimized and carried out the Dynamic combinatorial chemistry (DCC) along with Exapicheidou I. A. and, she was partially involved in the analysis. Additionally, she performed the sequence alignment, *Galleria mellonella* experiments and contributed to writing the manuscript.

<u>Publication C</u>: The author planned and performed the experiments for adaptation and optimization. Bousis S. established the basic methodology in different organism. Zeimetz L. contributed to the optimization of the assay during her six-month master's thesis. Haupenthal J. supervised and provided consultation throughout the study and oversaw the technical assistant, Amann S. Hirsch, Anna K. H. managed the overall project, acted as the team leader, and supervised all aspects of the study. She is also the corresponding author.

### **Abbreviations**

ECF Energy-coupling factor (ECF) transporters
 ABC ATP-Binding Cassette

ATP Adenosine Triphosphate
 AMR Antimicrobial resistance

• IspD 2-C-Methyl-D-Erythritol 4-Phosphate Cytidylyltransferase CYP

cytochrome P450 enzyme

• DXPS 1-Deoxy-D-Xylulose 5-Phosphate Synthase

TSA Thermal shift Assay

• DPhG Deutsche Pharmazeutische Gesellschaft

SPR Surface plasmon resonance

• EcfS S-component or Substrate-binding component of ECF transporters

• EcfT Energy-coupling transmembrane protein in ECF transporters

• EcfA/A' ATPase components of ECF transporters

• td-DCC target directed dynamic combinatorial chemistry

NBD Nucleotide-binding domain

• TMD Transmembrane domain

• BP Binding protein

• TCA Tricarboxylic acid cycle

• CoA Coenzyme A

• TMH Transmembrane helices

LB Lysogeny broth
 SM Structural motif
 THF Tetrahydrofolate

• S. pneumoniae Streptococcus pneumoniae (bacterium)

NAD Nicotinamide adenine dinucleotide

PDB Protein Data Bank

• NADP Nicotinamide adenine dinucleotide phosphate

• SAR Structure–activity relationship

WHO World Health Organization

• ECF-FolT2 Energy-coupling factor FolT2 transporter

• ECF-PanT Energy-coupling factor PanT transporter

DNA Deoxyribonucleic acid

RNA Ribonucleic acid

• MIC Minimum inhibitory concentration

• MW Molecular weight

• Co<sup>2+</sup> Cobalt ion

MDR Multidrug-resistant

• Ni<sup>2+</sup> Nickel ion

• SEC Size–exclusion chromatography

RoF Roseoflavin

B1 Thiamin (Vitamin B12)
 B2 Riboflavin (Vitamin B2)

• B3 Niacin (Vitamin B3)

• B5 Pantothenate (Vitamin B5)

• B6 Pyridoxal Phosphate (Active Form of Vitamin B6)

B7 Biotin (Vitamin B7)B9 Folate (Vitamin B9)

• B12 Cobalamin (Vitamin B12)

• B-complex A group of water-soluble vitamins (including B1, B2, B3, B5, B6, B7,

B9, B12)

• PPI Protein-protein interaction

• SBVS Structure-based virtual screening

• CG Coarse-grained

• MD Molecular dynamics

• CGMD Coarse-Grained Molecular Dynamics

Cryo-EM
 Cryo-electron microscopy

• PDB Protein Data Bank

SAR Structure-activity relationship

• DCC Dynamic combinatorial chemistry

• RoF Roseoflavin

• FMN Flavin Mononucleotide

• FAD Flavin Adenine Dinucleotide

OD Optical Density
 CO<sub>2</sub> Carbon Dioxide

DMSO Dimethyl Sulfoxide

• THM Todd–Hewitt Medium

SPR Surface Plasmon Resonance

• qPCR Quantitative Polymerase Chain Reaction

• β-lactam Beta-lactam (class of antibiotics)

• IspD 2-*C*-methyl-D-erythritol 4-phosphate cytidylyltransferase

• MEP Methylerythritol Phosphate

• MS Mass Spectrometry

• E. coli Escherichia coli (bacterium)

• Ab Acineobacter baumannii

• Mt Mycobacterium tuberculosis

• Ec Escherichia coli

• IPTG Isopropyl β-D-1-thiogalactopyranoside

• TSA Thermal Shift Assay

• SPR Surface Plasmon Resonance

• DXPS 1-deoxy-D-xylulose-5-phosphate synthase

• PfDXS Plasmodium falciparum DXS

• DrDXS Deinococcus radiodurans DXS

### **Table of Contents**

AC	KNOV	VLEDGMENTS	V
SU	MMA]	RY	VII
<b>7.</b> 11	SAMN	IENFASSUNG	VIII
PU.	BLIC	ATIONS INCLUDED IN THIS THESIS	. IX
PU	BLICA	ATIONS OF THE AUTHOR WHICH ARE NOT INCLUDED IN THIS THESIS	. IX
CO	NTRI	BUTION REPORT	. XI
ΑB	BREV	IATIONS	XII
		OF CONTENTS	
1		FRODUCTION	
1	1.1	Antimicrobial resistance (AMR)	
	1.1	Vitamins	
	1.3	ATP-binding cassette (ABC) transporters	
	1.3	Energy-coupling factor (ECF) transporters	
	1.5	Role of ECF transporters in pathogenic bacteria and vitamin uptake	
	1.6	Development of ECF inhibitors and their mechanism of action	
	1.7	Structural insights into ECF transporters	
	1.8	Conclusion and future directions	
2		MS OF THE THESIS	
3		SULTS	
·	3.1	Chapter A: Expression and characterization of pantothenate energy-coupling factor	
		porters as an anti-infective drug target <sup>55</sup>	. 14
	3.2	Chapter B: Hit optimization by dynamic combinatorial chemistry on Streptococcus	
	pneui	noniae energy-coupling factor transporter ECF-PanT <sup>51</sup>	46
	3.3	3.3 Chapter C: Investigation of the rescue effect of energy coupling factor inhibitors	
	agair	ast roseoflavin toxicity in Streptococcus pneumoniae	
4		VAL DISCUSSION	
	4.1	ECF transporter protein and its characterization	87
	4.2	Targeting ECF protein by specifically designed compounds	87
	4.3	Evaluation of binding, inhibitory Effect, and selectivity of ECF inhibitors	
	4.4	Qualitative mode of action in pathogens	
5	Ot	TLOOK	91
6	R	EFERENCES	92
7	Λп	DENINIV	00

7.1	Side projects	99
7.1.1	IspD project	99
7.1.2	DXPS Project	101
7.2	Conference Contributions	103
7.2.1	Poster presentations:	103
7.2.2	Oral presentation:	103

The references in chapter 6 refer to chapter 1, 3.3, 4, and 7 of this work. References for chapter 3.1 and 3.2 are listed in each subchapter, referring to the main text and the supporting information, respectively.

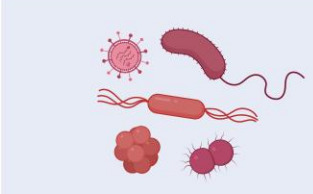
### 1 Introduction

### 1.1 Antimicrobial resistance (AMR)

AMR is one of the most pressing challenges in modern medicine, threatening decades of progress in treating bacterial infections. It occurs when bacteria acquire or develop mechanisms that render antibiotics ineffective, thereby allowing these microorganisms to survive and proliferate despite therapeutic intervention<sup>1</sup>. While the phenomenon of AMR is a natural evolutionary process, human activities such as the overuse and misuse of antibiotics in clinical and agricultural settings have accelerated its emergence and global spread<sup>2</sup>. This escalating crisis has profound implications for public health, as infections caused by resistant bacteria often lead to longer hospital stays, higher medical costs, and increased mortality<sup>3</sup>.

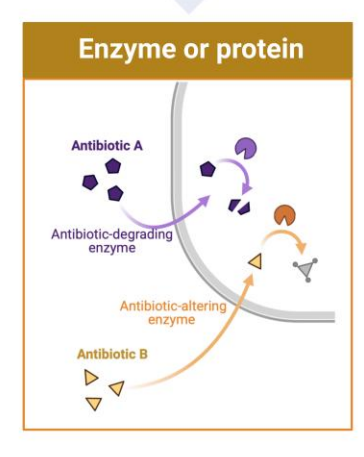
Bacterial resistance to antibiotics poses a significant public health challenge, rooted in both biochemical and genetic factors. Resistance can be intrinsic, where bacteria naturally evade certain antibiotics due to inherent structural or functional traits, or acquired, which arises through genetic mutations or the horizontal transfer of resistance genes. Key mechanisms include the enzymatic inactivation of antibiotics, structural modifications that prevent drugs from binding to their targets, active expulsion of antibiotics via efflux pumps, and reduced permeability of bacterial membranes to limit drug uptake (**Figure 1**). The remarkable genetic adaptability of bacteria, driven by mutations and gene exchange, enables rapid development and dissemination of resistance traits. These mechanisms collectively contribute to the growing prevalence of multidrug-resistant pathogens, underscoring the urgent need for innovative therapeutic strategies to combat antibiotic resistance and safeguard the efficacy of existing treatments<sup>4</sup>.

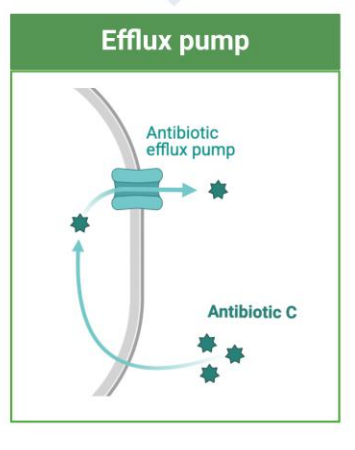
### Antimicrobial resistance (AMR)



- Bacteria, viruses, fungi, and parasites no longer respond to antimicrobial medicines.
- · Drug resistance makes antibiotics and other antimicrobial medicines ineffective.
- Infections become difficult or impossible to treat.
- Increased risk of disease spread, severe illness, disability, and death.
- AMR can affect anyone at any stage of life and anywhere in the world.

### **Common Antibiotic resistance mechanisms**





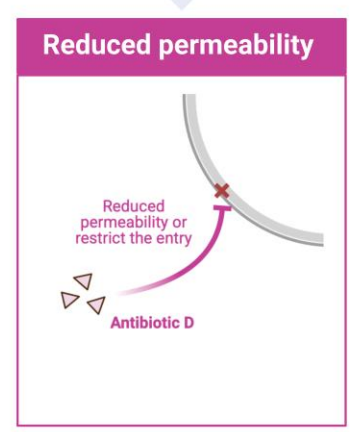


**Figure 1: Understanding antimicrobial resistance:** Schematic illustration of the common antibiotic resistance mechanisms in bacteria. Bacteria can alter or destroy antibiotics with enzymes or proteins, expel drugs using pumps, and restrict drug entry by modifying or reducing entryways and permeability. Created in BioRender. Shams, A. (2025)

The consequences of antibiotic resistance are severe. Common bacterial infections such as urinary–tract infections, pneumonia, and sepsis are becoming increasingly difficult to treat, with some infections now having limited treatment options using existing antibiotics<sup>4</sup>. Multidrug-resistant organisms, including *Escherichia coli*, *Klebsiella pneumoniae* and *Acinetobacter baumannii*, are spreading rapidly and causing outbreaks in healthcare facilities worldwide<sup>5</sup>.

The development of new antibiotics has significantly slowed down due to substantial financial and scientific challenges faced by pharmaceutical companies in creating and bringing novel drugs to the market<sup>6</sup>. Central to this effort is the implementation of antimicrobial stewardship programs, which aim to optimize the use of antibiotics to reduce unnecessary prescriptions and ensure effective treatment of infections<sup>7</sup>. Infection control measures, including enhanced hygiene practices and vaccination campaigns, can limit the spread of resistant pathogens<sup>8</sup>. Research into alternative therapies, such as bacteriophages, antimicrobial peptides, and immunomodulatory treatments, offers promising avenues for combating resistant infections<sup>9</sup>. Additionally, advancements in rapid diagnostic tools can aid clinicians in identifying

resistant infections promptly, enabling targeted therapy and minimizing the overuse of broad-spectrum antibiotics<sup>10</sup>.

Public awareness and education are equally critical in curbing AMR. Patients must be informed about the importance of adhering to prescribed treatments and the risks associated with self-medication and incomplete courses of antibiotics<sup>11</sup>. On a global scale, collaboration among governments, healthcare organizations, and regulatory bodies is essential to develop policies that promote responsible antibiotic use and support research into new therapeutic strategies<sup>12</sup>.

In conclusion, AMR represents a formidable challenge with far-reaching consequences for global health. Its resolution demands an integrated approach that combines scientific innovation, public health measures, and global collaboration. By prioritizing these efforts, we can mitigate the impact of resistance and preserve the effectiveness of antibiotics for future generations.

### 1.2 Vitamins

Vitamins are essential organic compounds that serve as crucial micronutrients for a wide range of biological processes, including growth, metabolic function, and the maintenance of overall health. The term "vitamin" from the word "vita," meaning life, and "amine," as they were originally thought to be amines necessary for life<sup>13</sup>. Since their discovery, vitamins have been recognized for their role in promoting proper cellular function and preventing various deficiencies. The discovery of these compounds has had a profound impact on the understanding of nutrition and health, especially in the context of deficiencies leading to disease<sup>14</sup>.

Vitamins are categorized into two primary groups based on their solubility: water-soluble and fat-soluble vitamins. Water-soluble vitamins, which include the eight members of the B-complex group and vitamin C (ascorbic acid), are absorbed directly into the bloodstream and are not stored in significant amounts within the body (**Figure 2**). As a result, they must be regularly replenished through diet<sup>15,16</sup>. Fat-soluble vitamins, which include vitamins A (retinol), D (calciferol), E (tocopherols), and K (quinones), are absorbed with dietary fat and can be stored in the body for longer periods, providing a reservoir for times of deficiency<sup>17</sup>. The roles of B-complex vitamins in cellular metabolism are summarized in **Table 1**, which highlights their involvement in key metabolic pathways critical for energy production and cellular function.

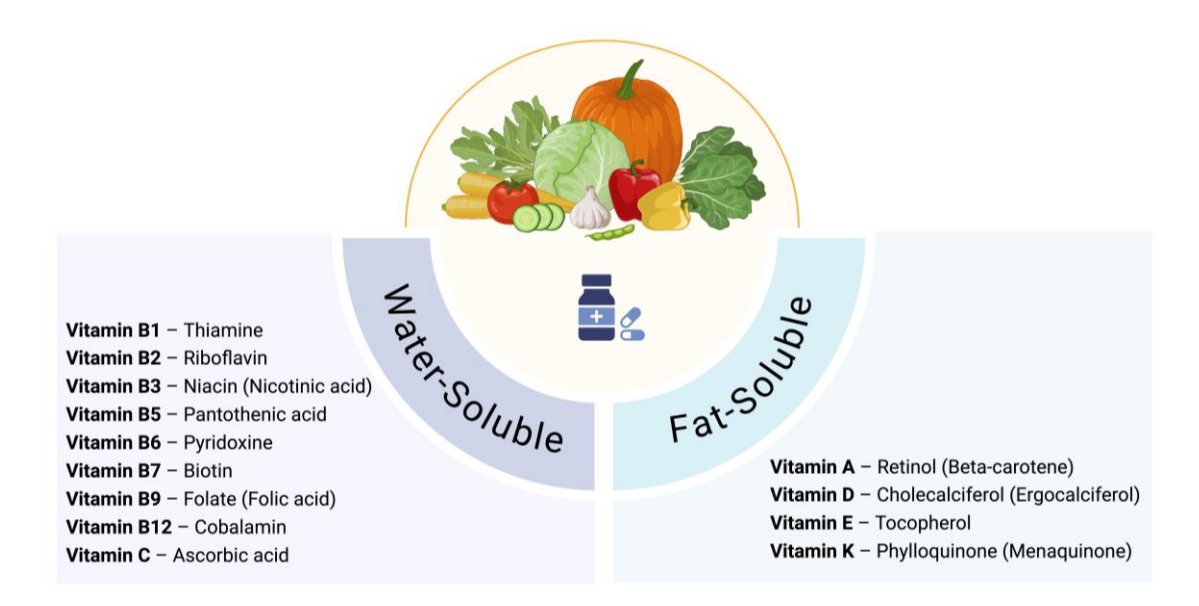


**Figure 2:** The figure shows a list of water and fat-soluble vitamins with their alternative names, highlighting their importance in maintaining overall health and supporting various bodily functions. Created in BioRender. Shams, A. (2025)

Deficiency in vitamins can lead to a variety of health conditions. For example, a lack of vitamin B9 (folic acid) results in macrocytic anemia and poor growth, while a deficiency in vitamin C (ascorbic acid) leads to scurvy, characterized by bleeding gums and weakened immune function<sup>18</sup>. In humans and animals, the investigation of vitamin deficiencies and their associated diseases has long been a subject of scientific research, as understanding these relationships has allowed for the development of therapeutic interventions and public health measures to prevent such conditions<sup>14</sup>.

Vitamins are not only essential for human health but also for the survival and growth of bacteria and archaea. While most prokaryotes are capable of synthesizing vitamins from primary metabolites, some species are auxotrophic, meaning they cannot produce certain vitamins and instead rely on environmental sources for these essential compounds<sup>19</sup>. This dependency on external vitamin uptake renders them vulnerable to environmental changes and offers an interesting target for antimicrobial drug development. Research into the transport mechanisms of vitamins within these microorganisms is thus a promising avenue for discovering novel antimicrobial agents that could disrupt these critical processes.

The role of vitamins in bacterial growth and survival underscores their importance not only for human health but also for microbial pathogenesis. Vitamin deficiencies in bacteria can severely disrupt cellular metabolism, impairing essential functions and hindering growth. Consequently, the study of vitamin transport and utilization mechanisms in bacteria could lead to the development of new therapeutic strategies aimed at combating resistant bacterial infections by targeting these essential metabolic pathways.

**Table 1:** B-type vitamins and their role in cellular metabolism<sup>20</sup>.

Vitamin	Structure	Role in pathogen
Thiamin or B1 <sup>21–25</sup>	$H_3C$ $NH_2$ $NH_3C$ $N^{\dagger}$	Precursor of cofactors for enzymes in various pathways:  • catabolism of carbohydrates and energy metabolism • pyruvate conversion • role in neurodegeneration and transient betterment
Riboflavin or B2 <sup>26,27</sup>	CH <sub>3</sub> NH NH OH OH	<ul> <li>Cofactor in redox metabolic reactions:</li> <li>energy generation from carbohydrates, fatty acids, ketone bodies, and proteins</li> <li>amino acid and fat metabolism</li> <li>mitochondrial function</li> <li>production of glutathione as an antioxidant</li> </ul>
Niacin or B3 <sup>28</sup>	ОН	Precursor of coenzymes NAD and NADP, which respectively are involved in:  • breaking down of fat, carbohydrate, protein, and alcohol along with cell signaling and DNA repair • building up fatty acids and cholesterol synthesis

Pantothenate or B5<sup>29</sup>

Precursor for biosynthesis of Coenzyme A, which is involved in:

- phospholipid biosynthesis
- fatty acid metabolism
- function of the tricarboxylic acid cycle

Pyridoxal phosphate or active form of vitamin B6<sup>33</sup>

Involved in different enzymatic reactions as coenzyme such as:

- transamination reactions
- ♦ beta-elimination reactions

Biotin or B7<sup>34</sup>

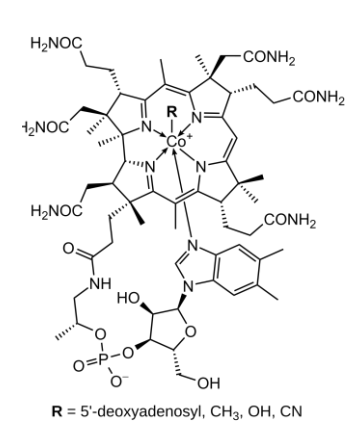
- cofactor for carboxylase enzymes
- involved in fatty acid biosynthesis, amino acid metabolism

Folate or B9<sup>35</sup>

Methylated derivation of folate (THF) involves in:

- ♦ single-carbon metabolism
- biosynthesis of DNA and RNA
- synthesis of methionine

Cobalamin or B12<sup>36</sup>



Used by many bacteria as a cofactor for various processes, including:

- ♦ Metabolism
- ♦ Gene regulation

Impacts host–microbe interactions by:

- ♦ Altering host physiology
- Modifying bacterial physiology

### 1.3 ATP-binding cassette (ABC) transporters

The cell membrane serves as a selectively permeable barrier, composed of a lipid bilayer interspersed with a diverse array of proteins. These proteins play vital roles in structural support, signal transduction, and the transport of molecules, contributing to the dynamic and complex nature of the membrane<sup>37</sup>. Among these, ATP-binding cassette (ABC) transporters are a prominent class of integral membrane proteins, recognized for their pivotal role in the active transport of substrates across membranes. As members of the transport system superfamily, ABC transporters are evolutionarily conserved and are found in organisms ranging from prokaryotes to eukaryotes<sup>38</sup>. ABC transporters have a tremendous structural diversity in their membrane-embedded domains. The structural differences between ABC exporters and importers may be related to the opposing directions in which the substrate is pumped or the range of transported substrates. The three different types of ABC importers (Type I, Type II, and ECF) have overlapping substrate specificities, but it is unclear why three importer folds have evolved<sup>39,40</sup>.

ABC transporters utilize ATP hydrolysis to drive the translocation of various substrates, including ions, lipids, drugs, and metabolic products, across biological membranes. Structurally, these transporters are composed of two transmembrane domains (TMDs) embedded in the lipid bilayer, which form the substrate translocation pathway, and two nucleotide-binding domains (NBDs) located in the cytoplasm. ATP molecules bind to the NBDs, initiating a cascade of events that includes ATP hydrolysis (**Figure 3**). The energy released from this process induces conformational changes in the TMDs, facilitating substrate movement across the membrane. This ATP-driven mechanism highlights the importance of energy coupling in maintaining directional substrate flow<sup>41</sup>.

In prokaryotes, the efficiency and specificity of substrate transport by ABC systems often depend on substrate-binding proteins (BPs). These proteins act as initial substrate recognizers and facilitators, capturing target molecules from the extracellular environment and delivering them to the transporter complex. In Gram-negative bacteria, BPs are predominantly located in the periplasmic space, where they operate within a confined and controlled environment. However, Gram-positive bacteria, which lack a periplasmic space, utilize alternative strategies. They employ either lipoproteins tethered to the external surface of the membrane or BPs directly associated with the TMDs of the transporter to ensure efficient substrate capture and delivery<sup>42</sup>.

The versatility and adaptability of ABC transporters in both prokaryotes and eukaryotes underscore their significance in cellular processes, including nutrient acquisition, toxin efflux, and resistance to antimicrobial agents<sup>38</sup>. Understanding their structure, function, and interaction with accessory proteins like BPs not only provides insights into their physiological roles but also opens avenues for developing therapeutic strategies targeting their function in pathogens.

# Substrate-binding protein Substrate Substrate binding & ATP-dependent NBD closure Nucleotide-binding domain (NBD)

**Figure 3: Illustration of the ABC influx transporter:** the interaction of the binding proteins (BPs) with the substrate, facilitate its transport into the cell through the ABC transporter. Created in BioRender. Shams, A. (2025)

### 1.4 Energy-coupling factor (ECF) transporters

Energy-coupling factor (ECF) transporters are a recently identified and distinct subfamily of ATP-binding cassette (ABC) transporters found exclusively in prokaryotes. Their role in the active transport of vital substrates, such as vitamin B complexes, cobalt ions (Co<sup>2+</sup>), and nickel ions (Ni<sup>2+</sup>), makes them promising targets for the development of anti-infective therapies. Targeting these essential transport mechanisms, ECF transporters could be exploited to combat bacterial pathogens<sup>43,44</sup>.

Structurally, ECF transporters are composed of four distinct domains: (a) two cytosolic ATPases, referred to as EcfA and EcfA', (b) a membrane-embedded substrate-binding protein, also called the S-component or EcfS, and (c) a transmembrane energy-coupling protein known as EcfT. The EcfT protein serves as an intermediary, linking the ATPases (EcfA and EcfA') with the substrate-specific S-component, ensuring coordinated transport activity<sup>45</sup>.

ECF transporters are classified into two distinct groups based on their organizational and functional differences:

- Group I: Each ECF module (ECFTA'A) is paired with a specific S-component, and the genes encoding these components are located within a single operon.
- Group II: Multiple S-components share a single ECF module and compete for access to it. Unlike Group I, the genes encoding the S-components are distributed across the chromosome, separate from those encoding the other domains<sup>20</sup>.

The transport mechanism in Group II ECF transporters is particularly intriguing. The EcfT protein features two elongated  $\alpha$ -helices that form an X-shaped structure<sup>20</sup>. Conformational changes in these helices facilitate substrate translocation. When ATP binds to the nucleotide-binding pockets of EcfA'A, its hydrolysis generates the energy required to move the  $\alpha$ -helices forward, causing the S-component to reorient. Initially, the S-component faces the extracellular space to bind its substrate. Following reorientation, the substrate-loaded S-component aligns with the cytoplasmic side, interacts with EcfT, and transfers the substrate through the membrane. In the resting state, the  $\alpha$ -helices of EcfT return to their original position, and the nucleotide-binding pockets remain unoccupied<sup>20</sup> (**Figure 4**).

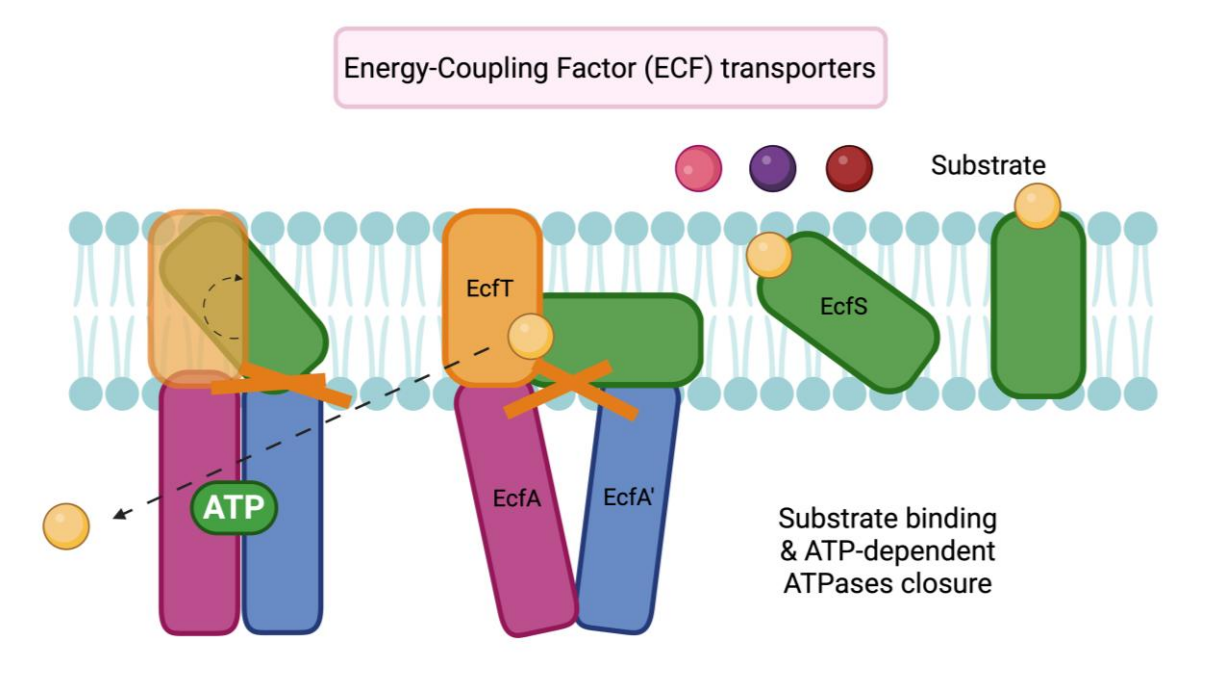


**Figure 4: Schematic representation of an ECF group-II transporter:** Upon binding of the S-component with its substrate, it topples over in the membrane. The interaction with the ECF module releases the substrate into the cytoplasm. ATP binding then releases the empty S-component, leading to the separation of the ECF module and the S-component in an outward-facing state. Created in BioRender. Shams, A. (2025)

The S-components (EcfS) of Group II transporters exhibit a high degree of sequence variability but share a common structural framework, characterized by six transmembrane helices (TMHs) arranged in a bundle. These helices, particularly SM4–6, interact with connecting loops (e.g., L1, L3, and L5) and conserved residues within the substrate-binding pocket<sup>46</sup>. This structural arrangement allows EcfS proteins to accommodate substrates of diverse sizes and shapes. A conserved AxxxA motif on the surface of the S-component is hypothesized to act as a binding site for the ECF module, further facilitating the transport process<sup>47</sup>. The diversity of S-component binding pockets is a key feature of ECF transporters, highlighting their adaptability in substrate recognition and transport.

### 1.5 Role of ECF transporters in pathogenic bacteria and vitamin uptake

Many pathogenic bacteria depend on the uptake of essential vitamins for their survival and growth, often facilitated by ECF transporters. These transporters allow bacteria to scavenge B-type vitamins from their environment, compensating for the absence or partial loss of *de novo* biosynthetic pathways. The presence and reliance on ECF transporters vary among different bacterial species. The vitamin acquisition strategies vary based on the pathogen and below is a list of seven key pathogens<sup>20</sup>:

- 1. *Staphylococcus aureus*: it encodes S-components for riboflavin, thiamine, and biotin. It has the capability to synthesize these vitamins *de novo*, reducing its dependence on external sources.
- 2. Streptococcus pneumoniae: it utilizes ECF transporters for pantothenate, niacin, riboflavin, and biotin. However, it lacks complete biosynthetic pathways for these vitamins, making uptake essential for its survival.
- 3. *Enterococcus faecium*: it fully dependent on vitamin uptake through ECF transporters, as it lacks the genetic machinery for de novo biosynthesis of essential vitamins.
- 4. *Enterococcus faecalis*: it can biosynthesize folic acid and pantothenate but requires external sources of niacin, riboflavin, thiamine, and biotin for optimal growth.
- 5. *Clostridium tetani*: it relies on ECF transporters for the uptake of folic acid, pantothenate, niacin, and biotin. However, it retains the ability to synthesize thiamine and riboflavin *de novo*.
- 6. *Clostridium novyi*: it is capable of synthesizing most essential vitamins, except folic acid and biotin, which must be obtained from the environment via transport systems.
- 7. *Clostridium difficile*: it possesses the biosynthetic pathways for pantothenate and riboflavin but depends on external biotin for survival.

The variations in vitamin acquisition strategies highlight the potential of ECF transporters as novel antimicrobial targets.

The ECF transporter studied in this Phd project is ECF-PanT from *Streptococcus pneumoniae*. *S. pneumoniae* is a Gram-positive bacterium that plays a central role in respiratory infections, such as pneumonia, as well as more severe conditions like meningitis and sepsis. It is primarily found in the nasopharynx of healthy individuals but can become pathogenic, especially in immunocompromised individuals, children, and the elderly. The bacterium's virulence is largely due to its polysaccharide capsule, which acts as a major virulence factor by preventing phagocytosis and aiding in immune evasion<sup>48</sup>. The ability of *S. pneumoniae* to survive and proliferate in diverse host environments requires it to acquire essential nutrients, including vitamins<sup>49</sup>. ECF transporters play a key role in bacterial growth and metabolism, particularly during infection when nutrient availability is limited, by facilitating the uptake of essential micronutrients. Disrupting these transporters could hinder bacterial survival, making it more vulnerable to the host's immune response. Targeting ECF transporters offers a promising strategy for

antimicrobial therapy, potentially complementing existing treatments and addressing the challenge of AMR.

### 1.6 Development of ECF inhibitors and their mechanism of action

Recent efforts have been directed toward identifying inhibitors of ECF transporters to hinder bacterial growth. In 2018, Bousis *et al.* identified 12 druggable pockets in the ECF-FoIT2 transporter using computational studies and, performed a sequence alignment of the ECF module in different pathogens showing conserved regions, indicating a broad-spectrum drug target<sup>20</sup>. Next, in 2023 Diamanti *et al.* performed a structure–based virtual screening (SBVS) on the ECF-FoIT2 from *Lactobacillus delbrueckii* (PDB ID: 5JSZ) to identify the first ECF inhibitors. The crystal and Cryo-EM structures for this ECF transporters gave us the opportunity to further explore our knowledge about these inhibitors. Coarse-grained (CG) molecular dynamics (MD) simulations were performed also to predict the binding and mechanism of action of a novel class of compounds to ECF transporters and interfere with their transport cycle. These compounds demonstrated potent inhibitory activity, highlighting the potential of targeting these transporters as a therapeutic strategy<sup>50</sup>. Additionally, we conducted a study in our group to identify and optimize compounds that inhibit ECF transporters<sup>51</sup>.

The mode of action of ECF inhibitors involves binding to the transporter and preventing the effective uptake of different vitamins, which is essential for bacterial survival. Diamanti *et al.* (2023) demonstrated that these inhibitors may bind at the interface between the S-component and ECF module. The compound might therefore interfere with the protein-protein interaction (PPI), thereby inhibiting transporter function and resulting in bacteriostasis<sup>50</sup>.

### 1.7 Structural insights into ECF transporters

The structural understanding of ECF transporters has been instrumental in the development of inhibitors. X-ray crystallography and cryo-electron microscopy (cryo-EM) have provided detailed structural models of the transporter, revealing key differences between ECF inhibitors and other ABC transporters. These structural insights facilitate the design of more effective and specific inhibitors that can bind to ECF transporters without affecting the human transport systems. Recent structural studies on ECF transporters have provided crucial insights into their mechanism and potential for inhibition. Crystal structures and biochemical analyses have revealed that ECF transporters use a unique transport mechanism involving the toppling of small integral membrane subunits (S-components)<sup>40</sup>. The structure of group II ECF transporter, specifically the pantothenate transporter from *Lactobacillus brevis* (LbECF-PanT) has elucidated how a single EcfAA'T module can interact with different S subunits in group II ECF transporters, identifying key residues essential for transporter activity and complex stability<sup>52</sup>. As mentioned above, Coarse-grained molecular dynamics simulations on ECF-FoIT2 and ECF-PanT have been used to profile the binding mode

and mechanism of inhibition for a promising class of inhibitors<sup>50</sup>. The conformational dynamics of ECF module support its role as a scaffold mediating interactions with various EcfS or S-component proteins<sup>53,54</sup>.

### 1.8 Conclusion and future directions

The identification and optimization of ECF transporter inhibitors is a promising strategy for the development of new antimicrobial therapies. These inhibitors could provide an alternative to traditional antibiotics, which are becoming increasingly ineffective due to rising antibiotic resistance. However, further research is needed to refine the potency and selectivity of these inhibitors, as well as to evaluate their efficacy in clinical settings. Additionally, understanding the structural biology of ECF-PanT will be crucial for designing inhibitors that can effectively target bacterial pathogens without affecting human transport systems.

### 2 Aims of the thesis

ECF transporters are integral membrane protein complexes that facilitate the uptake of essential micronutrients, such as vitamins, in prokaryotic organisms. Their pivotal role in bacterial metabolism, coupled with their absence in humans, renders them attractive targets for the development of novel antibacterial agents, especially in the context of rising antibiotic resistance.

The primary objective of this thesis was the purification and characterization of the *Streptococcus* pneumoniae ECF-PanT transporter to elucidate its structural and functional properties. *In silico* studies were employed to guide the design and optimization of inhibitors targeting its allosteric sites. Subsequent efforts focused on optimizing these inhibitors and assessing their *in vivo* efficacy using the *Galleria* mellonella infection model.

In previous work conducted at the Helmholtz institute for pharmaceutical research Saarland (HIPS), a SBVS of ECF-FolT2, a homolog of ECF-PanT, was performed. This screening led to the identification of initial hits, which were synthesized and tested in various functional assays in collaboration with the University of Groningen. These studies aimed to establish a structure–activity relationship (SAR) for the most promising compounds, encompassing comprehensive biophysical and biological characterization, as well as the resynthesis of lead compounds and their derivatives.

Building upon these foundations, the second part of this work focused on the discovery and optimization of ECF inhibitors. A dynamic combinatorial chemistry (DCC) approach was employed, facilitating the identification of a new class of ECF inhibitors with improved activity. The application of DCC enabled the efficient exploration of chemical space, leading to the discovery of potent inhibitors. These compounds were further evaluated for cytotoxicity, and computational modeling studies were conducted to rationalize their binding modes. Notably, docking studies revealed that the acylhydrazone linker maintained crucial interactions within the binding site.

Additionally, an efficient bacterial uptake assay was developed to screen for inhibitors of ECF transporters. This assay provided a robust platform for evaluating the inhibitory potential of compounds, thereby streamlining the identification of promising ECF transporter inhibitors.

Collectively, these efforts contribute to a deeper understanding of ECF transporter inhibition and offer a promising avenue for the development of novel antibacterial therapies targeting ECF-PanT.

### 3 Results

3.1 Chapter A: Expression and characterization of pantothenate energy-coupling factor transporters as an anti-infective drug target<sup>55</sup>

Shams A.; Bousis S.; Diamanti E.; Elgaher W. A. M.; Zeimetz L.; Haupenthal J.; Slotboom Dirk J.; Hirsch Anna K. H: Expression and characterization of pantothenate energy-coupling factor transporers as an anti-infective drug target. *Protein Sci* 2024. DOI: 10.1002/pro.5195

Accepted: 9 October 2024

DOI: 10.1002/pro.5195

### RESEARCH ARTICLE



### Expression and characterization of pantothenate energy-coupling factor transporters as an anti-infective drug target

Atanaz Shams<sup>1,2</sup> | Spyridon Bousis<sup>1,2,3</sup> | Eleonora Diamanti<sup>1,4</sup> | Walid A. M. Elgaher<sup>1</sup> | Lucie Zeimetz<sup>1,2</sup> | Jörg Haupenthal<sup>1</sup> | Dirk J. Slotboom<sup>5</sup> | Anna K. H. Hirsch<sup>1,2</sup>

<sup>1</sup>Helmholtz Institute for Pharmaceutical Research Saarland (HIPS) - Helmholtz Centre for Infection Research (HZI). Department of Drug Design and Optimization, Saarbrücken, Germany <sup>2</sup>Saarland University, Department of Pharmacy, Saarbrücken, Germany <sup>3</sup>Stratingh Institute for Chemistry and Technology, Faculty of Science and Engineering, University of Groningen, Groningen, The Netherlands <sup>4</sup>Department of Pharmacy and Biotechnology, Alma Mater Studiorum-Università di Bologna, Bologna, Italy <sup>5</sup>Groningen Biomolecular Sciences and Biotechnology Institute, University of Groningen, Groningen, The Netherlands

### Correspondence

Anna K. H. Hirsch, Helmholtz-Institut für Pharmazeutische Forschung Saarland (HIPS), Campus E8.1, 66123 Saarbrücken, Germany.

Email: anna.hirsch@helmholtz-hips.de

### **Funding information**

European Research Council Starting Grant, Grant/Award Number: 757913; Helmholtz-Association, Grant/Award Number: Initiative and Networking Fund; Erasmus+; Saarland University

Review Editor: Aitziber L. Cortajarena

### Abstract

This study investigates the potential of energy-coupling factor (ECF) transporters as promising anti-infective targets to combat antimicrobial resistance (AMR). ECF transporters, a subclass of ATP-binding cassette (ABC) transporters, facilitate the uptake of B-vitamins across bacterial membranes by utilizing ATP as an energy source. Vitamins are essential cofactors for bacterial metabolism and growth, and they can either be synthesized de novo or absorbed from the environment. These transporters are considered promising drug targets, underscoring the need for further research to harness their medicinal potential and develop selective inhibitors that block vitamin uptake in bacteria. Herein, we focused on the ECF transporter for pantothenate (vitamin B5) from Streptococcus pneumoniae and the ECF transporter for folate (vitamin B9) from Lactobacillus delbrueckii as a reference protein. We also included the energizing module for pantothenate along with both full transporter complexes. Initially, we transformed and purified the transporters, followed by an assessment of their thermal stability under various buffer composition, pH, and salt concentrations. Additionally, we monitored the melting temperature over six days to confirm their stability for further assays. We then measured the binding affinities of six ECF inhibitors using surface plasmon resonance (SPR) and evaluated their inhibitory effects through in vitro assays, including bacterial growth assay, whole-cell uptake, and transport-activity assays. After determining cytotoxicity in two human cell lines, we established an in vivo infection model using Galleria mellonella larvae to further validate our findings.

### KEYWORDS

antimicrobial resistance (AMR), B-vitamins, energy-coupling factor (ECF) transporters, *Galleria mellonella* infection model, pantothenate (vitamin B-5), *Streptococcus pneumoniae*, surface plasmon resonance

This is an open access article under the terms of the Creative Commons Attribution License, which permits use, distribution and reproduction in any medium, provided the original work is properly cited.

© 2024 The Author(s). Protein Science published by Wiley Periodicals LLC on behalf of The Protein Society.

SHAMS ET AL.



ATPases (EcfA and EcfA') and the S-component

(Figure 1) (Zhang, 2013).

### 1 | INTRODUCTION

Antimicrobial resistance (AMR) is a major global public health threat that endangers humans. It occurs when a microbe gains the ability to evade the effect of anti-infectives (Murray et al., 2022). The World Health Organization (WHO) list of global-priority, drug-resistant pathogens in 2024 includes macrolide-resistant Group A Streptococci, penicillin-resistant Group B Streptococci, macrolide-resistant Streptococcus pneumoniae, and Haemophilus influenzae, underscoring the urgent need to address their public health impacts, particularly for vulnerable populations in resource-limited settings. This highlights the critical necessity to discover novel anti-infective therapies, especially those with unprecedented modes of action.

The energy-coupling factor (ECF) transporters are a subfamily of the ATP-binding cassette (ABC) transporters that mediate the uptake of substrates such as B-type vitamins, Ni<sup>2+</sup>, and Co<sup>2+</sup> through the membrane of prokaryotes. Due to their specific role in the bacterial homeostasis, they might represent a new avenue to treat infections caused by bacteria that rely on these transporters for survival (Henderson et al., 1979; Rempel et al., 2019; Rodionov et al., 2009).

We selected *S. pneumoniae* as a suitable target pathogen to study the function of ECF transporters as it lacks the biosynthetic route for pantothenate (vitamin B-5), biotin (vitamin B-7), and folate (vitamin B-9), and it depends on their uptake from the environment (Bousis et al., 2018). *S. pneumoniae* is a Gram-positive pathogen that causes pneumonia and meningitis by targeting and colonizing the respiratory tract. Although many pneumococcal infections can be treated using antibiotics, mutated *S. pneumoniae* strains appear with resistance against current antibiotics (Cillóniz et al., 2018).

Vitamins are indispensable for the survival of bacteria, archaea as well as humans. Prokaryotes can synthesize vitamins from primary metabolites or conversely, they can be auxotrophic and rely on the uptake of vitamins from the environment (Bousis et al., 2018). In the latter case, bacteria cannot synthesize vitamins de novo or do not have access to their entire biosynthetic pathway (Jaehme & Slotboom, 2014).

Intrigued by the critical role the ECF transporters played in the uptake of B-type vitamins, the focus of this work is directed toward the study of ECF transporter for pantothenate in *S. pneumoniae*.

Structurally, ECF transporters contain four domains: two cytosolic ATPases named EcfA and EcfA', a membrane-embedded substrate-binding protein known as EcfS or S-component, and a transmembrane protein called EcfT that connects the two

Two classifications are found for ECF transporters. In group I, each ECF module (EcfTAA') interacts with its specific S-component, and a single operon is responsible for the genes encoding all different domains. In group II, multiple S-components compete for the same ECF module, engaging in shared competition. The genes encoding S-components are distinct from the other three domains and are scattered across the chromosome (Slotboom, 2014).

To explore ECF transporters for pantothenate in S. pneumoniae, we expressed and isolated three proteins: (i) the S. pneumoniae full ECF transporter complex for pantothenate (ECF-PanT) with PanT as the S-component, (ii) the S. pneumoniae EcfTAA' (ECF module), and (iii) the L. delbrueckii full ECF transporter complex for folic acid (ECF-FolT2) as a comparative model. We evaluated the stability of ECF-PanT and the ECF module using thermal shift assay (TSA) and determined the binding affinities and inhibitory activities of a series of compounds previously identified by our group (Bousis et al., 2021; Diamanti et al., 2023; Drost et al., 2022) using various biochemical and biophysical assays. Ultimately, assessed the compounds in vivo against S. pneumoniae using Galleria mellonella larvae infection

This study serves as a proof-of-concept investigation aimed at exploring and validating the feasibility of our experimental approaches and hypotheses. By focusing on the purification and characterization of the ECF-PanT transporter and its interactions with various inhibitors, we seek to establish a foundational understanding of these systems. The insights gained from this work are intended to guide further research and development in the field, particularly in the context of targeting ECF transporters for therapeutic applications.

### 2 | RESULTS

### 2.1 | Sequence alignment and protein homology determination

Comparative genome sequence analysis indicated that the energy-coupling modules are conserved among bacteria (Rodionov et al., 2009). Previously, we carried out sequence alignment of the ECF modules across seven pathogens, including Staphylococcus aureus, S. pneumoniae, Enterococcus faecium, Enterococcus faecalis, Clostridium tetani, Clostridium novyi, and Clostridium difficile, highlighting the presence of highly conserved regions within the ECF modules. In particular, the



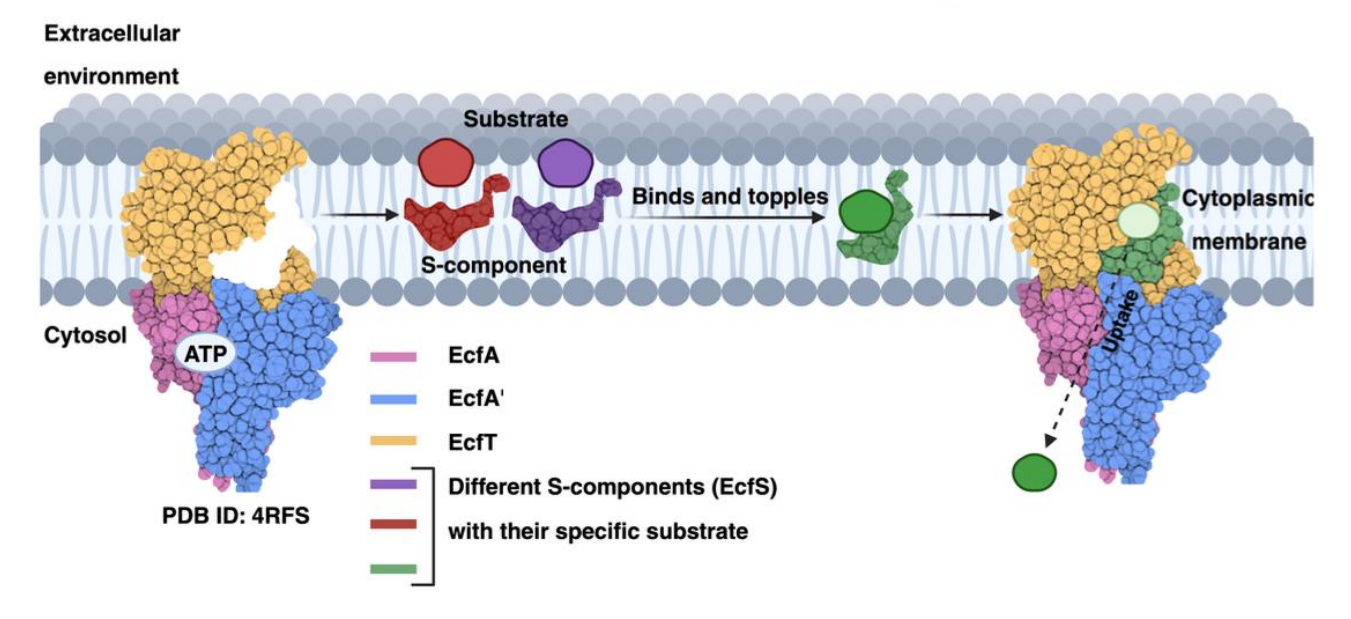


FIGURE 1 Schematic representation of the ECF transporters subunits and mechanism of transport. The ECF transporters use the integral-membrane S proteins (EcfS) to bind to a substrate and transport it into the cytoplasm in an ATP-dependent process (Zhang, 2013; Zhang et al., 2014). Source: Created with BioRender.com.

ATP-binding pocket and the interfaces between EcfA, EcfA', and EcfT subunits, are quite conserved suggesting that these regions are critical for the transport function and could serve as potential drug targets (Bousis et al., 2018).

In this study, we further aligned the ECF-PanT sequence from *S. pneumoniae* with three other ECF transporters, for which crystal structures have been determined, namely ECF-FolT2 from *L. delbrueckii* (PDB: 5JSZ) (Swier et al., 2016), ECF-PanT sequences from *L. delbrueckii* (PDB: 6ZG3) (Setyawati et al., 2020), and *Levilactobacillus brevis* (PDB: 4RFS) (Zhang et al., 2014) using the NCBI BLAST tool (Altschul et al., 1997, 2005). ECF-FolT2 was used as protein model for comparison in our analysis (Swier et al., 2016). The results indicated sequence homology across the queries with >40% identity for *L. delbrueckii* ECF-PanT *L. delbrueckii* ECF-FolT2, and >36% identity was observed in *L. brevis* ECF-PanT, in agreement with previous findings (Figure S1, Tables S1 and S2).

Consequently, we built a homology model of *S. pneumoniae* ECF-PanT employing AlphaFold-generated structures for the four ECF-PanT domains (Jumper et al., 2021) and the structure of *L. delbrueckii* ECF-FolT2 (PDB ID: 5JSZ) as a template for assembling the four protein subunits (Figure S2a). The homology model of *S. pneumonaie* ECF-PanT revealed structural similarities with *L. delbrueckii* ECF-FolT2 with an overall root mean square deviation (RMSD) of 3.25 Å. In particular, the two ATPase subunits (EcfA and EcfA') showed

RMSD values of 1.71 and 2.12 Å, respectively, which are consistent with their conserved functional roles, whereas high RMSD value was observed for the PanT component (5.12 Å) (Figure S2b), indicating potential structural divergence, possibly related to differences in substrate specificity. It is worth mentioning that high structural similarity were also observed between the *L. delbrueckii* ECF-FolT2 and ECF-PanT structures (Setyawati et al., 2020).

### 2.2 | Stability determination

We investigated the stability of ECF-PanT, ECF module, and ECF-FolT2 proteins using the thermal shift assay (TSA). Furthermore, we used TSA to identify the buffer conditions that optimize protein stability for binding assays, specifically surface plasmon resonance (SPR). The optimal concentrations of GloMelt and ROX dyes in complex with ECF-PanT in TSA were found to be 1× and 0.5 µM, respectively. Under these conditions, clear melting curves and the highest melting temperature  $(T_m)$ , indicating maximal biomolecule stability, determined (Table \$4). Subsequently, we identified the optimal concentrations of ECF-PanT, ECF module, and ECF-FolT2 along with their respective melting temperatures (Figure S6). The ECF-FolT2 from L. delbrueckii exhibits an average Tm of 54.6°C, which is higher than that of the S. pneumoniae ECF transporter. This difference may be attributed to the fact that L. delbrueckii ssp.

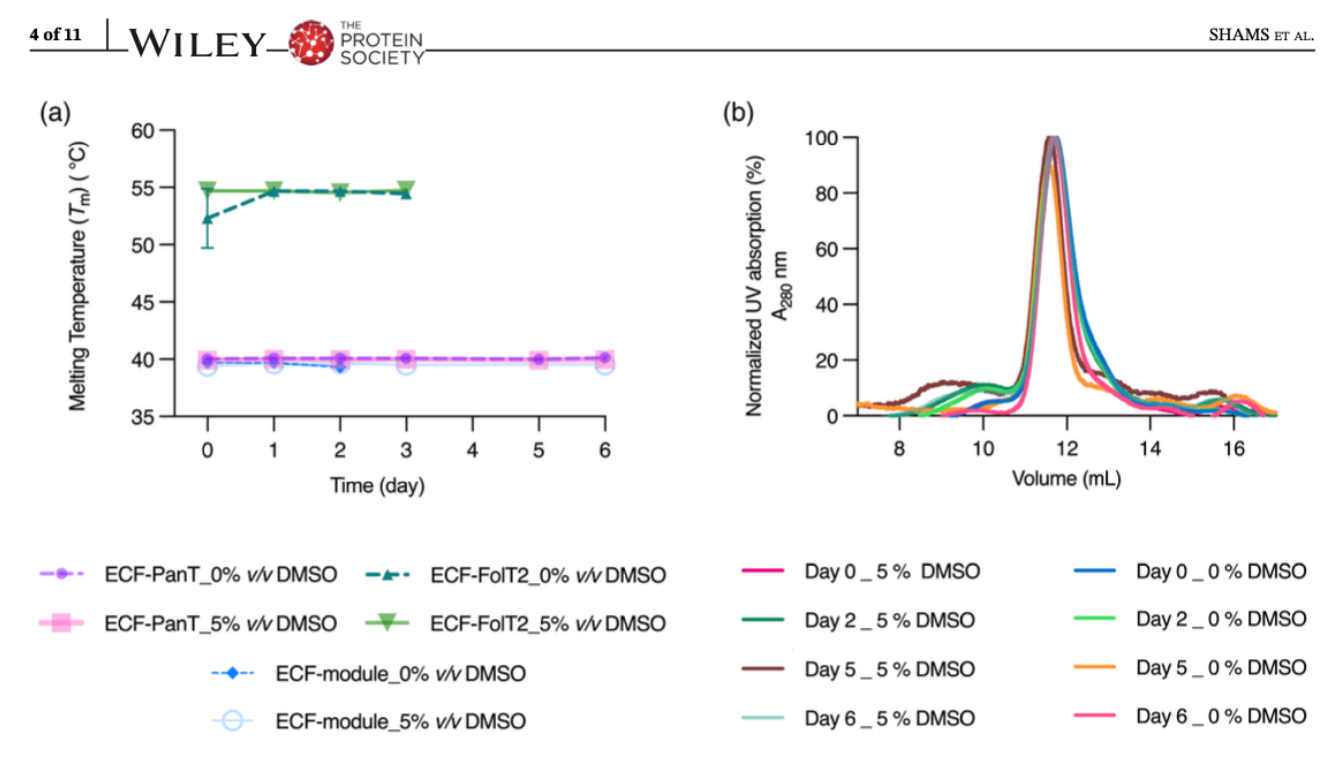


FIGURE 2 Assessment of ECF-PanT stability with and without DMSO. (a) Stability of ECF-PanT, ECF-FoIT2, and ECF-module was evaluated by monitoring melting temperatures ( $T_{\rm m}$ ) at room temperature over 6 days with 0% and 5% (v/v) DMSO. The data represent the mean and standard deviation from two independent experiments. (b) To assess protein stability, ECF-PanT samples were incubated at room temperature in an optimal buffer (50 mM KPi pH 7.5, 50 mM NaCl, 0.05% DDM) with or without 5% DMSO. UV absorption at 280 nm was measured using size exclusion chromatography (SEC) to determine the consistency of protein absorbance over time. Measurements were performed in technical duplicate to ensure accuracy.

bulgaricus can withstand heat exposure up to  $55\,^{\circ}$ C (Gouesbet et al., 2001). In contrast, the ECF-PanT and ECF-module from S. pneumoniae show average  $T_{\rm m}$  values of 39.7 and 39.5°C, respectively. The difference is not statistically significant and although this interpretation requires further validation, the derivative melting temperature graphs for the ECF-PanT protein (Figure S8) reveal two peaks: a major peak around  $39^{\circ}$ C that might corresponds to the ECF module and a smaller peak near  $60^{\circ}$ C possibly representing the S-component. This hypothesis matches the known melting temperature of the ECF module at approximately  $39^{\circ}$ C.

Building on this information, we systematically screened a wide range of buffers with various pH values and salt concentrations to investigate their effect on the stability of ECF-PanT (Figure S7).

Non-ionic detergent n-dodecyl  $\beta$ -D-maltoside 0.05% (DDM) (Rouse et al., 2013) and sodium chloride (50 mM) were added to maintain the solubility of proteins and ionic strength of the buffer; further details are reported in Appendix S1.

Then, after selecting the  $KP_i$  buffer due to the highest  $T_{\rm m}$ , we investigated the stability of the ECF-PanT, ECF-module and ECF-FolT2 using TSA for 6 days at room temperature. For ECF-PanT, we chose the so-called

"optimal buffer" that showed the highest  $T_{\rm m}$  (50 mM KP<sub>i</sub> pH 7.5, 50 mM NaCl, 0.05% DDM) (Figure 2), while the ECF-module and ECF-FolT2 were incubated in the SEC purification buffer. All the above-mentioned conditions were tested both in the absence and presence of 5% DMSO (v/v). The addition of DMSO was intended to mimic the SPR conditions used during our compound screening, ensuring consistency throughout the experiments.

Importantly, the melting temperature results, complementary to the corresponding curve shape, indicate that ECF-FolT2 and the ECF-module are stable for up to 3 days (Figure 2a), while ECF-PanT is stable for up to 6 days. In both cases, the buffer contains 5% DMSO (Figures S8–S10). To further validate these results, we loaded the samples on a SEC column followed by SDS-PAGE, where all four bands exhibited no significant degradation (Figures 2b and S11).

### 2.3 | Evaluation of known smallmolecule ECF transporter inhibitors

After identifying the optimal buffer and assessing the stability of the ECF transporter proteins, we proceeded to

TABLE 1 Chemical structures of known ECF inhibitors (1-6) with their IC<sub>50</sub> values resulted from the *Lactobacillus casei* whole-cell uptake assay as well as their respective MIC values using *Streptococcus pneumoniae* DSM-20566 strain.

 $^{a}$ The mean IC $_{50}$  values for the compounds was determined from two independent biological replicates. The range of IC $_{50}$  values observed was 6–500 μM, indicating substantial variability in the standard deviation (SD).

determine the binding affinity  $(K_d)$  of small-molecule inhibitors using SPR. This label-free technique allows for the investigation of protein-ligand interactions in real time and requires protein immobilization (GE Healthcare Life Science, 2012). Specifically, for the three ECF transporters, we used capture immobilization rather than standard immobilization because it offers several advantages, such as the ordered and uniform orientation of the protein, which does not compromise the protein's binding sites, and the ability to regenerate the surface afterward. The ECF-PanT, ECF-module, and ECF-FolT2, each bearing a histidine tag, were immobilized on a highaffinity poly-nitrilotriacetic acid (poly-NTA) sensor chip, which was initially activated using NiCl2. The His-tagged proteins were then injected over the Ni<sup>2+</sup>-activated surface to strongly bind to the metal (Knecht et al., 2009). The immobilization resonance unit (RU) levels were 12,000-15,000 for ECF-PanT, 9000-12,000 for the ECFmodule, and 6000-9000 for ECF-FolT2.

The SPR assay was used to test in-house ECF inhibitors **1–6** (Table 1) on the ECF-PanT, ECF-module, and ECF-FolT2 (Bousis et al., 2021; Diamanti et al., 2023; Drost et al., 2022).

As shown in Table 2, compounds 2 and 3 exhibited the lowest dissociation rate constants ( $k_d$ ) and the highest affinities for both ECF-PanT and ECF-FolT2 (Figures S12 and S13). Interestingly, no binding responses were observed for any of the compounds at concentrations up to 200  $\mu$ M when injected over the ECF module (Figure S14). These data may be consistent with our previous molecular-dynamics simulations, which predicted compound 1 binding at the interface between the ECF

module and the S-component (Diamanti et al., 2023). The absence of binding to the ECF-module alone, while showing binding to ECF-FolT2 and ECF-PanT, suggests that the S-component is necessary for compound binding. Moreover, these results can be further explained by considering the conformational changes in the ECF transporter proteins. In fact, the ECF-module undergoes a conformational change when forming the full ECF complex, which is different from that one of the ECF-module alone (Thangaratnarajah et al., 2023). On the other hand, the compounds exhibit a consistent binding trend to both ECF-FolT2 and ECF-PanT, indicating no substrate dependence. Thus, these findings support the idea that our compounds might act as allosteric inhibitors by binding at the interface between the ECF-module and the S-component.

It is worth mentioning that slightly higher inhibitory activities of the compounds were observed in the whole-cell assays (Table 1) compared to their binding affinities (Table 2). This variation may be attributed to the dynamic mechanism of action of ECF transporters, in contrast to the relatively 'locked' conformation observed in the SPR conditions from the EcfA side, where the Histag is attached.

### 2.4 | Transport-activity assay of ECF-PanT from S. pneumoniae

Based on the reported transport activity assay on *L. delbrueckii* (Swier et al., 2016), for the first time, we adapted this assay to a pathogenic bacterium. To do so,

ABLE 2 Binding affinities  $(K_D)$  and kinetic parameters of compounds 1–6 for the ECF transporter proteins<sup>8</sup>

	Streptococcu	Streptococcus pneumoniae				Lactobacillus delbrueckii	delbrueckii		
ECF transporter	ECF-PanT				ECF- module	ECF-FolT2			
Compound	$\frac{k_a}{(M^{-1} s^{-1})} \qquad k_d (s^{-1})$	$k_{\rm d}  ({ m s}^{-1})$	Kinetic, K <sub>D</sub> (μM)	Equilibrium, K <sub>D</sub> (μM)	K <sub>D</sub> (μM)	$k_{\rm a}  ({\rm M}^{-1}  {\rm s}^{-1})  k_{\rm d}  ({\rm s}^{-1})$	$k_{\rm d} ({ m s}^{-1})$	Kinetic, K <sub>D</sub> (μM)	Equilibrium, $K_{\rm D}~(\mu{ m M})$
1	$472 \pm 6$	$0.130\pm0.001$	276 ± 4	277 ± 5	n.a.	$620 \pm 10$	$0.181 \pm 0.003$	294 ± 6	$300 \pm 20$
2	384 ± 4	$0.0661 \pm 0.0004$	$172 \pm 2$	$170 \pm 5$	n.a.	$411 \pm 6$	$0.0760 \pm 0.0007$	185 ± 3	$190 \pm 20$
3	$6 \pm 059$	$0.0643 \pm 0.0006$	$99 \pm 1$	8 <del>∓</del> 96	n.a.	$570 \pm 10$	$0.0755 \pm 0.0008$	$132 \pm 3$	$128 \pm 9$
4	399 ± 4	$0.127 \pm 0.001$	$317 \pm 3$	304 ± 6	n.a.	$325 \pm 5$	$0.115\pm0.001$	353 ± 5	$340 \pm 10$
5	348 ± 7	$0.157 \pm 0.002$	$451 \pm 8$	$420 \pm 10$	n.a.	$570 \pm 10$	$0.187\pm0.003$	328 ± 6	$300 \pm 30$
9	376 ± 6	$0.147 \pm 0.002$	391 ± 6	374 ± 6	n.a.	$(1\\\pm 0.1)\times 10^5$	22 ± 3	231 ± 5	230 ± 10
Abhreviation: n a no	t amplicable due	Abhravistion: ns not sunlicable due to wew wast interaction or no hinding	on or no hinding						

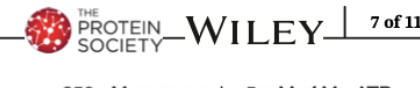
between the contraction of the contraction of the contraction of the contraction of the n=2

we purified the ECF-PanT transporter, reconstituted it into proteoliposomes, and carried out transport assays with radiolabeled pantothenate. Upon the addition of MgATP, the radiolabeled pantothenate is translocated across the membrane via an ATP-dependent mechanism. MgATP at 5 mM served as a positive control, supplying the proteins with the energy needed to complete the transport cycle, while MgADP at 5 mM was used as a negative control. The uptake of the radiolabeled substrate into proteoliposomes was measured using a scintillation counter.

As shown in Figure 3, all compounds (1-6) exhibited inhibition levels higher than 60% at the tested concentration of 250 µM. Compared to the inhibitory activities observed in the Lactobacillus casei whole-cell uptake assays, which ranged from 38.7% to 95.4% (Bousis et al., 2021; Diamanti et al., 2023; Kiefer et al., 2022), the compounds demonstrated higher inhibition in our transport-activity assay. The observed disparity in activity may be attributed to several factors, including dissimilarities in the ECF transporter sequences between L. casei and S. pneumoniae, as well as variations in compound concentrations. However, it is important to note that our study did not provide direct evidence to conclusively link these sequence differences to the observed variations in activity. In addition to sequence variations, differences in assay conditions such as the use of proteoliposome-based versus whole-cell uptake assays can also contribute to differences in compound activity and efficacy. Variations in cellular contents and assay conditions, as discussed by Dvorak et al. (2021), can impact the observed results. Further research is needed to explore these potential factors in more detail.

### 2.5 | Cytotoxicity evaluation

To investigate the cytotoxic potential of compounds 1-6 and to further support the prospective therapeutic use of ECF inhibitors, we evaluated their effect on the viability of human hepatoma (HepG2) and lung cancer (A549) cells. At a concentration of 100 μM, compounds 1 and 2 exhibited substantial cytotoxicity in HepG2 cells (Table 3), reducing viability to 20% and 23%, respectively. In contrast, only minimal effects were observed in A549 cells (viability >100%), suggesting selective toxicity toward liver cells. Also compound 3 displayed moderate cytotoxicity in HepG2 cells (49% viability) and lower toxicity in A549 cells (86% viability). Compound 4 was only slightly toxic in both cell lines, with 88% viability in HepG2 and 80% in A549 cells. Compounds 5 and 6 were non-toxic against both cell types.



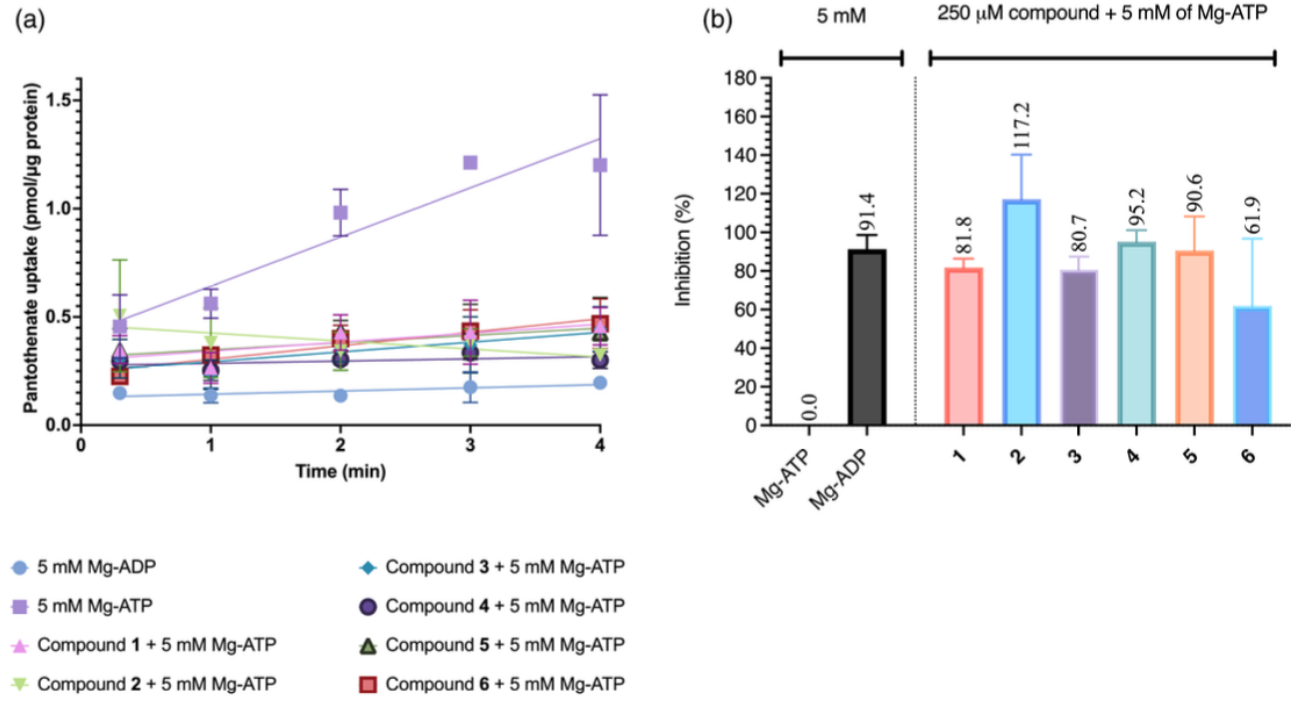


FIGURE 3 Transport activity assay of reconstituted *S. pneumoniae* ECF-PanT with a protein-to-lipid ratio of 1:125. (a) Time-course traces of pantothenate uptake over 4 min, showing transport activity in the presence of inhibitors with 5 mM Mg-ATP. The controls were 5 mM Mg-ADP (negative control) and 5 mM Mg-ATP (positive control) alone. The data demonstrate the uptake rates for each condition and was performed in duplicates. (b) Percentage inhibition of pantothenate uptake in presence of ECF inhibitors 1–6, calculated relative to the activity observed with 5 mM Mg-ATP.

TABLE 3 ECF inhibitors 1–6 were tested for toxicity against HepG2 and A549 cells to investigate their effect on cell viability.

	Percent (%) cell viability at 100 μM		
Compound	HepG2 cells	A549 cells	
1	$20 \pm 2$	$111 \pm 6$	
2	$23 \pm 7$	$124 \pm 15$	
3	$49 \pm 3$	$86 \pm 11$	
4	88 ± 9	$80 \pm 10$	
5	$106 \pm 8$	$102\pm17$	
6	$105 \pm 3$	$103 \pm 7$	

## 2.6 | Galleria mellonella infection model studies using S. pneumoniae

Next, we examined the antibacterial effect of the ECF inhibitors under in vivo conditions by using *G. mellonella* larvae. This model was adopted based on the work of Alhayek et al. (2022) and serves to assess the efficacy of ECF inhibitors against *S. pneumoniae* induced infection. Larvae were injected with the overnight culture of *S. pneumoniae* DSM-20566, incubated for 3 days at 37°C and 5% CO<sub>2</sub> without shaking, and survival rates were monitored daily for 3 days (Figure 4).

Based on the MIC, cytotoxicity, and affinity data, compounds 2, 3, and 4 were selected for further investigation. Compound 2 exhibited the strongest antibacterial activity, with a MIC of 8 μM against S. pneumoniae and a moderate IC<sub>50</sub> of 59 μM in the *L. casei* whole-cell uptake assay. Compound 3 also demonstrated potent antibacterial activity, with a MIC value of 16 µM and good inhibitory activity (IC<sub>50</sub> of 49.2 μM). While both compounds showed some cytotoxicity in HepG2 cells (in contrast to A549 cells), the dilution effect in vivo would mitigate this potential concern. Compound 4, despite having a higher MIC of 64 µM, exhibited lower cytotoxicity, making it a safer candidate for further studies. In the G. mellonella model, S. pneumoniae at an OD<sub>600</sub> of 1.5 reduced larval survival to 30% after 3 days. The controls (no injection and PBS injection) showed no effect on survival. Treatment with 10 and 50 µM of compound 2 increased survival by up to 70% compared to PBSinjected larvae, while compound 3 increased the survival to 60% at 10  $\mu$ M and 50% at 50  $\mu$ M. Compound 4 improved the survival rate to 40% at 10 µM and 60% at 50 µM. The differences in survival rates between the two concentrations might be attributed to a balance between effective antibacterial activity and cytotoxicity. For compound 2, the substantial survival rate at 50 µM suggests that its antibacterial effects outweigh potential cytotoxicity. In contrast, the decreased survival of compound 3 at 50 µM indicates that

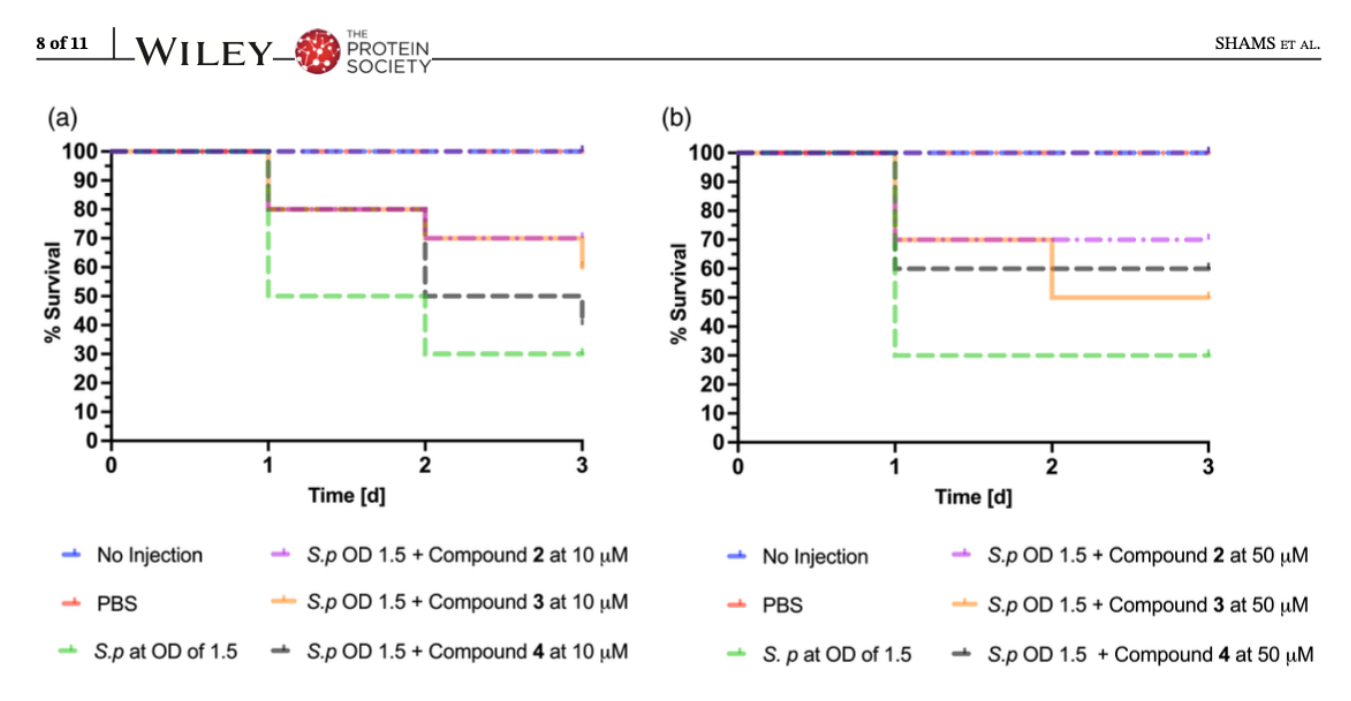


FIGURE 4 Simple survival analysis (Kaplan–Meier) was performed using GraphPad Prism. (a) The larvae were injected with S. pneumoniae (S.p) at  $OD_{600}$  of 1.5 in the absence and presence of compounds 2–4 at 10  $\mu$ M. The control groups are with no injection and PBS. (b) The larvae were injected with S. pneumoniae (S.p) at  $OD_{600}$  of 1.5 in the absence and presence of compounds 2–4 at 50  $\mu$ M. The control groups are with no injection and PBS.

increased cytotoxic effects may limit its efficacy. Notably, compound 4 demonstrated enhanced survival with higher concentrations, indicating its potential as a safer candidate. These results validate our inhibitors as promising candidates for targeting ECF transporters and confirm that the boost in inhibitory activity observed in vitro translates to an improved in vivo effect.

#### 3 | DISCUSSION

Membrane proteins pose challenges as drug targets, with stability being a crucial factor for experimental success. Using the thermal shift assay (TSA), we demonstrated that the ECF-module and full complex ECF-PanT from *S. pneumoniae*, as well as the full complex ECF-FolT2 from *L. delbrueckii*, are stable over 6 days. This study marks the first report of the isolation, purification, and use of a stable *S. pneumonia* ECF-module (or EcfTAA'). We further evaluated their stability under assay conditions (room temperature, with and without 5% DMSO) using TSA. This information is essential for drug discovery, serving as a foundation for developing new bioassays.

Notably, the established protocol for membrane proteins can be readily adapted to other ECF membrane proteins, providing vital stability data and assisting in the selection of optimal storage buffers for functional and/or binding assays.

Additionally, we successfully developed a surface plasmon resonance (SPR) protocol to determine the

binding affinities of six ligands against three noncovalently immobilized ECF transporters. This method is particularly effective with His-tagged target proteins, ensuring uniform binding and orientation on the chip. To our knowledge, we pioneered the use of SPR for assessing ligand binding affinities to transmembrane proteins, identifying HEPES (10 mM HEPES, 50 mM NaCl, 50 µM EDTA, 0.05% (v/v) DDM, pH 7.5) as the optimal buffer for SPR. In this proof-of-concept study, we successfully investigated the binding of six small-molecule inhibitors to three ECF proteins. Furthermore, these conditions can be adapted to a 384-well plate format, making SPR an accessible and robust screening method for identifying new ECF transporter inhibitors. We also optimized the G. mellonella infection model for S. pneumoniae to evaluate ECF inhibitors in vivo. These findings pave the way for the exploration and medicinal exploitation of ECF transporters, potentially leading to significant advancements in the treatment of bacterial infections.

#### 4 | MATERIALS AND METHODS

## 4.1 | Transformation, overexpression, and purification

The transformation was carried out using prepared chemically competent *E. coli* cells of strain *MC1061* and modified p2BAD His-ECF PanT-StrepII plasmid from *S. pneumoniae NCTC7465*, modified p2BAD His-ECF



from *S. pneumoniae NCTC7465*, and modified p2BAD His-ECF FolT2 plasmid from *L. delbrueckii* subsp. *bulgaricus ATCC 11842*. The transformed *E. coli* cultures were grown at 37°C overnight on LB-agar plates with ampicilin, and the cell pellets were stored in 60% glycerol at -80°C. Protein expression and purification followed established protocols (Swier et al., 2016). Supplementary figures corresponding to these methods can be found in Appendix S1 (Figures S3–S5 and Table S3).

## **4.2** | Determination of protein stability using TSA

TSA procedure requires incubation of protein and dye in a 96-well plate (Huynh & Partch, 2015). All the experiments were performed in biological and technical duplicate or triplicate, as stated in the following.

In each step, the end volume was set to  $20~\mu L$ . The four main components are protein, buffer, and both the GloMelt and ROX reference dye, which were accordingly set to have the desired concentrations. (Table S1 and Figure S6).

The second step is buffer screening for the optimization of protein stability. The composition of each condition in the well plates was set according to Appendix S1 (Figure S7).

The third step was investigating the stability in two different conditions. For this purpose, two conditions were prepared at seven times more than the total volume and incubated at room temperature for almost 1 week, and each day the melting temperature was monitored by running TSA. More detailed procedures can be found in Appendix S1 (Figures S8–S10).

#### 4.3 | Surface plasmon resonance

In this assay, we used HEPES buffer (10 mM HEPES, 50 mM NaCl, 50  $\mu$ M EDTA, 0.05% (v/v) DDM, and a pH value of 7.5) as recommended by Xantec Bioanalytics, with a slight modification made to create a more favorable environment for the ECF proteins, enabling their stability to be maintained throughout the assay. Additionally, the protein was maintained in the buffer containing 5% (v/v) DMSO. For a more in-depth description of the procedures, please refer to Appendix S1.

#### 4.4 | Transport-activity assay

The assay was performed based on the published protocol (Swier et al., 2016). The only modification was

reconstitution of *S. pneumoniae* ECF-PanT in a 1:125 (w/w) ratio of protein to *E. coli* polar lipids into large unilamellar vesicles and using radiolabeled pantothenate for uptake.

#### 4.5 | HepG2 in vitro MTT assay

The assay was performed based on the published protocol (Haupenthal et al., 2007), with some modifications, which can be found in Appendix S1.

#### 4.5.1 | G. mellonella infection model

G. mellonella larvae were used as an in vivo infection model to test selected ECF inhibitors, following the methodology established by Alhayek et al. (2022). S. pneumoniae DSM-20566 was cultured in Todd-Hewitt medium with 0.1% choline at 37°C with 5% CO<sub>2</sub> until an OD600 of 1.5 or higher was reached. Larvae were infected by injecting 10 μL of the culture into the left proleg and incubated at 37°C, 5% CO<sub>2</sub> for 72–96 h. Survival was monitored daily. Control groups received either PBS or no injection. Compounds 2–4 significantly improved larvae survival compared to the untreated control. The larvae used in this study were purchased from VALOMO-LIA Company (Strasbourg, France).

#### **AUTHOR CONTRIBUTIONS**

Atanaz Shams: Writing - original draft; conceptualization; methodology; formal analysis; validation; investigation; writing - review and editing; visualization; supervision. Spyridon Bousis: Conceptualization; writing - review and editing; methodology; supervision. Eleonora Diamanti: Conceptualization; writing - review and editing; methodology; supervision. Walid A. M. Elgaher: Writing - review and editing; formal analysis; supervision; methodology; validation; visualization. Lucie Zeimetz: Formal analysis; investigation. Jörg Haupenthal: Supervision; writing - review and editing; validation. Dirk J. Slotboom: Conceptualization; supervision; writing - review and editing; validation. Anna K. H. Hirsch: Project administration; resources; funding acquisition; supervision; conceptualization; writing - review and editing.

#### **ACKNOWLEDGMENTS**

The authors thank Jeannine Jung, Jannine Seelbach and Andreas Kany for their support in performing the *L. casei* whole-cell uptake assay and planning the MTT assay performance, respectively. A. K. H. H. appreciates support by an ERC starting grant (European Research Council

SHAMS ET AL.



Starting Grant, 757913) and the Helmholtz-Association Initiative and Networking Fund. A. S. is grateful for funding via Erasmus+ and GradUS of Saarland University. Open Access funding enabled and organized by Projekt DEAL.

#### CONFLICT OF INTEREST STATEMENT

The authors declare no conflicts of interest.

#### DATA AVAILABILITY STATEMENT

The data that support the findings of this study are available from the corresponding author upon reasonable request.

#### ORCID

Atanaz Shams https://orcid.org/0000-0002-7352-2876

Jörg Haupenthal https://orcid.org/0000-0003-3991-2800

Anna K. H. Hirsch https://orcid.org/0000-0001-8734-4663

#### REFERENCES

- Alhayek A, Abdelsamie AS, Schönauer E, Camberlein V, Hutterer E, Posselt G, et al. Discovery and characterization of synthesized and FDA-approved inhibitors of clostridial and bacillary collagenases. J Med Chem. 2022;65:12933–55.
- Altschul SF, Madden TL, Schäffer AA, Zhang J, Zhang Z, Miller W, et al. Gapped BLAST and PSI-BLAST: a new generation of protein database search programs. Nucleic Acids Res. 1997;25: 3389–402.
- Altschul SF, Wootton JC, Gertz EM, Agarwala R, Morgulis A, Schäffer AA, et al. Protein database searches using compositionally adjusted substitution matrices. FEBS J. 2005;272: 5101–9.
- Bousis S, Setyawati I, Diamanti E, Slotboom DJ, Hirsch AKH. Energy-coupling factor transporters as novel antimicrobial targets. Adv Ther. 2018;2:1800066.
- Bousis S, Winkler S, Haupenthal J, Fulco F, Diamanti E, Hirsch AK. An efficient way to screen inhibitors of energy-coupling factor 2 (ECF) transporters in a bacterial uptake assay 3. Int J Mol Sci. 2021;23:2637.
- Cillóniz C, Garcia-Vidal C, Ceccato A, Torres A. Antimicrobial resistance among *Streptococcus pneumoniae*. In: Fong I, Shlaes D, Drlica K, editors. Antimicrobial resistance in the 21st century. USA: Springer International Publishing; 2018. p. 13–38.
- Diamanti E, Souza PCT, Setyawati I, Bousis S, Gómez LM, Swier LJYM, et al. Identification of inhibitors targeting the energy-coupling factor (ECF) transporters. Commun Biol. 2023; 6:1182.
- Drost M, Diamanti E, Fuhrmann K, Goes A, Shams A, Haupenthal J, et al. Bacteriomimetic liposomes improve antibiotic activity of a novel energy-coupling factor transporter inhibitor. Pharmaceutics. 2022;14:4.
- Dvorak V, Wiedmer T, Ingles-Prieto A, Altermatt P, Batoulis H, Bärenz F, et al. An overview of cell-based assay platforms for the solute carrier family of transporters. Front Pharmacol. 2021;12:722889.

- GE Healthcare Life Science. Biacore TM assay handbook. Sweden: GE Healthcare Life Science; 2012. p. 1–78 Retrieved from https://rrc.uic.edu/wp-content/uploads/sites/112/2020/02/Biac oreAssayHandbook.pdf
- Gouesbet G, Jan G, Boyaval P. Lactobacillus delbrueckii ssp. bulgaricus thermotolerance. Lait. 2001;81:301–9.
- Haupenthal J, Baehr C, Zeuzem S, Piiper A. RNAse A-like enzymes in serum inhibit the anti-neoplastic activity of siRNA targeting polo-like kinase 1. Int J Cancer. 2007;121:206–10.
- Henderson GB, Zevely EM, Huennekens FM. Mechanism of folate transport in *Lactobacillus casei*: evidence for a component shared with the thiamine and biotin transport systems. J Bacteriol. 1979;137(3):1308–14.
- Huynh K, Partch CL. Analysis of protein stability and ligand interactions by thermal shift assay. Curr Protoc Protein Sci. 2015;79: 28.9.1–28.9.14.
- Jaehme M, Slotboom DJ. Diversity of membrane transport proteins for vitamins in bacteria and archaea. BBA Gen Subj. 2014;1850: 565-76.
- Jumper J, Evans R, Pritzel A, Green T, Figurnov M, Ronneberger O, et al. Highly accurate protein structure prediction with AlphaFold. Nature. 2021;596:583-9.
- Kiefer AF, Bousis S, Hamed MM, Diamanti E. Structure-guided optimization of small-molecule folate uptake inhibitors targeting the energy-coupling factor transporters. J Med Chem. 2022; 65:8869–80.
- Knecht S, Ricklin D, Eberle AN, Ernst B. OligoHis-tags: mechanisms of binding to Ni<sup>2+</sup>-NTA surfaces. J Mol Recognit. 2009; 22(4):270–9.
- Murray CJ, Ikuta KS, Sharara F, Swetschinski L, Robles Aguilar G, Gray A, et al. Global burden of bacterial antimicrobial resistance in 2019: a systematic analysis. Lancet. 2022; 399:629–55.
- Rempel S, Stanek W, Slotboom D, Arjatscls S. ECF-type ATP-binding cassette transporters. Annu Rev Biochem. 2019;88: 551–76.
- Rodionov DA, Hebbeln P, Eudes A, ter Beek J, Rodionova IA, Erkens GB, et al. A novel class of modular transporters for vitamins in prokaryotes. J Bacteriol. 2009;191(1):42-51.
- Rouse SL, Marcoux J, Robinson CV, Sansom MSP. Dodecyl maltoside protects membrane proteins in vacuo. Biophys J. 2013;105: 648-56.
- Setyawati I, Stanek WK, Majsnerowska M, Swier LJYM, Pardon E, Steyaert J, et al. In vitro reconstitution of dynamically interacting integral membrane subunits of energy-coupling factor transporters. Elife. 2020;22(9):e64389. https://doi.org/10.7554/eLife.64389
- Slotboom DJ. Structural and mechanistic insights into prokaryotic energy-coupling factor transporters. Nat Rev Microbiol. 2014; 12:79–87.
- Swier LJYM, Guskov A, Slotboom DJ. Structural insight in the toppling mechanism of an energy-coupling factor transporter. Nat Commun. 2016;7:11072.
- Thangaratnarajah C, Nijland M, Borges-Araújo L, Jeucken A, Rheinberger J, Marrink SJ, et al. Expulsion mechanism of the substrate-translocating subunit in ECF transporters. Nat Commun. 2023;14:4484.
- Zhang M, Bao Z, Zhao Q, Guo H, Xu K, Wang C, et al. Structure of a pantothenate transporter and implications for ECF module



sharing and energy coupling of group II ECF transporters. Proc Natl Acad Sci U S A. 2014;111:18560–5.

Zhang P. Structure and mechanism of energy-coupling factor transporters. Trends Microbiol. 2013;21:652-9.

#### SUPPORTING INFORMATION

Additional supporting information can be found online in the Supporting Information section at the end of this article. How to cite this article: Shams A, Bousis S, Diamanti E, Elgaher WAM, Zeimetz L, Haupenthal J, et al. Expression and characterization of pantothenate energy-coupling factor transporters as an anti-infective drug target. Protein Science. 2024;33(11):e5195. https://doi.org/10.1002/pro.5195

## Expression and characterization of pantothenate energy-coupling factor (ECF) transporters as an anti-infective drug target

<u>Atanaz Shams<sup>1,2</sup></u>, Spyridon Bousis<sup>1,2,3</sup>, Eleonora Diamanti<sup>4,1</sup>, Walid A. M. Elgaher<sup>1</sup>, Lucie Zeimetz<sup>1,2</sup>, Jörg Haupenthal<sup>1</sup>, Dirk. J. Slotboom<sup>5,2</sup>, Anna K. H. Hirsch<sup>1,2\*</sup>

<sup>1</sup> Helmholtz Institute for Pharmaceutical Research Saarland (HIPS) – Helmholtz Centre for Infection Research (HZI), Department of Drug Design and Optimization, 66123, Saarbrücken, Germany

<sup>2</sup> Saarland University, Department of Pharmacy, Campus Building E8.1, 66123, Saarbrücken, Germany

<sup>3</sup> Stratingh Institute for Chemistry and Technology, Faculty of Science and Engineering, University of Groningen, Nijenborgh 4, 9747AG, Groningen, The Netherlands

<sup>4</sup> Department of Pharmacy and Biotechnology, Alma mater studiorum - Università di Bologna - Via Zamboni, 33 - 40126 Bologna

<sup>5</sup> Groningen Biomolecular Sciences and Biotechnology Institute, University of Groningen, Nijenborgh 4, 9747AG, Groningen, The Netherlands

\*Corresponding author: Anna K. H. Hirsch, Helmholtz-Institut für Pharmazeutische Forschung Saarland (HIPS), Campus E8.1, 66123 Saarbrücken, +4968198806-2100, anna.hirsch@helmholtz-hips.de.

- Supplementary Material -

#### **Table of Contents**

Sequence alignment	3
Building of S. pneumonaie ECF-PanT homology model	7
Transformation, overexpression, and purification	8
Stability determination	10
Optimal concentrations for protein and dye	10
S. pneumoniae ECF-PanT buffer screening	11
Protein thermal stability: 6-Day study	13
Evaluation of stability data resulted from TSA	15
Protein-ligand interaction study using TSA	15
Surface plasmon resonance (SPR)	16
In vitro cytotoxicity evaluation	19

#### Sequence alignment

The NCBI BLAST program was utilized to conduct the BLAST analysis with specific parameters, including Blastp and an E-value threshold of 0.05 and scoring matrix of BLOSUM62 (Altschul et al., 1997, 2005). The subject protein under examination was *S. pneumoniae* ECF-PanT while the query proteins were *L. delbrueckii* ECF-FolT2 (Swier et al., 2016), *L. delbrueckii* ECF-PanT (Setyawati et al., 2020), and *Levilactobacillus brevis* ECF-PanT (Zhang et al., 2014) (Table S1).

Table S1: List of proteins with their respective source organisms, Protein Data Bank (PDB) identifiers, and UniProtKB accession numbers.

Protein name	PDB ID	UniProtKB	UniProtKB	UniProtKB	UniProtKB
		ID EcfS	ID EcfT	ID EcfA1	ID EcfA2
S. pneumoniae ECF-PanT	n.a.a	A0A064C5C4	A0A4L7ULF4	Q04HV7	Q97N51
L. delbrueckii ECF-FoIT2	5JSZ	Q1G929	A0A061BSU4	Q1GBJ0	Q1GBI9
L. delbrueckii ECF-PanT	6ZG3	Q1GBG0	Q1GBI8	Q1GBJ0	Q1GBI9
Levilactobacillus. brevis ECF-PanT	4RFS	Q03SM0	Q03PY7	Q03PY5	Q03PY6

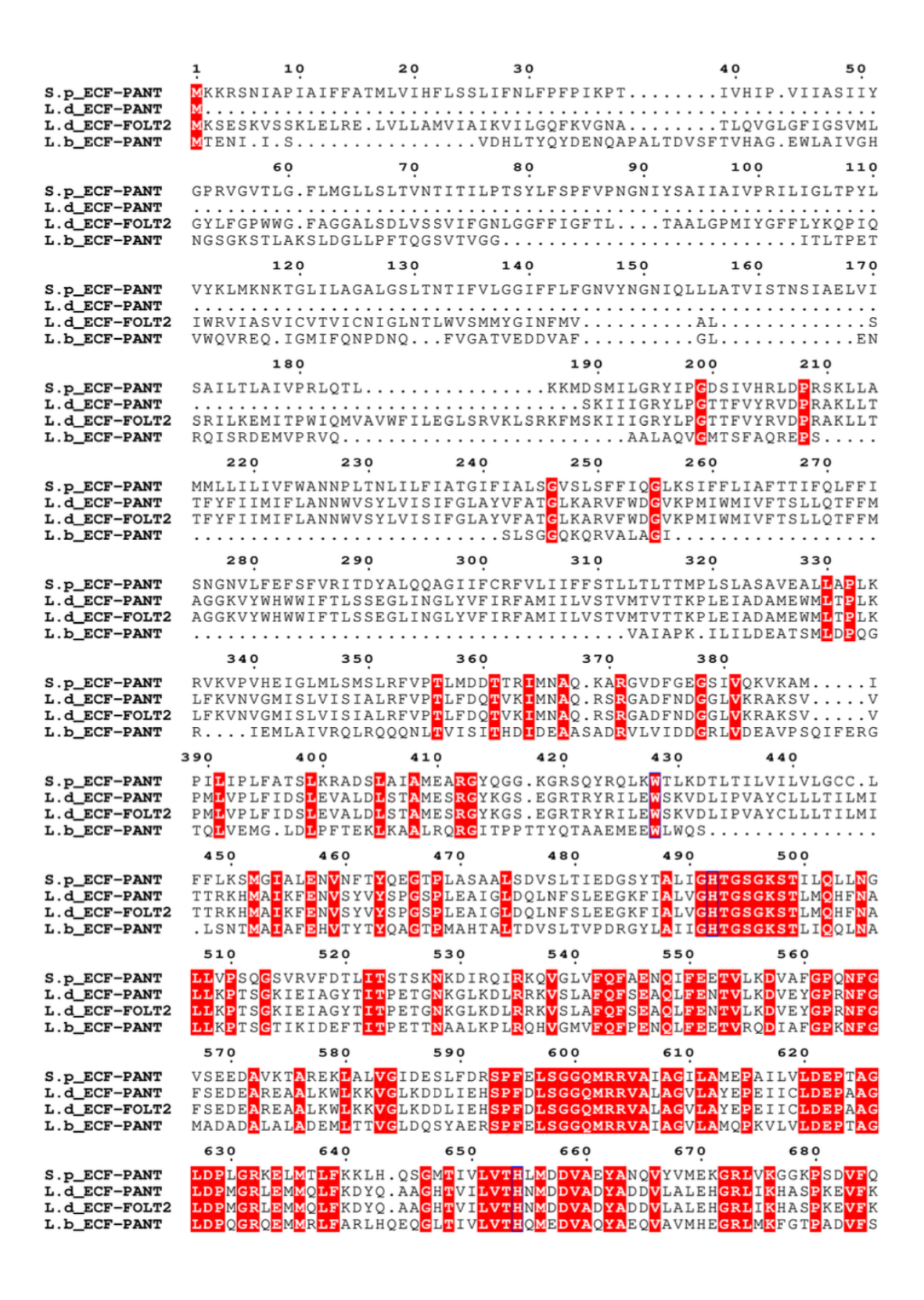
a not applicable.

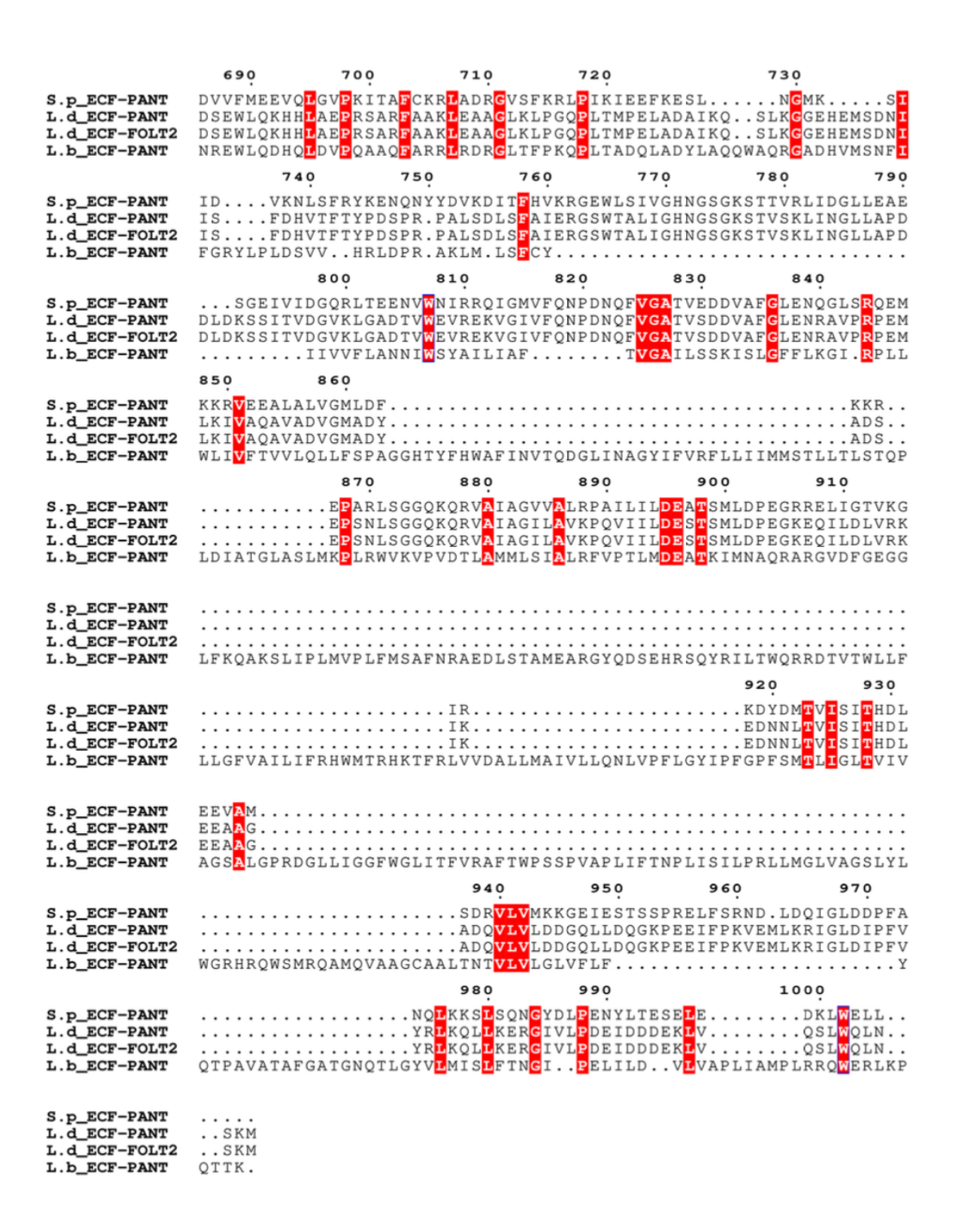
Table S2 provides an overview of the BLAST results, suggesting moderate sequence similarity between the subject protein, *S. pneumoniae* ECF-PanT, and the query proteins. *L. delbrueckii* ECF-PanT appears to exhibit the closest match, with a Max Score of 776, 99% query coverage, and 40.80% identity, implying a relatively strong alignment. Similarly, *L. delbrueckii* ECF-FolT2 shows a Max Score of 745, 95% coverage, and 40.61% identity, indicating a comparable degree of similarity. *L. brevis* ECF-PanT, on the other hand, displays a lower Max Score of 341 but a significantly higher Total Score of 1308, with 95% coverage and 36.36% identity, which might point to a slightly weaker sequence similarity, though the alignment still spans a substantial portion of the sequence. These results suggest a varying degree of conservation across the proteins, but further analysis would be required to confirm their functional relationships.

Table S2: Summary of BLAST search results for the protein sequences analyzed in this study. The table includes the maximum and total scores, query coverage (%), percent identity (%), E-values, and accession length. These metrics provide insights into the similarity and alignment quality between the query proteins and the target sequences.

description	Max	Total	Query	E Value	Per.	Acc.	Accession
	Score	Score	Cover		Ident	Len	
L. delbrueckii ECF-PanT	776	776	99%	0.0	40.80%	1041	Query_7093401
L. delbrueckii ECF-FolT2	745	745	95%	0.0	40.61%	1010	Query_7093402
L. brevis ECF-PanT	341	1308	95%	1e-104	36.36%	1038	Query_7093403

In this study, the multiple sequence alignment with all the query and subject proteins was produced by T-Coffee (Di Tommaso et al., 2011; Notredame, Higgins, & Heringa, 2000), and ESPript 3.0 was employed to improve the visual representation of the multiple sequence alignments, enabling clearer depiction of sequence similarities and conservation patterns. For consistency with the BLAST analysis, the BLOSUM62 substitution matrix was selected as the scoring system for visualizing sequence similarity (Figure S1). (Robert & Gouet et al., 2014.)





**Figure S1.** Visualization of multiple sequence alignment (MSA) performed by T-Coffee, visualized using ESPript online tool.

#### Building of S. pneumonaie ECF-PanT homology model

The ECF-PanT homology model was generated using Molecular Operating Environment (MOE), version 2022.02, Chemical Computing Group ULC, 910–1010 Sherbrooke St. W. Montreal, Quebec, H3A 2R7, Canada.

The sequences of *L. delbrueckii* ECF-FolT2 (PDB ID: 5JSZ), and the AlphaFold-predicted *S. pneumoniae* ECF-A (AF-Q04HV7-F1-v4), ECF-A' (AF-Q97N51-F1-v4), ECF-T (AF-A0A4L7ULF4-F1-v4), and PanT S-component (AF-A0A064C5C4-F1-v4) were imported into the sequence editor window, and each subunit of the *S. pneumoniae* ECF-PanT transporter was allocated to the corresponding chain of the *L. delbrueckii* ECF-FolT2. From protein panel, homology model option was selected and the sequence of *S. pneumoniae* ECF-PanT was indicated as source, and the *L delbrueckii* ECF-FolT2 as template with align sequence to template option was chosen. Model scoring was set to RMSD to mean, and refinement gradient limit to 0.5.

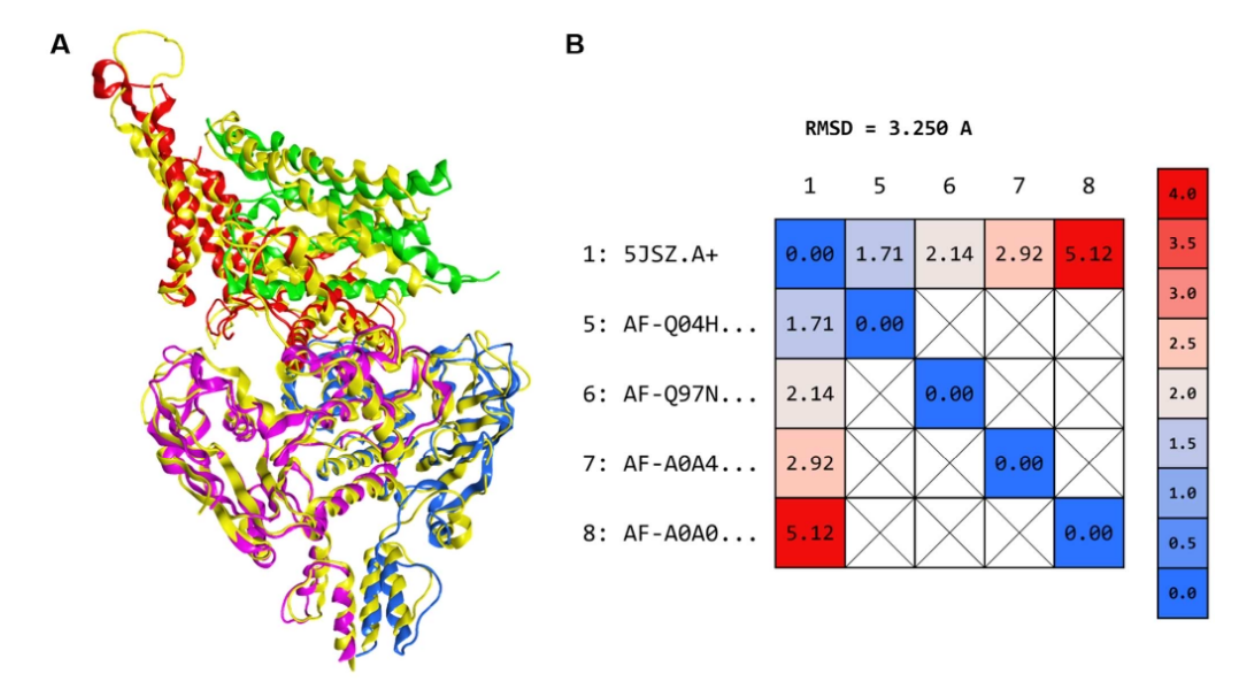


**Figure S2.** (A) Alignment of *L. delbrueckii* ECF-FoIT2 structure (yellow) (PDB ID: 5JSZ) and *S. pneumonaie* ECF-PanT homology model: ECF-A (blue), ECF-A' (magenta), ECF-T (red), and PanT S-component (green). (B) RMSD values of the whole homology structure and individual subunits.

#### Transformation, overexpression, and purification

The transformation, expression and purification were performed according to established procedures (Swier et al., 2016)

For confirmation of protein presence and effectiveness of purification, SDS-PAGE was carried out (Figure S3–S5). The molecular weight of each component of ECF-PanT, ECF-module, and ECF-FolT2 was computed using ExPASY (Table S3).

Table S3. The molecular weight (MW) of ECF-PanT, ECF-module from S. pneumoniae, and ECF-FolT2 from L. delbrueckii.

Protein	S. pneumoniae ECF-PanT (MW in KDa)	S. pneumoniae ECF-module (MW in KDa)	L. delbrueckii ECF-FolT2 (MW in KDa)
EcfT	29,47758	29,47758	30,26036
EcfA	32,53077	32,53077	31,63017
EcfA'	30,55329	30,55329	30,84509
EcfS	21,31286	-	19,42754
Total	113,8745	92,56164	112,16316

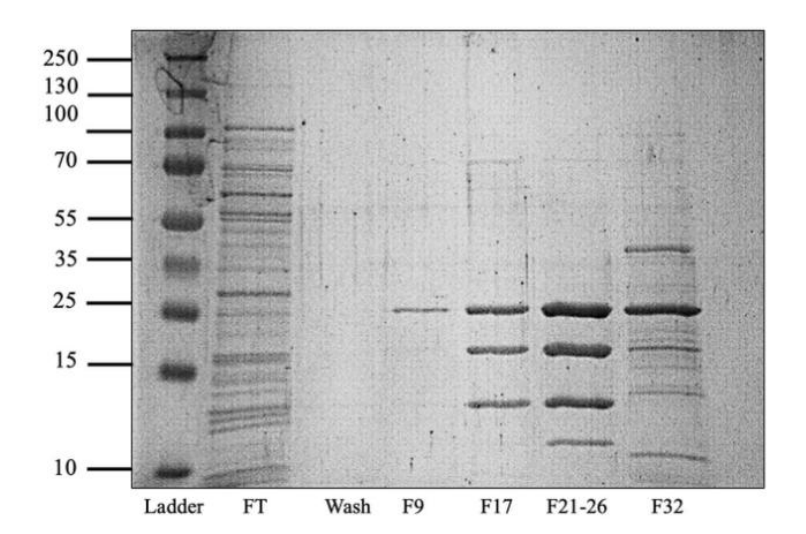


**Figure S3**. The 12% SDS-PAGE from purified ECF-PanT. FT represents the flow through the sample, the wash is the sample collected after wash, and F9, F17, F21-26, and F32 represent the elution fractions, from which A21-26 is considered the purified protein with separation of 4 different components of energy-coupling factor transporter.

Figure S4 shows SDS-PAGE for ECF-FolT2. This time additionally we investigated the effect of temperature as well as freezing and thawing on the protein. For this purpose, we had two conditions, in which the protein was incubated at 95 °C and room temperature (RT) to investigate the purity of the protein after purification. The two ATP-binding protein bands are observable at 95 °C and after one thaw, but EcfT and EcfS (FolT2) bands are not present at 95 °C, which can probably be due to protein precipitation at 95 °C, although a high concentration of SDS is present. As a result, heating the mixture should be avoided.

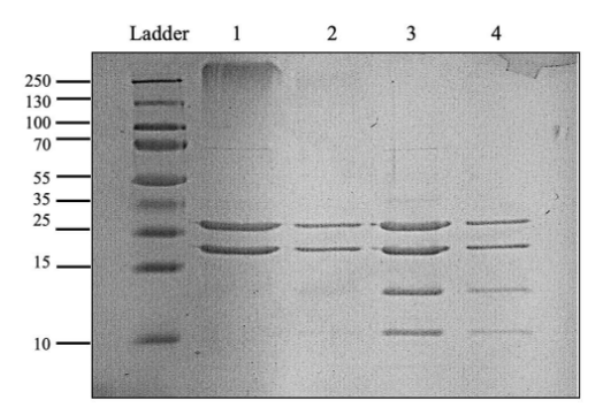


**Figure S4.** 12% SDS-PAGE gel from Purified ECF-FoIT2 fractions. 1) incubated at 95 °C for 5min 2) after one-time thaw incubated at 95 °C for 5 min 3) incubated at RT for 5min 4) after one-time thaw incubated at RT for 5min.

In the following (Figure S5), 12% SDS-PAGE was performed to confirm the purity of the ECF-module. Indeed, the ECF-module contains the three domains EcfT, EcfA, and EcfA'.

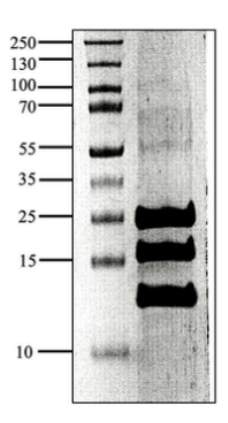


Figure S5. 12% SDS-PAGE gel from Purified ECF-module resulting from SEC.

SDS-PAGE results for ECF transporter proteins show four bands that do not align with their expected molecular weights. It could be due to protein conformational changes which means that the structural changes or conformational flexibility in proteins can influence their electrophoretic mobility. If the ECF transporter proteins due to release from their native environment undergo conformational changes that affect their shape or charge distribution, it can lead to different migration patterns on SDS-PAGE.

#### Stability determination

#### Optimal concentrations for protein and dye

TSA was used to determine the optimal concentrations of GloMelt dye and the ECF-PanT protein. To do so, we monitored how the melting temperature and shape of the curve changed as a function of different concentrations of ECF-PanT protein and GloMelt dye. Subsequently, by adding various final concentrations of protein, starting from 0.73 mg/mL which was the highest concentration of protein after purification, to 0.05 mg/mL (Table S2), as well as different concentrations of GloMelt (2x, 1x, and 0.5x). The effect of ROX 0.5  $\mu$ M was investigated by addition to different concentrations of GloMelt; the total volume was set to 20  $\mu$ L as well but the volume for each component was altered to keep the desired concentration. Then, the well plate was centrifuged, and the melting temperature was measured using a StepOnePlus® instrument. In run-setup, the start- and end-temperature were set to 20 °C and 95 °C, respectively; the heating rate was set to 0.5 °C per minute. The melting temperatures were analyzed using protein thermal shift software.

The lowest concentration of dye 0.5x and the protein 0.05 mg/mL were not enough to generate a good signal (Table S4). The experiment was carried out in two biological replicates for biological variability and two technical replicates for experimental precision.

**Table S4. Optimization of dye and the ECF-PanT protein concentration.** Orange-color highlight exhibits inadequate concentrations either due to low value or unclear curve shape.

ECF-PanT (mg/mL)	GloMelt	T <sub>m</sub> (°C)		
	2 x	$39.53 \pm 0$		
0.73	1 x	$39.45 \pm 0.07$		
	0.5 x	$39.55 \pm 0.02$		
	2 x	39.68 ± 0.14		
0.20	1 x	40.04 ± 0.07		
	0.5 x	$40.43 \pm 0$		
	2 x	$39.83 \pm 0$		
0.10	1 x	$40.49 \pm 0.07$		
	0.5 x	41.18 ± 0.14		
	2 x	Unknown		
0.05	1 x	Unknown		
	0.5 x	Unknown		

As a result, the optimal concentrations of GloMelt and ROX dyes were the same as the recommended amount for real-time PCR Instrument x1 and 0.5  $\mu$ M (4). In the next step, consequently, the concentration of dyes was kept constant, while the protein concentrations for ECF-PanT, ECF-module, and ECF-FoIT2 proteins were set to be between approximately 0.2 and 1 mg/mL. In Figure S6, a summary of the melting temperatures of all three proteins is shown. With this information, we can conclude the control melting temperature and start to screen different buffers and their effect on protein  $T_{\rm m}$  and finally investigate the stability.

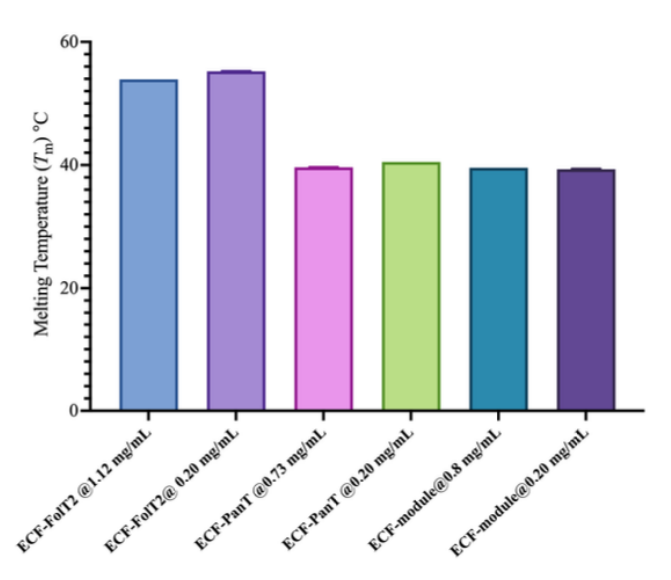
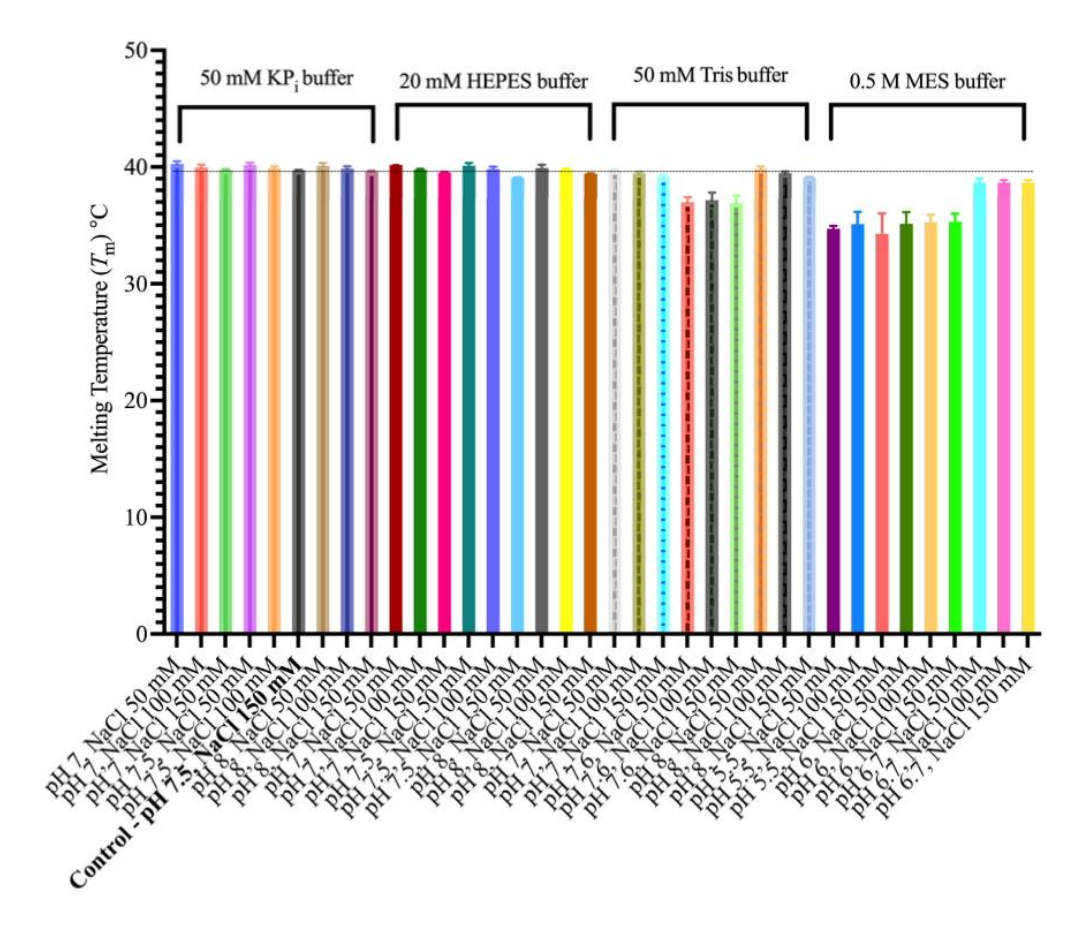


Figure S6. The melting temperature ( $T_{\rm m}$ ) of the targeted proteins with constant GloMelt and ROX dye at x1 and 0.5  $\mu$ M and different concentrations of proteins. The highest concentration is 10  $\mu$ L of each protein stock from purification in the final volume of 20  $\mu$ L, and the lowest concentration is approximately a quarter of the high value.

#### S. pneumoniae ECF-PanT buffer screening

For buffer screening (Figure S7), four different buffers were chosen: 50 mM KP<sub>i</sub>, 0.5 M MES, 20 mM HEPES, and 50 mM Tris buffer. For each buffer, three different pH values, and for each pH, three different salt concentrations were selected. In addition, 0.05% DDM was added to each buffer. The optimal protein concentration of 0.5 mg/mL was used for this step. The ROX and GloMelt dye concentrations were 0.5  $\mu$ M and 1x, respectively. The total volume was set to 20  $\mu$ L with a similar setup as explained above

As a negative control, no protein was added which shows no melting temperature and wasn't included in the graphs. The positive control was the size exclusion chromatography (SEC) purification buffer *e.g.*, 50 mM KP<sub>i</sub> buffer, pH 7.5 with 150 mM NaCl, and 0.05 % DDM which also is used for storage and most of the experiments and is shown in bold format.



**Figure S7.** Buffer screening for *S. pneumoniae* ECF-PanT, using four different buffers with three different pH and salt concentrations for each. The control is 50 mM KP<sub>i</sub> buffer, pH 7.5 with 150 mM NaCl and 0.05 % DDM.

Among all the conditions tested (Figure S7), potassium phosphate (KPi), as well as HEPES buffers show approximately the same melting temperature (i.e., Tm of 39.7 °C) as the control buffer e.g. size exclusion chromatography (SEC) buffer (e.g., 50 mM KPi buffer, pH 7.5 with 150 mM NaCl, and 0.05 % DDM). Tris buffer with a pH value of 7.6 and MES buffer at all tested pH values (especially pH 5.5 and 6), showed lower melting temperatures for ECF-PanT (i.e., average Tm of 35.4 °C). Based on these results, it was determined that KP<sub>i</sub> and HEPES buffers generally exhibited higher melting temperatures compared to the control buffer used for SEC purification and storage.

#### Protein thermal stability: 6-Day study

Based on this observation, we proceeded to investigate the stability of all three proteins over a period of 6 days, with the proteins incubated in the selected buffer. For the ECF-PanT protein, we selected the optimal buffer based on the results obtained from the buffer screening process, which exhibited a higher melting temperature (Tm). This buffer was denoted as the "optimal buffer" and comprised, for instance, 50 mM KP<sub>i</sub> at pH 7.5, 50 mM NaCl, and 0.05% DDM. Conversely, the ECF-module and ECF-FolT2 proteins were incubated in the buffer employed during the size exclusion chromatography (SEC) purification, namely 50 mM KP<sub>i</sub> buffer at pH 7.5, with 150 mM NaCl and 0.05% DDM. *T<sub>m</sub>* for each condition was monitored every day. One condition is incubating the protein with 5 % DMSO and the other one is 0 % DMSO. The percentage of DMSO in the wells during the TSA will be set to 2.5 %. The final ROX and GloMelt concentrations were set to 0.5 μM and 1x, respectively. Figure S8 depicts the corresponding curves for the ECF-PanT protein, illustrating the first derivative of fluorescence emission as a function of temperature. The first derivative of fluorescence emission provides valuable insights into the thermal stability characteristics of the proteins under investigation. (Huynh & Partch, 2015)

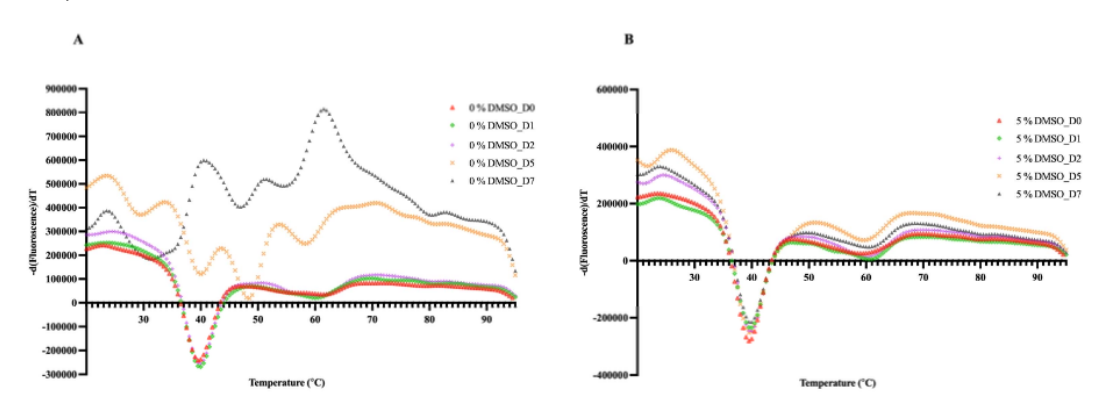


Figure S8. Corresponding ECF-PanT protein curves with A) 0% and B) 5% of DMSO.

In Figure S8-A, it can be observed that ECF-PanT, when incubated in the optimal buffer without DMSO (0% DMSO), remains stable for 3 days. However, beyond this period, the protein exhibits multiple melting temperatures, suggesting a loss of stability. Although a peak with approximately  $T_m$  of 39.66 °C is visible, it cannot be definitively concluded that the protein remains stable under these conditions. On the other hand, Figure S8-B illustrates the stability of ECF-PanT in the respective buffer containing 5% DMSO. In this case, the protein remains stable throughout the incubation period, indicating that the presence of 5% DMSO helps to maintain its stability. The small variation between the starting intensities could be due to an error in pipetting which could cause a difference in concentration. In Figures S9 and S10, the corresponding curves for ECF-module and ECF-FolT2 are presented, respectively. These curves provide insights into the stability profiles of these proteins under the specified experimental conditions.

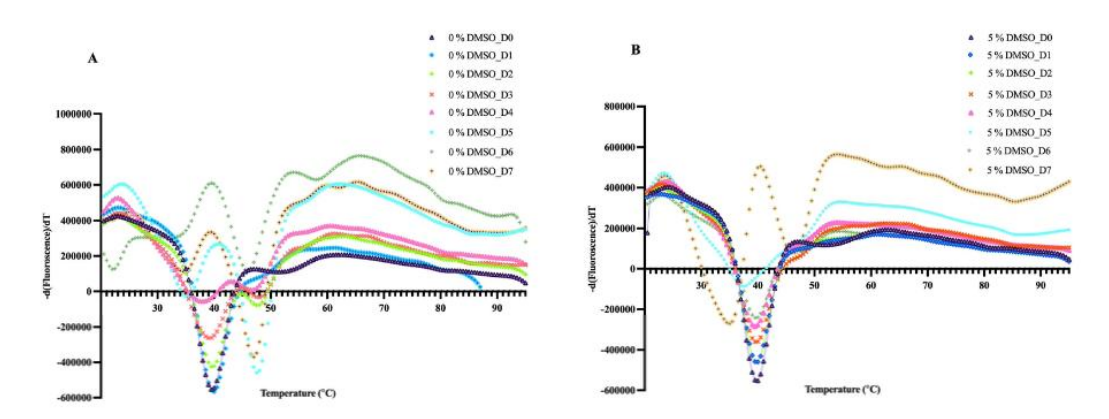


Figure S9. Corresponding ECF-module protein curves with A) 0% and B) 5% of DMSO.

In Figure S9-A, it is evident that the ECF-module with approx.  $T_m$  of 39.45 °C, when incubated in the buffer without DMSO (0% DMSO), remains stable for 3 days. This indicates that the protein maintains structural integrity and stability during this timeframe. On the other hand, in Figure S9-B, when the ECF-module is incubated in the buffer containing 5% DMSO, it exhibits stability for an extended period of 3-4 days.

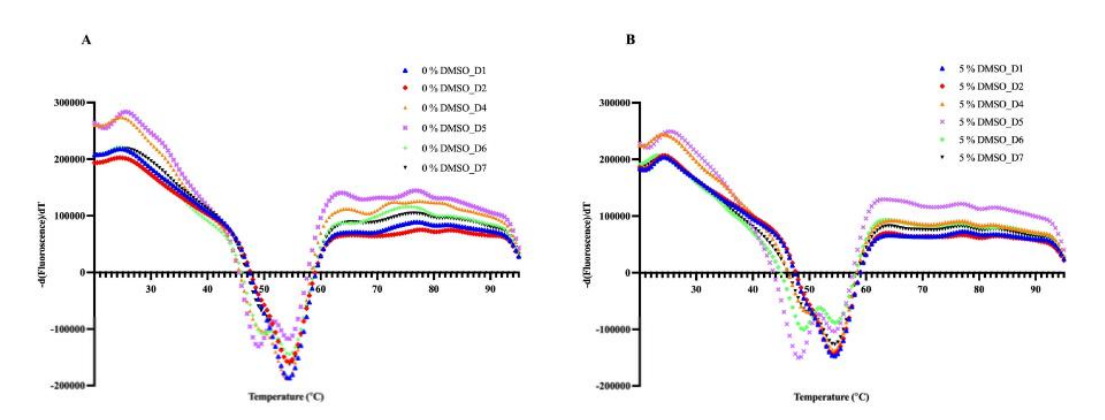
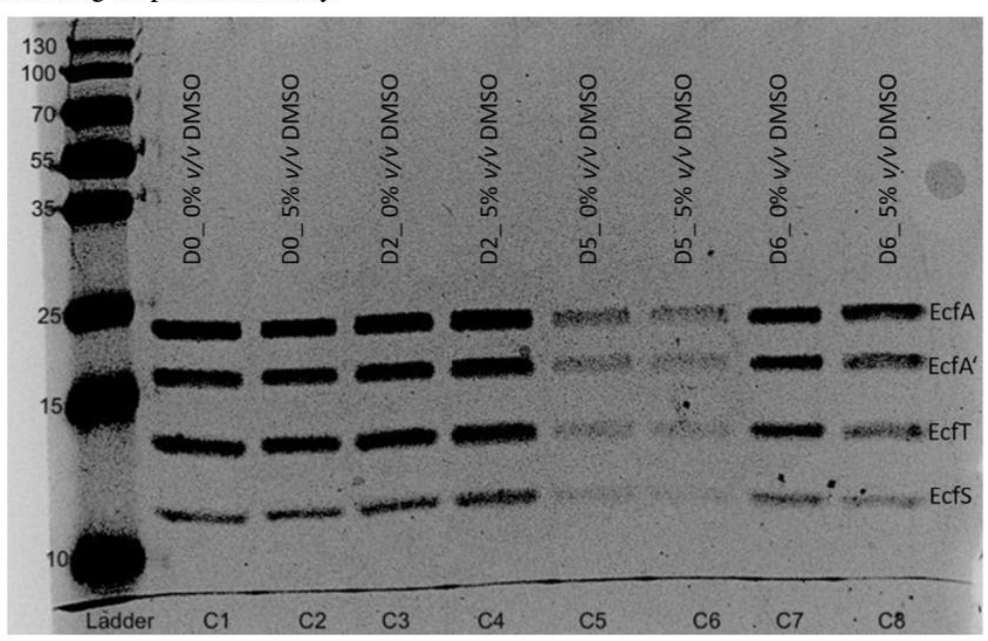


Figure S10. Corresponding ECF-FolT2 protein curves with A) 0% and B) 5% of DMSO.

Figure S9 shows that ECF-FolT2 is stable for 4 days with  $T_m$  of approx. 54.57 °C, and after that, the curve shape and the fluorescence intensity start to change in both 0% and 5% of DMSO. The comparison between the two figures highlights the influence of DMSO on the stability of the ECF proteins, with the addition of 5% DMSO providing an advantage in terms of prolonging the protein's stability.

#### Evaluation of stability data resulted from TSA

To evaluate the stability of ECF-PanT, we incubated the protein at room temperature in the optimal buffer (50 mM KPi pH 7.5, 50 mM NaCl, 0.05% DDM) under two conditions: with and without 5% DMSO. The stability was monitored by analyzing UV absorption at 280 nm using Size Exclusion Chromatography (SEC) to ensure consistent absorbance (see Figure 2B). Technical duplicates were used to confirm the reliability of the results. Following SEC, fractions were further analyzed by Sodium Dodecyl Sulfate-Polyacrylamide Gel Electrophoresis (SDS-PAGE) to verify the presence and integrity of the protein bands. The results are shown in Figure S11, confirming the expected bands and demonstrating the protein's stability.



**Figure S11. SEC Fractions on SDS-PAGE (12% Gel).** Each condition indicated by **C** can be described respectively as **C1**) Day 0 (D0) without DMSO (0%). **C2**) Day 0 (D0) with 5% DMSO. **C3**) Day 2 (D2) without DMSO (0%). **C4**) Day 2 (D2) with 5% DMSO. **C5**) Day 5 (D5) without DMSO (0%). **C6**) Day 5 (D5) with 5% DMSO. **C7**) Day 6 (D6) without DMSO (0%). **C8**) Day 6 (D6) with 5% DMSO.

As depicted in **Figure S11**, all four bands corresponding to the protein of interest were observed throughout the experimental period. However, it is noteworthy that on day 5, the protein volume injection was lower compared to the other days. The presence of all four bands confirms the persistence of the protein fragments.

#### Protein-ligand interaction study using TSA

The experimental setup, including run parameters, total volume, protein and dye concentrations, as well as the selection of the optimal buffer, remained consistent with previous procedures. All the compounds were diluted in 100% DMSO and for each compound, a specific range of concentration was chosen. The volumes for each component were 10  $\mu$ L of protein, 2.5  $\mu$ L of ROX, 2  $\mu$ L of GloMelt, 1 $\mu$ L of the compound in 100% DMSO (or 100% DMSO only as control), and 4.5  $\mu$ L of the buffer.

#### Surface plasmon resonance (SPR)

The SPR binding studies were performed using a Reichert 4SPR surface plasmon resonance spectrometer (Reichert Technologies, Buffalo, NY, USA), and medium-density NTA derivatized polycarboxylate hydrogel NiHC200M sensor chips (XanTec Bioanalytics, Düsseldorf, Germany). The experimental procedure involved two rounds of nickel activation and one immobilization step at a concentration of 200 nM. The proteins ECF-module (92,56146 kDa), ECF-PanT (113,8745 kDa), and ECF-FolT2 (112,16316 kDa) were immobilized in flow cells 1, 2, and 3, respectively according to the standard protocol as provided by Xantec bioanalytics with a slight modification based on the recombinant proteins. The flow-cell 4 was left blank to serve as a reference.

The immobilization buffer employed for the immobilization process consisted of 10 mM HEPES with a pH of 7.5, 50 mM NaCl, 50  $\mu$ M EDTA, and 0.05% DDM without DMSO. Following the immobilization step, for the binding study of the compounds, the running buffer was exchanged for the mentioned buffer with 5%  $\nu/\nu$  DMSO. This was done to ensure consistency in the percentage of DMSO present in the solutions containing the respective testing inhibitors, as these inhibitors were soluble in the DMSO solvent. By maintaining the same DMSO concentration, we aimed to minimize any potential solvent-related effects on the assay results. All running buffers were filtered and degassed before use.

The system was initially primed with 5 mM NiCl<sub>2</sub> with an association and dissociation time of 2 min for each to activate the NTA sensor chip. Then, the recombinant proteins with a concentration of 200 nM were injected at a flow rate of 10  $\mu$ L/min for 8 min. Finally, the baseline check with the running buffer showed a stable immobilization level of approximately 9.000 RU, 14.000 RU, and 6.000 RU for the ECF-module, ECF-PanT, and ECF-FolT2, respectively.

First, the calibration curve for correction of the DMSO effect was prepared; the concentrations were 3%, 3.5% 4%, 4.5%, 5%, 5.5%, 6%, 6.5%, and 7% v/v and were diluted with SPR buffer. Then, the concentration of compounds started from 800  $\mu$ M to 1.56  $\mu$ M with a dilution factor of 2. The concentration of DMSO in all the samples was set to 5% v/v DMSO. The samples (200  $\mu$ L) were loaded on a 96-well plate and were injected at a flow rate of 50  $\mu$ L/min. Single-cycle kinetics were applied for  $K_D$  determination. The association time was set to 60 s, and the dissociation phase was recorded for 120 s. For surface regeneration, 0.35 M EDTA (pH 8.5) and 0.1 M NaOH were used. Data processing and analysis were performed by Scrubber software (Version 2.0c, 2008, BioLogic Software). Sensorgrams were calculated by sequential subtractions of the corresponding curves obtained from the reference flow cell and the running buffer (blank). SPR responses were expressed in the resonance unit (RU). The  $K_D$  values were calculated by global fitting of the kinetic curves as well as fitting of the steady state binding responses to a 1:1 Langmuir interaction model. The calculated values are in the same range.

The SPR experiments were conducted at least two times, representing independent replicates. The response-time and response-concentration curves for each compound, illustrating the binding interactions, are presented in Figure S12 for ECF-PanT, Figure S13 for ECF-FolT2, and Figure S14 for ECF-module. These curves provide insights into the kinetics and concentration-dependent responses of compounds **1–6** when interacting with the immobilized proteins.

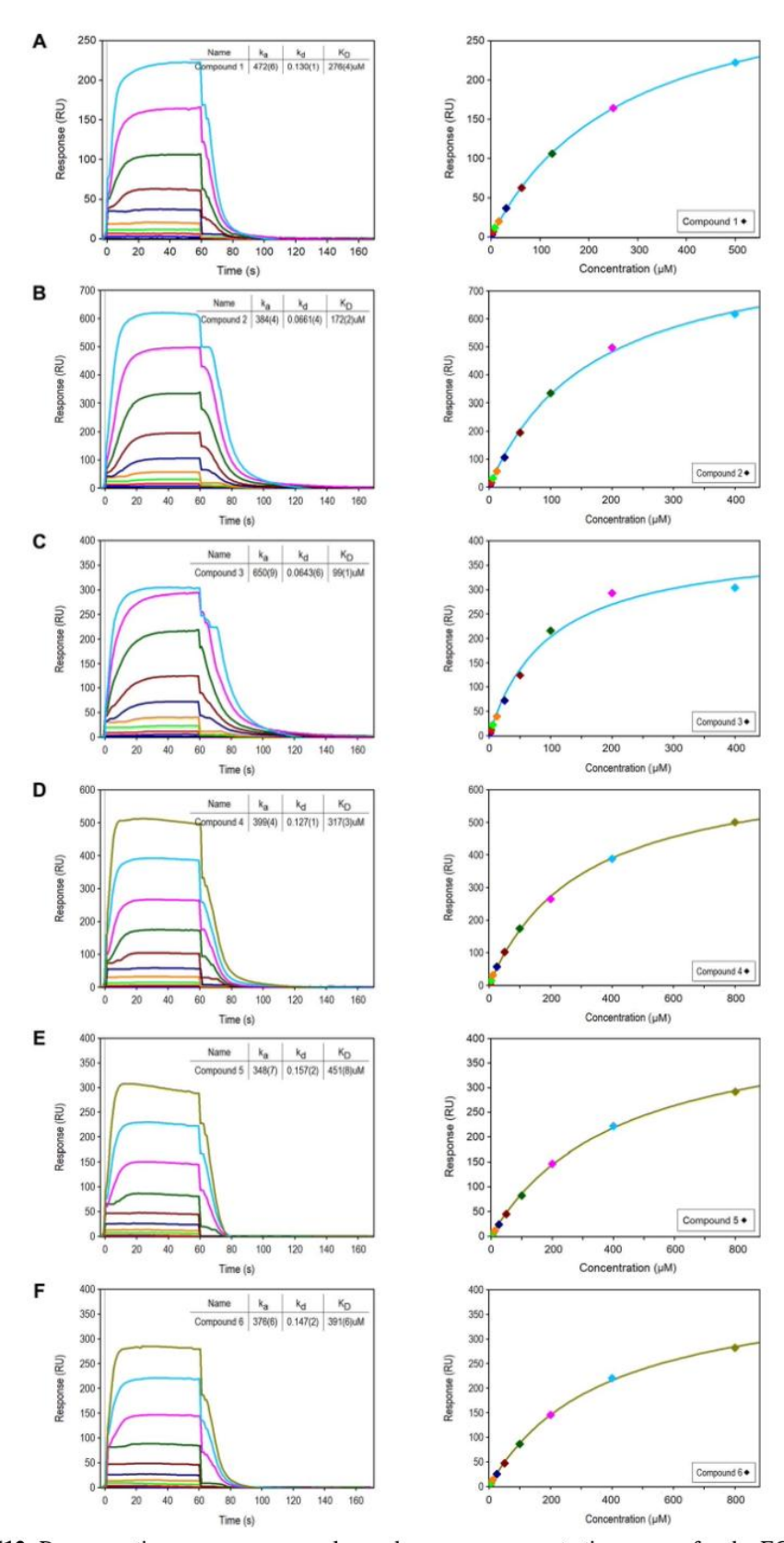


**Figure S12.** Response–time sensorgram overlay and response–concentration curves for the ECF-PanT protein upon injection of compounds 1–6, denoted as A to F, respectively. Each compound is associated with a unique curve, elucidating the temporal evolution of the ECF-PanT protein's response as well as its response at different compound concentrations.

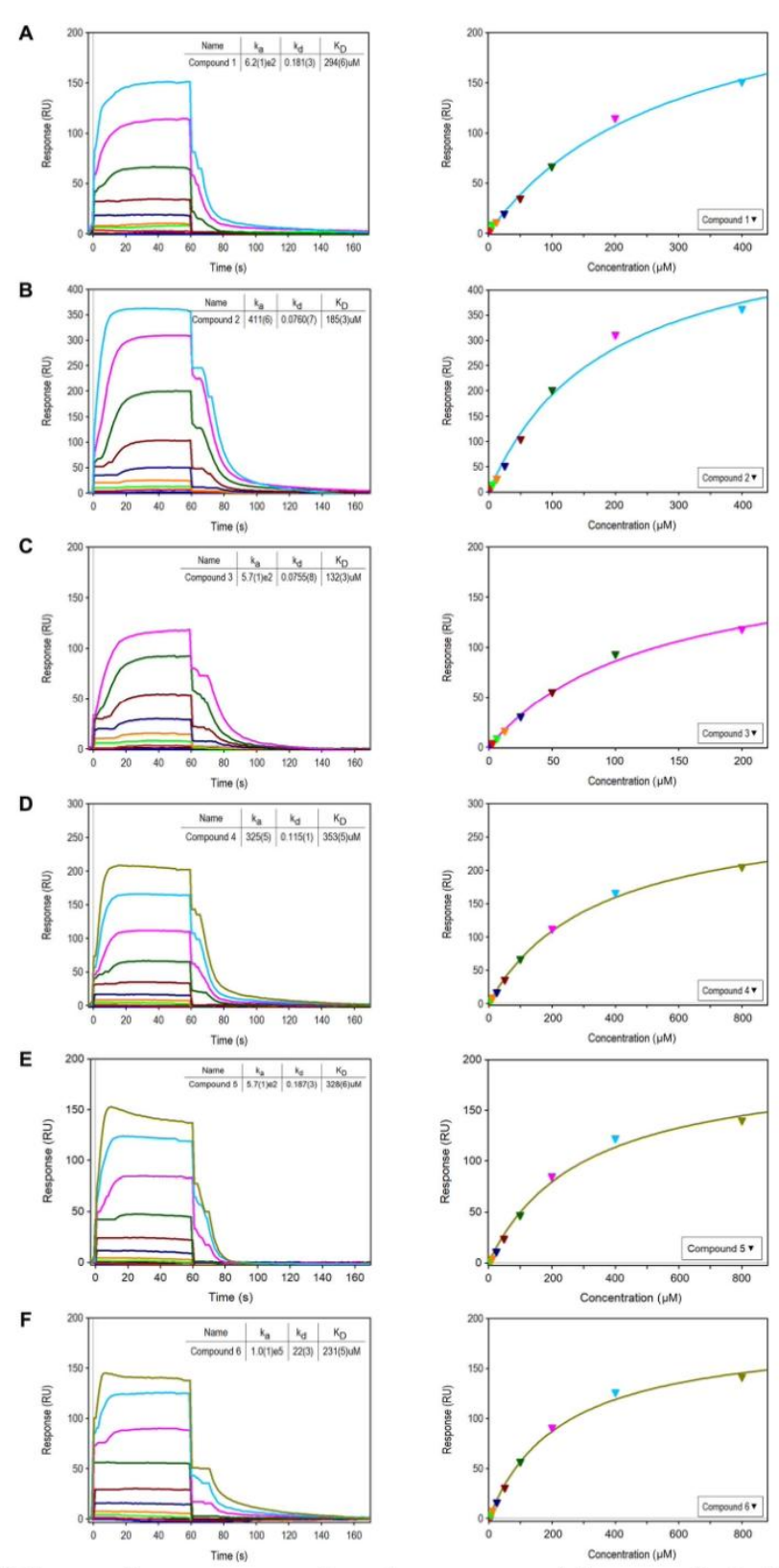


**Figure S13.** Response–time sensorgram overlay and response–concentration curves for the ECF-FoIT2 protein upon injection of compounds 1–6, denoted as A to F, respectively. Each compound is associated with a unique curve, elucidating the temporal evolution of the ECF-FoIT2 protein's response as well as its response at different compound concentrations.

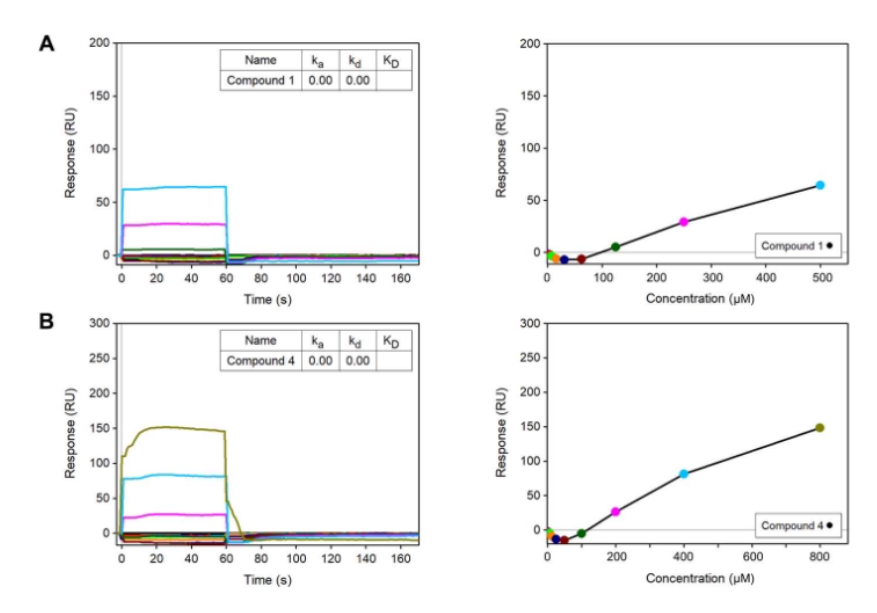


Figure S14. Response—time sensorgram overlay and response—concentration curves for the ECF-module upon injection of compounds 1 and 4 as representative of the two classes, denoted as A and B, respectively.

#### In vitro cytotoxicity evaluation

As previously noted, this assay was conducted following the methodology of Haupenthal et al., 2007, with minor modifications, which will be detailed below.

To obtain information regarding the toxicity of our compounds, their impact on the viability of human cells was investigated. HepG2 and A549 cells ( $2 \times 10^4$  cells per well) were seeded in 96-well, flatbottomed culture plates in 100 µL culture medium (DMEM containing 10% fetal calve serum, 1% penicillin-streptomycin). Twenty-four hours after seeding the cells, medium was removed and replaced by medium containing test compounds in a final DMSO concentration of 1%. Compounds were tested in duplicates at a single concentration in 1% DMSO/medium. Epirubicin and doxorubicin were used as positive controls in serial dilutions starting from 10 µM, and rifampicin was used as a negative control (at 100 µM). The living cell mass was determined 48 h after treatment with compounds by adding 0.1 volumes of 3-(4,5-dimethylthiazol-2-yl)-2,5-diphenyltetrazolium bromide (MTT) solution (5 mg/mL sterile PBS) (Sigma, St. Louis, MO) to the wells. After incubating the cells for 30 min at 37 °C (atmosphere containing 5% CO<sub>2</sub>), medium was removed and MTT crystals were dissolved in 75 µL of a solution containing 10% SDS and 0.5% acetic acid in DMSO. The optical density (OD) of the samples was determined photometrically at 570 nm in a PHERAstar Omega plate reader (BMG labtech, Ortenberg, Germany). To obtain percent viability for each sample, their ODs were related to those of DMSO controls. At least two independent measurements were performed for each compound. The calculation of IC50 was performed using the nonlinear regression function of GraphPad Prism 10 (GraphPad Software, San Diego, CA, USA).

#### References

- Altschul SF, Madden TL, Schäffer AA, Zhang J, Zhang Z, Miller W, Lipman DJ (1997) Gapped BLAST and PSI-BLAST: a new generation of protein database search programs. Nucleic Acids Research, 25:3389–3402.
- Altschul SF, Wootton JC, Gertz EM, Agarwala R, Morgulis A, Schäffer AA, Yu YK (2005) Protein database searches using compositionally adjusted substitution matrices. FEBS J 272:5101–5109.
- Di Tommaso, P., Moretti, S., Xenarios, I., Orobitg, M., Montanyola, A., Chang, J. M., Notredame, C. (2011). T-Coffee: A web server for the multiple sequence alignment of protein and RNA sequences using structural information and homology extension. Nucleic Acids Research, 39(SUPPL. 2).
- Haupenthal J, Baehr C, Zeuzem S, Piiper A (2007) RNAse A-like enzymes in serum inhibit the antineoplastic activity of siRNA targeting polo-like kinase 1. Int. J. Cancer 121: 206–210.
- Huynh, K., & Partch, C. L. (2015). Analysis of Protein Stability and Ligand Interactions by Thermal Shift Assay. (February), 1–14. doi: 10.1002/0471140864.ps2809s79
- Notredame, C., Higgins, D. G., & Heringa, J. (2000). T-coffee: A novel method for fast and accurate multiple sequence alignment. Journal of Molecular Biology, 302(1), 205–217.
- Robert, X, Gouet, P (2014) Deciphering key features in protein structures with the new ENDscript server. Nucleic Acids Research, 42:W320–W324. doi:10.1093/nar/gku316
- Setyawati I, Stanek WK, Majsnerowska M, Swier LJYM, Pardon E, Steyaert J, Guskov A, Slotboom DJ (2020) In vitro reconstitution of dynamically interacting integral membrane subunits of energy-coupling factor transporters. Elife. 22;9:e64389. doi: 10.7554/eLife.64389.
- Swier, L. J. Y. M., Guskov, A., & Slotboom, D. J. (2016). Structural insight in the toppling mechanism of an energy-coupling factor transporter. Nature Communications, 7.
- Zhang M, Bao Z, Zhao Q, Guo H, Xu K, Wang C, Zhang P (2014) Structure of a pantothenate transporter and implications for ECF module sharing and energy coupling of group II ECF transporters. Proc Natl Acad Sci U S A 111:18560–18565.

## 3.2 Chapter B: Hit optimization by dynamic combinatorial chemistry on *Streptococcus* pneumoniae energy-coupling factor transporter ECF-PanT <sup>51</sup>

Exapicheidou I. A.  $\perp$ ; Shams A.  $\perp$ ; Ibrahim H.; Tsarenko A.; Backenköhler M.; Hamed M.; Diamanti E.; Volkamer A.; Slotboom Dirk J.; Hirsch Anna K. H: Hit optimization by dynamic combinatorial chemistry on *Streptococcus pneumoniae* energy-coupling factor transporter ECF-PanT. *Chem. Commun* **2024**. DOI: 10.1039/D3CC04738E

<sup>⊥</sup> these authors contributed equally

# Hit optimization by dynamic combinatorial chemistry on *Streptococcus pneumoniae* energy-coupling factor transporter ECF-PanT

I. A. Exapicheidou, A. Shams, H. Ibrahim, A. Tsarenko, M. Backenköhler, M. M. Hamed, E. Diamanti, A. Volkamer, D. J. Slotboom and A. K. H. Hirsch, *Chem. Commun.*, 2024, **60**, 870 **DOI:** 10.1039/D3CC04738E

To request permission to reproduce material from this article, please go to the <u>Copyright Clearance Center request page</u>.

If you are an author contributing to an RSC publication, you do not need to request permission provided correct acknowledgement is given.

If you are the author of this article, you do not need to request permission to reproduce figures and diagrams provided correct acknowledgement is given. If you want to reproduce the whole article in a third-party publication (excluding your thesis/dissertation for which permission is not required) please go to the <u>Copyright Clearance Center request page</u>.

Read more about <u>how to correctly acknowledge RSC</u> <u>content</u>.

## ROYAL SOCIETY OF **CHEMISTRY**

#### ChemComm

#### COMMUNICATION

View Article Online
View Journal | View Issue



Cite this: Chem. Commun., 2024,

Received 23rd September 2023, Accepted 11th December 2023

DOI: 10.1039/d3cc04738e

rsc.li/chemcomm

### Hit optimization by dynamic combinatorial chemistry on Streptococcus pneumoniae energycoupling factor transporter ECF-PanT†

Ioulia Antonia Exapicheidou, (1) ‡ab Atanaz Shams, (1) ‡ab Hamza Ibrahim, c Aleksei Tsarenko, d Michael Backenköhler, d Mostafa M. Hamed, 📭 a Eleonora Diamanti,<sup>a</sup> Andrea Volkamer, oac Dirk J. Slotboom<sup>d</sup> and Anna K. H. Hirsch P\*ab

Herein, we present the first application of target-directed dynamic combinatorial chemistry (tdDCC) to the whole complex of the highly dynamic transmembrane, energy-coupling factor (ECF) transporter ECF-PanT in Streptococcus pneumoniae. In addition, we successfully employed the tdDCC technique as a hitidentification and -optimization strategy that led to the identification of optimized ECF inhibitors with improved activity. We characterized the best compounds regarding cytotoxicity and performed computational modeling studies on the crystal structure of ECF-PanT to rationalize their binding mode. Notably, docking studies showed that the acylhydrazone linker is able to maintain the crucial interactions.

Energy-coupling factor (ECF) transporters are underexplored transmembrane proteins involved in the uptake of vitamins in a wide range of bacteria, predominantly in Gram-positive species such as Streptococcus pneumoniae, Enterococcus faecium and faecalis.1 They are essential for bacterial survival and absent in humans, making them attractive drug targets. They comprise a substrate-specific binding protein termed the S-component and an energizing module (ECF module) that consists of a membrane-embedded scaffold protein (ECFT) and two cytosolic nucleotide binding domains (ECFA) and (ECFA'). ECF transporters are divided into two groups. We focus on group II, where a single inhibitor can block the uptake of multiple vitamins at once given that multiple S-components compete for the same ECF module (Fig. 1).2,3

These intriguing transporters are proposed to use a highly dynamic bilayer-mediated toppling mechanism for the transport of the substrates from the external environment to the cytosol. Molecular dynamics (MD) simulations and cryo-EM spectroscopy revealed that the protein-induced membrane deformations enable the toppling of the S-component across the membrane and its interaction with the ECF module. 4,5 This unique architecture and mechanism of action make the ECF transporters fascinating and challenging targets. Over the past decade, several structural and functional studies have unravelled their mechanism of transport. In 2016, we solved the crystal structure of Lactobacillus delbrueckii ECF-FolT2.5,6 Later, we determined the crystal structure of ECF-PanT in L. delbrueckii by generating antibodies, which were used as a crystallization chaperone.7 In addition, the crystal structure of the ECF-PanT from L. brevis was determined in 2014 by M. Zhang et al.8 Recently, our group managed to express and purify S. pneumoniae ECF-PanT,9 but unfortunately, structural information on this protein is still lacking.

Herein, we aimed to expand the currently limited repertoire of ECF inhibitors and to investigate the applicability of the

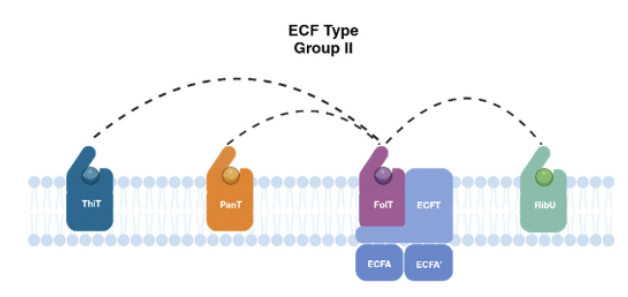


Fig. 1 Architecture of group II ECF transporters. All S-components (shown in different colors) interact with a shared ECF module (ECFAAT) shown in blue, thereby mediating the uptake of multiple vitamins.

<sup>&</sup>lt;sup>a</sup> Helmholtz Institute for Pharmaceutical Research Saarland (HIPS) - Helmholtz Centre for Infection Research (HZI), 66123, Saarbrücken, Germany, E-mail: anna.hirsch@helmholtz-hips.de

<sup>&</sup>lt;sup>b</sup> Saarland University, Department of Pharmacy, Campus Building E8.1, 66123, Saarbrücken, Germany

<sup>&</sup>lt;sup>c</sup> Data Driven Drug Design Group, Center for Bioinformatics, Saarland Informatics Campus E2.1, Saarland University, Saarbrücken 66123, Germany

<sup>&</sup>lt;sup>d</sup> Groningen Biomolecular Sciences and Biotechnology Institute, University of Groningen, Nijenborgh 4, 9747, AG, Groningen, The Netherlands

<sup>†</sup> Electronic supplementary information (ESI) available. See DOI: https://doi.org/ 10.1039/d3cc04738e

<sup>±</sup> The authors contributed equally.

View Article Online

Communication ChemComm

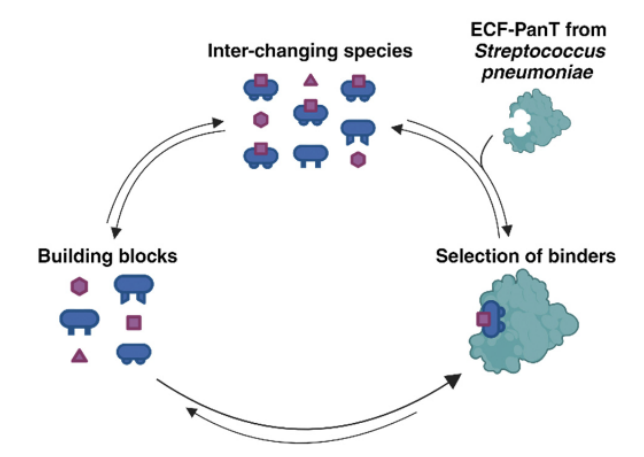


Fig. 2 Application of target-directed dynamic combinatorial chemistry (tdDCC) approach to ECF-PanT from S. pneumoniae.

dynamic combinatorial chemistry (DCC) approach to the full complex of a highly dynamic, transmembrane protein from S. pneumoniae (Fig. 2). Previously, our group reported the applicability of DCC solely on the S-component from a nonpathogenic organism L. lactis, while here we managed to extend the applicability of DCC to the entire transmembrane protein.

DCC is a powerful tool that generates compound libraries under reversible conditions.10 The combination of all building blocks through covalent or noncovalent interactions leads to the formation of a mixture of interchanging products under thermodynamic control. Upon addition of the target, the library composition alters as the members that have higher affinity for the target are selected and stabilized at the expense of the nonrecognized species. Hence, this efficient technique allows the target to select its own binders and circumvents the need for synthesis and evaluation of all individual compounds.11

Among the reported reversible reactions, the acylhydrazone formation became appealing for DCC in medicinal chemistry, 12 as aldehyde and hydrazide building blocks are commercially available. In addition, the acylhydrazone is a relatively stable amide-type linkage and also offers hydrogen-bond donor and -acceptor sites. The aldehyde-hydrazide ratio ensures the pseudo first-order behavior of the reaction and allows the fast formation of all possible products. 13,14 Under acidic conditions, the equilibrium is reached rapidly, while this process is slower at neutral pH. The addition of a nucleophilic catalyst such as aniline leads to fast equilibration and fully reversible dynamic combinatorial libraries (DCLs), allowing the freezing of the reaction.14

To date, only a few applications of the DCC approach to transmembrane proteins have been reported. In 2017, our group used DCC as a fragment-growing method to identify ligands of ThiT, the S-component of the ECF transporter for thiamine in L. lactis. 15 Herein, we apply DCC for the first time to the entire complex of ECF-PanT from the pathogen S. pneumoniae. According to the WHO, S. pneumoniae is a medium-priority pathogen with an increasing number of antibiotic-resistant strains. Furthermore, it is a suitable target

for the study of ECF transporters as it lacks the endogenous pathway for the biosynthesis of pantothenate and folic acid and depends entirely on their uptake from the environment.1

For this study, we chose a DCL that relies on the reversible acylhydrazone formation, while ECF-PanT from S. pneumoniae was selected as the target protein. The template effect of ECF-PanT in the DCL was determined by comparing the blank library (without protein) with the templated one (in presence of the protein) by high-resolution mass spectrometry (HR-MS). At the outset, as we are applying this technique for the first time to the whole transporter, we had to optimize the experimental conditions (temperature, pH, buffer influence) as well as the protein stability in the presence of the DCL. To do so, we took advantage of our group's recent data,9 where we report the determination of the protein stability at different pHs and buffers over time using the thermal shift assay (TSA).9 Among all the screened conditions, we selected the KP<sub>i</sub> buffer (pH 7.5) ensuring the stability of ECF-PanT over six days.

Having established the optimal conditions for the stability of our protein, we proceeded with the design of three tdDCC experiments as initially planned. The first tdDCC (tdDCC-1) served as a pilot to establish the essential conditions and confirm the applicability of tdDCC to ECF-PanT, by choosing an "unbiased" library of commercially available in-house building blocks (see details in ESI†). Then, we followed a standard DCC workflow: (i) identification of when the blank library reaches equilibrium; (ii) determination of the relative peak areas (RPAs); (iii) analysis of the samples via HR-MS.

Subsequently, we used tdDCC as a hit optimization method to further advance our research endeavors. To the best of our knowledge, the only ECF inhibitors described to date emerged from a structure-based virtual screening (SBVS) approach. 16-18 Hence, we decided to design a DCL bearing key motifs of the two already-known series of ECF inhibitors namely 1 and 217,18 with the aim to further optimize their in vitro and whole-cell activities. Therefore, we designed a library containing two aldehydes that resemble 1 and 2 (Scheme 1A). Aldehyde A4 retained the salicylic acid moiety, which is known to be essential for the activity from a previous structure-activity relationship (SAR) study.<sup>17</sup> Thus, we decided to explore it further. Accordingly, aldehyde A5 was based on 2 for which an SAR study revealed that the "Western moiety" is the optimum growth vector.18 After our rational choice of the two aldehydes (A4, A5), we selected seven diverse hydrazides (H9-H15), encompassing both aliphatic and aromatic variations, as well as a range of molecular sizes to explore a broad chemical space and capture a wide spectrum of potential interactions. This ECF-focused DCC experiment was called in this study tdDCC-2. Under the conditions already described, aldehydes and hydrazides were mixed in phosphate buffer (pH 7.5) with an excess of aniline and 5% DMSO. Having reached the equilibrium, we determined the composition of the blank library. After 28 hours, the RPAs of the products did not show any significant changes, indicating the end of the experiment. By comparing the chromatogram of the blank library to the two protein-templated ones, we observed the amplification of A5H9

View Article Online

ChemComm Communication

Scheme 1 (A) Design of target-directed dynamic combinatorial chemistry i.e. tdDCC-2 and 3 experiments based on the initial hits 1 and 2. (B) Structures of the amplified compounds 4, 5 and 6 that showed inhibition against ECF transporter.

(5) and A5H10 (4) only in the mixture containing ECF-PanT and proceeded with their synthesis (Fig. S2, ESI†).

Next, we decided to further expand our set of compounds and designed a third tdDCC experiment referred to as tdDCC-3 with a primary objective of hit identification and optimization. In this context, we selected a more diverse library of aldehydes, including those with larger substituents such as A7 and A8, as well as A6 (Fig. 2 and Fig. S3, ESI†), which features an amide bond in place of the carboxylic acid found in compound 1. Additionally, the hydrazides (H16-H23) chosen for this library were also bulkier in order to explore more chemical space. The experiment was performed under the same conditions as before (Fig. S3a, ESI†). Following the same workflow, this time acylhydrazones A6H19 (6), A7H15 and A7H19 were amplified and then synthesized (Fig. 2 and Fig. S3, ESI†).

Next, we synthesized acylhydrazone 3 as an analogue to 1 and used both of them as references in our study. All the compounds synthesized were tested in a whole-cell uptake assay. 18 The data reported in Table 1 showed that we swiftly improved the activity of our parent compounds. Despite 1 showing an IC<sub>50</sub> value of 315  $\pm$ 15 μM, compound 3 was comparably active. In fact, there is a three-fold improvement of activity of our tdDCC-3 binder A6H19 (6), compared to 1. We were pleased to see that 6 showed an IC<sub>50</sub> value of 99.5  $\pm$  0.7  $\mu$ M. In addition, the tdDCC-2 binders **A5H10** (4), and A5H9 (5), exhibited IC<sub>50</sub> values of 152.8  $\pm$  43  $\mu$ M and 56  $\pm$ 6.3 µM, respectively. These values represent several-fold improved potencies compared to 2, which showed less than 10% inhibition in the same whole-cell assay.<sup>18</sup> We also evaluated the monomers within the same assay, which confirmed that the observed activity was attributed to the acylhydrazone products. Additionally, we assessed the most promising compounds in a proteoliposome uptake assay with ECF-PanT. To further profile our ECF

Table 1 Biological evaluation of the compounds for inhibition in the whole-cell uptake assay and in the proteoliposome uptake assay

Compound	Whole-cell up	Uptake assay into proteoliposome	
	% Inh. 200 μM	IC <sub>50</sub> μM	% Inh. @ 250 μM
1	$42.7 \pm 8.9$	$315 \pm 15$	$34 \pm 9$
2	<10	n.d.	<10
3	$11.6 \pm 1.3$	$308 \ n = 1$	$72.5 \pm 16$
A5	< 10	n.d.	n.d.
A6	<10	n.d.	n.d.
H9	< 10	n.d.	n.d.
H10	< 10	n.d.	n.d.
H19	< 10	n.d.	n.d.
4	$59.5 \pm 10.2$	$152.8\pm43$	$85.8 \pm 4$
5	$68.5 \pm 3.5$	$56 \pm 6.3$	52.2
6	$81.3\pm0.9$	$99.5\pm0.7$	$43.4\pm23$
n.d. = Data no	ot determined.		

inhibitors, we evaluated 4, 5 and 6 for their antibacterial activity and their toxic effects on three different human cell lines, namely liver cancer cells (HepG2), embryonic kidney 293 cells (HEK293) and adenocarcinoma alveolar basal epithelial cells (A549) using an MTT assay. Encouragingly, none of them showed significant toxicity against any of the cell lines used. (Table S4, ESI†).

To rationalize the binding mode of the three most active ECF inhibitors, 4, 5 and 6, computational modeling was performed (methods, ESI†). This study started from an unbiased coarse-grained (CG) molecular dynamics (MD) simulation previously performed by our group on ECF-PanT.<sup>17</sup> Importantly, another short 60 picosecond MD simulation revealed that the three selected compounds, behaved similarly to compound 1, binding more stably to the so-called P9 pocket at the interface between the S-component and the ECF module

View Article Online

Communication ChemComm

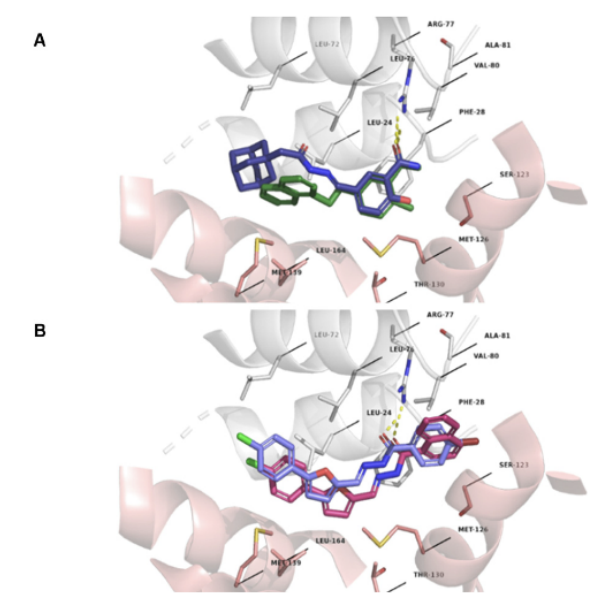


Fig. 3 Ligand poses and main interacting residues from chain C (white) and chain D (light red) within pocket P9 guided by SeeSAR. (A) Overlay of hit 1 (blue), from the unbiased CG MD simulation and the selected pose of 6 (green). (B) Overlay of compounds 4 (violet) and 5 (pink).

(Fig. S8, ESI†). Thus, this buried pocket was used for the docking experiments with SeeSAR. 19 Most of the generated docking poses interact with the S-component (chain-C) and ECF module (chain-D) primarily through hydrophobic interactions (mainly Phe28-C and Leu164-D) on both ends of the compounds. As shown before, 17 hydrogen bonds are formed with the Arg77-C residue (Fig. 3 and Fig. S9, ESI†) in 72% of all generated poses. In most poses, the salicylic acid of 6, or the acylhydrazones of 4 and 5 form a hydrogen bond with Arg77-C (Fig. S9, ESI†). We also observed a significant overlap of the common structural motifs between the selected pose pairs, i.e., the salicylic acid moieties of 1 and 6 from the CG-MD snapshot. The orientation of the common parts of 4 and 5 poses also overlap, while a shift along the longitudinal axis is observed. This variation may result from the differing space required for the bromophenyl and naphthyl rings, respectively (Fig. 3). The stability of the selected poses was further investigated in a short 60 ps MD simulation. The selected poses remained stable in the binding pocket (root mean square deviation (RMSD) = 3.18 Å) and the hydrogen-bond interactions with Arg77-C remained intact (mean distance = 2.96 Å, Fig. S10, ESI†).

In conclusion, we successfully established and applied the conditions of the DCC strategy on the full complex of ECF-PanT from S. pneumoniae, which represents a challenging target in the design of innovative anti-infectives due to its highly dynamic mechanism of transport. In addition, we confirmed the applicability of tdDCC as a hit-optimization method as we were able to enhance the potency of the already reported ECF inhibitors 1 and 2 to derivatives 4, 5 and 6. We further profiled these compounds for their cytotoxicity and found them nontoxic. We also performed docking studies to gain insights into the binding mode of these compounds, which showed that 6 is predicted to bind similarly to 1, whereas in 4 and 5 the acylhydrazone linker acts as alternative interaction site. These results further demonstrate the value of using the acylhydrazone linker in DCC for the discovery and optimization of novel ligands for challenging targets such as transmembrane proteins with dynamic pockets.

I. A. E. designed and performed the DCC experiments and synthesized the amplified products. A. S. purified ECF-PanT, performed the DCC experiments and together with A. T performed the uptake assay. I. H. and M. B. performed the docking studies and A.V. supervised the work. A. K. H. H. and I. A. E. together with E. D and M. M. H. conceived the study and A. K. H. H. supervised the research.

Work by I. A. E. and A. S. was supported by the GradUS program and Erasmus+ from Saarland University. A. V. thankfully announces funding from Saarland University for the Next AID project through which the position of M. B. is supported. A. K. H. H. gratefully acknowledges funding from the European Research Council (ERC Starting grant 757913) and from the Helmholtz Association's Initiative and Networking Fund. The authors thank J. Jung, J. Seelbach and J. Haupenthal for excellent technical support.

#### Conflicts of interest

There are no conflicts to declare.

#### Notes and references

- 1 S. Bousis, I. Setyawati, E. Diamanti, D. J. Slotboom and A. K. H. Hirsch, Adv. Ther., 2019, 2, 1800066.
- 2 S. Rempel, W. K. Stanek and D. J. Slotboom, Annu. Rev. Biochem., 2019, 88, 551-576.
- 3 T. Wang, G. Fu, X. Pan, J. Wu, X. Gong, J. Wang and Y. Shi, Nature, 2013, 497, 272-276.
- 4 I. Faustino, H. Abdizadeh, P. C. T. Souza, A. Jeucken, W. K. Stanek, A. Guskov, D. J. Slotboom and S. J. Marrink, Nat. Commun., 2020, 11, 1763.
- 5 C. Thangaratnarajah, J. Rheinberger, C. Paulino and D. J. Slotboom, Proc. Natl. Acad. Sci. U. S. A., 2021, 118, e2105014118.
- 6 L. J. Swier, A. Guskov and D. J. Slotboom, Nat. Commun., 2016, 7, 11072.
- I. Setyawati, W. K. Stanek, M. Majsnerowska, L. Swier, E. Pardon, J. Steyaert, A. Guskov and D. J. Slotboom, eLife, 2020, 9, e57322.
- 8 M. Zhang, Z. Bao, Q. Zhao, H. Guo, K. Xu, C. Wang and P. Zhang, Proc. Natl. Acad. Sci. U. S. A., 2014, 111, 18560-18565.
- 9 A. Shams et al., unpublished work.
- 10 O. Ramström and J. M. Lehn, Nat. Rev. Drug Discovery, 2022, 1, 26-36.
- A. M. Hartman, R. M. Gierse and A. K. H. Hirsch, Eur. J. Org. Chem., 2019, 3581-3590.
- 12 R. P. Jumde, M. Guardigni, R. M. Gierse, A. Alhayek, D. Zhu, Z. Hamid, S. Johannsen, W. A. M. Elgaher, P. J. Neusens, C. Nehls, J. Haupenthal, N. Reiling and A. K. H. Hirsch, *Chem.* Sci., 2021, 12, 7775-7785.
- 13 M. Mondal and A. K. Hirsch, Chem. Soc. Rev., 2015, 44, 2455-2488.
- 14 V. T. Bhat, A. M. Caniard, T. Luksch, R. Brenk, D. J. Campopiano and M. F. Greaney, Nat. Chem., 2010, 2, 490-497.
- 15 L. Monjas, L. Swier, I. Setyawati, D. J. Slotboom and A. K. H. Hirsch, ChemMedChem, 2017, 12, 1693-1696.
- 16 A. F. Kiefer, S. Bousis, M. M. Hamed, E. Diamanti, J. Haupenthal and A. K. H. Hirsch, J. Med. Chem., 2022, 65, 8869-8880.
- 17 E. Diamanti, P. C. T. Souza, I. Setyawati, S. Bousis, L. M. Gómez, L. J. Y. M. Swier, A. Shams, A. Tsarenko, W. K. Stanek, M. Jäger, S. J. Marrink, D. J. Slotboom and A. K. H. Hirsch, Commun. Biol., 2023, 6, 1182.
- 18 S. Bousis, S. Winkler, J. Haupenthal, F. Fulco, E. Diamanti and A. K. H. Hirsch, Int. J. Mol. Sci., 2022, 23, 2637.
- 19 SeeSAR (version 9.2), BioSolveIT, Sankt Augustin, Germany, 2019.

Electronic Supplementary Material (ESI) for ChemComm. This journal is © The Royal Society of Chemistry 2023

#### **Supporting Information**

#### Hit optimization by dynamic combinatorial chemistry on Streptococcus pneumoniae energy-coupling factor transporter ECF-PanT

Ioulia Antonia Exapicheidou, ‡a,b Atanaz Shams, ‡a,b Hamza Ibrahim,c Aleksei Tsarenko,d Michael Backenköhler,c Mostafa Hamed, a Eleonora Diamanti, a Andrea Volkamer, a,c Dirk J. Slotboom, d Anna K. H. Hirsch\*a, b

See DOI: 10.1039/x0xx00000x

\*Corresponding author Prof. A. K. H. Hirsch e-mail: anna.hirsch@helmholtz-hips.de

e Helmholtz Institute for Pharmaceutical Research Saarland (HIPS) – Helmholtz Centre for Infection Research (HZI), 66123, Saarbrücken, Germany.

b. Saarland University, Department of Pharmacy, Campus Building E8.1, 66123, Saarbrücken, Germany.

<sup>&</sup>lt;sup>c</sup> Data Driven Drug Design Group, Center for Bioinformatics, Saarland Informatics Campus E2.1, Saarland University, 66123 Saarbrücken, Germany <sup>d</sup> Groningen Biomolecular Sciences and Biotechnology Institute, University of Groningen, Nijenborgh 4, 9747, AG, Groningen, The Netherlands.

<sup>†</sup>Electronic Supplementary Information (ESI) available.

Table of Contents	
General information	3
Chemicals	3
General procedure for DCC experiments	3
DCL preparation (GP-1)	3
Protein-templated DCL preparation (GP-2	3
General procedure for acylhydrazone formation (GP-3):	4
DCC-experiments	4
DCC-1:	4
DCC-2:	4
DCC-3:	5
Characterization of acyl hydrazones	6
Identification of different conformers of acylhydrazone	6
Biological evaluation of synthesized compounds	
Protein homology sequence and structure identity determination	9
Computational Modelling	13

#### **General information**

All reactions using oxygen- and/or moisture-sensitive materials were carried out in dry solvents (vide infra) under a nitrogen atmosphere using oven-dried glassware. Reactions were monitored by a liquid chromatography-mass spectrometry (LC-MS) system equipped with a Dionex UltiMate 3000 pump, autosampler, column compartment, detector, and ESI quadrupole MS (MSQ Plus or ISQ EC) from Thermo Fisher Scientific, Dreieich, Germany. Purification of the final products, when necessary, was performed using preparative HPLC (Dionex UltiMate 3000 UHPLC+ focused, Thermo Scientific) on a reversed-phase column (C18 column, 5 µM, Macherey-Nagel, Germany). The solvents used for the chromatography were water (0.1% formic acid) and MeCN (0.1% formic acid). High-resolution mass (HRMS) of final products was determined by LCMS/MS using a Thermo Scientific Q Exactive Focus Orbitrap LC-MS/MS system. NMR data were collected on a Bruker Avance Neo 500 MHz (1H at 500.0 MHz; 13C at 126.0 MHz; <sup>19</sup>F NMR at 470 MHz), equipped with a Prodigy Cryo-probe. Chemical shifts are reported in parts per million (ppm) relative to residual solvent peak (DMSO-d<sub>6</sub>, <sup>1</sup>H: 2.54 ppm; <sup>13</sup>C: 39.9 ppm). Coupling constants are reported in Hertz (Hz). Multiplicity is reported with the usual abbreviations (s: singlet, br s: broad singlet, d: doublet, dd: doublet of doublets, ddd: doublet of doublet of doublets, t: triplet, dt: doublet of triplets, q: quartet, p: pentet, dp: doublet of pentets, m: multiplet). The periodic progress and analysis of DCC experiments were monitored by UPLC-MS (ThermoScientific Dionex Ultimate 3000 UHPLC System coupled to a ThermoScientific Q Exactive Focus with an electrospray ion source) using an Acquity Waters Column (BEH, C8 1.7  $\mu$ m, 2.1 × 150 mm, Waters, Germany) at a flow rate of 0.250 mL/min with detection set at 210, 254, 290, and 310 nm, and the mass spectrum recorded in a positive mode in the range of 100-700 m/z. The solvent system was 0.1% formic acid in H<sub>2</sub>O (Solvent-A) and 0.1% formic acid in MeCN (Solvent-B). The gradient program began with 5% of Solvent-B for 1 min and was then increased to 95% of Solvent-B over 17 min and held for 2 min, followed by a decrease of Solvent-B to 5% over 0.1 min, where it was held for 2 min. Compounds were purified by prep. HPLC eluting with an alternating gradient of 5−100% ACN with 0.05% FA in H₂O with 0.05% FA. All the compounds have a purity > 95% according to LC-MS.

#### Chemicals

Unless indicated otherwise, reagents and substrates were purchased from commercial sources and used as received. Solvents not required to be dry were purchased as technical-grade and used as received. All new compounds were fully characterized by <sup>1</sup>H- and <sup>13</sup>C-NMR and HRMS techniques. The purity of all the final products was determined by LC-MS and found to be >95%.

#### **General procedure for DCC experiments**

DCL preparation (GP-1):

To a 1.5 mL Eppendorf Tube® containing phosphate buffer (Phosphate buffer, pH 7.5) were added hydrazides (150  $\mu$ M each, in DMSO), aldehydes (50  $\mu$ M each, in DMSO), aniline (5 mM, in DMSO), and an additional amount of DMSO to reach a final concentration of 5% in the DCL with 500  $\mu$ L of end-volume. The DCL was allowed to gently mix on a rotating wheel (7 rpm) at room temperature and was frequently monitored via UPLC-MS. For analysis, 20  $\mu$ L of the corresponding library was mixed with 28  $\mu$ L acetonitrile and 2  $\mu$ L of NaOH (2 M), the mixture was centrifuged, and the supernatant was used for the analysis. <sup>1</sup>

#### Protein-templated DCL preparation (GP-2):

To a 1.5 mL Eppendorf Tube® containing phosphate buffer (pH 7.5) were added hydrazides (150  $\mu$ M each, in DMSO), alldehydes (50  $\mu$ M each, in DMSO), aniline (5mM, in DMSO), *Streptococcus pneumoniae* ECF-PanT (11.77 – 13.17  $\mu$ M) in phosphate buffer at pH 7.5,² and an additional amount of DMSO to reach a final concentration of 5% in the DCL with 500  $\mu$ L of end-volume. The DCL with the protein was allowed to gently mix on a rotating wheel (7 rpm) at room temperature, was frequently monitored via UPLC-MS ,and the traces were compared with the blank composition. For analysis, 20  $\mu$ L of the corresponding library were mixed with 28  $\mu$ L acetonitrile and 2  $\mu$ L of NaOH (2 M), the mixture was centrifuged and the supernatant was used for the analysis.¹ Note: The protein-templated DCL-1, -2 and -3 were run as duplicates.

#### Assessment of DCL composition

The library composition was assessed after the equilibrium of acylhydrazone formation was reached as reported in the literature. All the DCLs in this study reached an equilibrium after four to twenty eight hours. The "amplification factor" was determined with the relative peak area (RPA), which is the percent of each peak when the sum of all peak areas was set to 100%. The "normalized RPA" was used for the final assessment of amplification of the acylhydrazone products in the DCL.<sup>1, 3</sup>

amplification factor = RPA(templated) RPA(blank)

 $normalized\ change\ of\ RPA = (RPA(templated) - RPA(blank))\ RPA(blank)$ 

#### **DCC-experiments**

#### tdDCC-1 for establishing the DCC conditions using ECF-PanT for the first time:

Initially, we built our first DCL library by choosing a diverse set of commercially available aldehydes and hydrazides with the aim to find the optimal conditions for our protein and at the same time identify new hits as potential ECF inhibitors.

The composition of DCL-1 is depicted in Fig. S1A, ESI† and includes three aldehydes (A1—A3) and eight differently substituted hydrazides (H1—H8). From the results of the tdDCL-1, we observed that the products formed did not show significant changes after 28 hours (Fig. S1B, ESI†). Then, the blank library was compared to the two protein-templated ones. The analysis of this experiment showed that the ECF protein altered the equilibrium and, thus, the composition of the DCL, as acylhydrazones A1H6, A1H7, A1H5, A2H5 and A3H8 were amplified (Fig. S1, ESI†) and then synthesized for testing.

**DCL-1 (20 mol% protein):** The DCC-experiment was carried out according to GP-1 (blank) and GP-2 (protein-templated) in phosphate buffer at pH 7.5 and 5% DMSO.

Table 1: Composition of dynamic combinatorial library 1 (DCL-1) of target-directed dynamic combinatorial chemistry experiment 1 (tdDCC-1)

Entry		Blank		Protein-templated (I)		Protein-templated (II)	
,	Amount	Final conc. in DCL	Amount	Final conc. in DCL	Amount	Final conc. in DCL	
Buffer phosphate pH 7.5*	475 μL	-	222 μL	-	222 μL	-	
Aldehyde 100 mM	3 × 5 (15 μL)	(3 × 50 μM)	3 × 5 (15 uL)	(3 × 50 μM)	3 × 5° (15 μL)	(3 × 50 μM)	
Hydrazide 100 mM	8×5 (40 μL)	(8 × 150 μM)	8×5 (40 μL)	(8 × 150 μM)	8 × 5 <sup>b</sup> (40 μL)	(8 × 150 μM)	
Aniline 1M in DMSO	5 μL	5 mM	5 μL	5 mM	5 uL	5 mM	
DMSO	13.25 μL	-	13.25 μL	-	13.25 μL	-	
Streptococcus pneumoniae ECF-PanT (11.77 uM)	0	-	253 μL	10 μΜ	253 μL	10 μΜ	

\*The buffer is 50mM KP<sub>i</sub>, pH= 7.5 with 50 mM NaCl and 0.05 %(w/v) DDM. <sup>a</sup>To minimize the error, the 15 µL stock solution was prepared by mixing 5 µL of each aldehyde from the initial 100 mM stock, and 0.75µL were taken from this stock. <sup>b</sup>To minimize the error, the 40 µL stock solution was prepared by mixing 5 µL of each hydrazide from the initial 100 mM stock, and 6 µL were taken from this stock.

#### DCC-2:

This experiment library consisted of two aldehydes (A4-A5) and eight hydrazides (H9-H15) as shown in S2A.

DCL-2 (20 mol% protein): The DCC-experiment was carried out according to the GP-1 (blank) and GP-2 (protein-templated) in phosphate buffer at pH 7.5 and 5% DMSO.

Table 2: Composition of dynamic combinatorial library 2 (DCL-2) of target-directed dynamic combinatorial chemistry experiment 2 (tdDCC-2)

		Blank	Prote	in-templated (I)	Protein-templated (II)	
Entry	Amount	Final conc. in DCL	Amount	Final conc. in DCL	Amount	Final conc. in DCL
Buffer phosphate pH 7.5*	475 μL	-	52 μL	-	52 μL	-
Aldehyde 100 mM	2 × 5 (10 μL)	(2 × 50 μM)	2 × 5 (10 μL)	(2 × 50 μM)	2 × 5° (10 μL)	(2 × 50 μM)
Hydrazide 100 mM	7 × 5 (35 μL)	(7× 150 μM)	7 × 5 (35 uL)	(7 × 150 μM)	7 × 5 <sup>b</sup> (35 μL)	(7 × 150μM)
Aniline 1M in DMSO	5 μL	5 mM	5 μL	5 mM	5 μL	5 mM
DMSO	13.25 μL	-	13.25 μL	-	13.25	-
Streptococcus pneumoniae ECF-PanT (11.77 uM)	0	-	424 μL	10 μΜ	424 μL	10 μΜ

<sup>\*</sup>The buffer is 50mM KP<sub>i</sub>, pH= 7.5 with 50mM NaCl and 0.05 %(w/v) DDM. \*To minimize the error, the 10 µL stock solution was prepared by mixing 5 µL of each aldehyde from the initial 100 mM stock, and 0.5 µL were taken from this stock. \*To minimize the error, the 35 µL stock solution was prepared by mixing 5 µL of each hydrazide from the initial 100 mM stock, and 5.25 µL were taken from this stock.

#### DCC-3:

This experiment library consists of three aldehydes (A6-A8) and seven hydrazides (H1-H7) as shown in S3A.

DCL-3 (20 mol% protein): The DCC-experiment was carried out according to the GP-1 (blank) and GP-2 (protein-templated) in phosphate buffer at pH 7.5 and 5% DMSO. The DCL composition is depicted in Table 3.

Table 3: Composition of dynamic combinatorial library 3 (DCL-3) of target-directed dynamic combinatorial chemistry experiment 3 (tdDCC-3)

Entry	Blank		Protein-tei	Protein-templated (I)		Protein-templated (II)	
	Amount	Final conc. in DCL	Amount	Final conc. in DCL	Amount	Final conc. in DCL	
Buffer phosphate pH 7.5*	475 μL	-	95.4 μL	-	95.4 μL	-	
Aldehyde 100 mM	3×5	(3 × 50 μM)	3×5	(3 × 50 μM)	3 × 5ª	(3 × 50 μM)	
	(15 μL)		(15 μL)		(15 μL)		
Hydrazide 100 mM	8 × 5	(8 × 150 μM)	8 × 5	(8 × 150 μM)	8 × 5 <sup>b</sup>	(8 × 150 μM)	
	40 μL		(40 μL)		(40 μL)		
Aniline 1M in DMSO	5 μL	5 mM	5 μL	5 mM	5 μL	5 mM	
DMSO	13.25 μL	-	13.25	-	13.25	-	
S. pneumoniae ECF-PanT	0	-	379.6 μL	10 μΜ	379.6 μL	10 μΜ	
(13.17 uM)	1						

<sup>\*</sup>The buffer is 50mM KP $_{\nu}$  pH= 7.5 with 50 mM NaCl and 0.05 %(w/v) DDM. a To minimize the error, the 15  $\mu$ L stock solution was prepared by mixing 5  $\mu$ L of each aldehyde from the initial 100 mM stock, and 0.75 $\mu$ L were taken from this stock. b To minimize the error, the 40  $\mu$ L stock solution was prepared by mixing 5  $\mu$ L of each hydrazide from the initial 100 mM stock, and 6  $\mu$ L were taken from this stock.

#### A) Aldeh B) 3.35 min 6.19 min → 3.67 min → 7.42 min 5.29 min 7.82 min 5.81 min 8.21 min ◆ 6.02 min ◆ 8.3 min 9.41 min 9.97 min -10.95 min -11.82 min 60000 Peak area of product: 50000 40000 30000 20000 10000 H7 AcylHydrazones etention time 3.34 mi C) A3H3 A1H4 alized change of RPA (%) 5.29 min A1H4 A1H3 A3H2 & A1H1 A3H7 A2H4 A2H1 & A3H6 A2H3 A1H7 & A3H8 A3H5 A1H6 A2H7 A1H5 A2H6 A2H6 A2H5 amplification factor 5.80 min 6.02 min 6.19 min 7.42 mi 7.61 mi 7.82 min 8.22 min 9.41 min 9.96 min 10.07 min 10.95 min 11.82 min 3.34 4.01 5.29 5,0 6.02 6.19 7.42 7.61 7.82 8.22 8.31 9.41 96'6 min D) A2H5 11.82 mir E) A1H7 and A3H8 A1H6 A1H5 Protein templated I RT 8 00 - 12 1

Target-directed dynamic combinatorial chemistry experiment 1 (tdDCC-1):

Figure S.1. A) Dynamic combinatorial library 1 (DCL-1) composition, B) evaluation of the equilibrium state in the blank DCL-1 by comparing relative peak areas (RPA) of products formed over time, C) amplification factor and normalized change of RPA of products, D) amplified acylhydrazones in protein-templated target-directed dynamic combinatorial chemistry 1 (tdDCC-1). E) Comparison between blank and protein-templated tdDCC-1 samples at twenty-height hours.

## A) Aldehydes B) → 5.01 min ---5.36 min -7.27 min → 7.67 min --- 9.24 min --- 9.31 min -9.49 min --- 9.7 min -11.5 min -- 12.31 min --- 12.43 min --- 12.71 min 30000 25000 Peak area of products 15000 10000 5000 H12 H13 H14 C) Acylhydrazones Retention time A4H4 5.01 min A4H11 A5H14 A4H9 5.36 min 7.27 min 7.67 min zed change of RPA (%) A4H13 A5H14, A4H10 9.24 min 9.31 min 0.2 9.49 min 9.7 min A5H14 11.5 min A5H10<sub>isomer-1</sub> A5H9<sub>isomer-1</sub> 12.31 min 12.43 min 7.34 9.32 A5H12 12.71 min 7.76 (A5H9+A5H10)<sub>isc</sub> 12.79 min 13.12 min D) A5H10 A5H9 12.31 and 12.79 min 12.43 and 12.79 min E)

Target-directed dynamic combinatorial chemistry experiment 2 (tdDCC-2):

Figure S.2. A) Dynamic combinatorial library 2 (DCL-2) composition, B) evaluation of the equilibrium state in the blank DCL-2 by comparing relative peak areas (RPA) of products formed over time, C) amplification factor and normalized change of RPA of products, D) amplified acylhydrazones in protein-templated target-directed dynamic combinatorial chemistry 2 (tdDCC-2). E) Comparison between blank and protein-templated tdDCC-2 samples at twenty-height hours.

## Target-directed dynamic combinatorial chemistry experiment 3 (tdDCC-3):

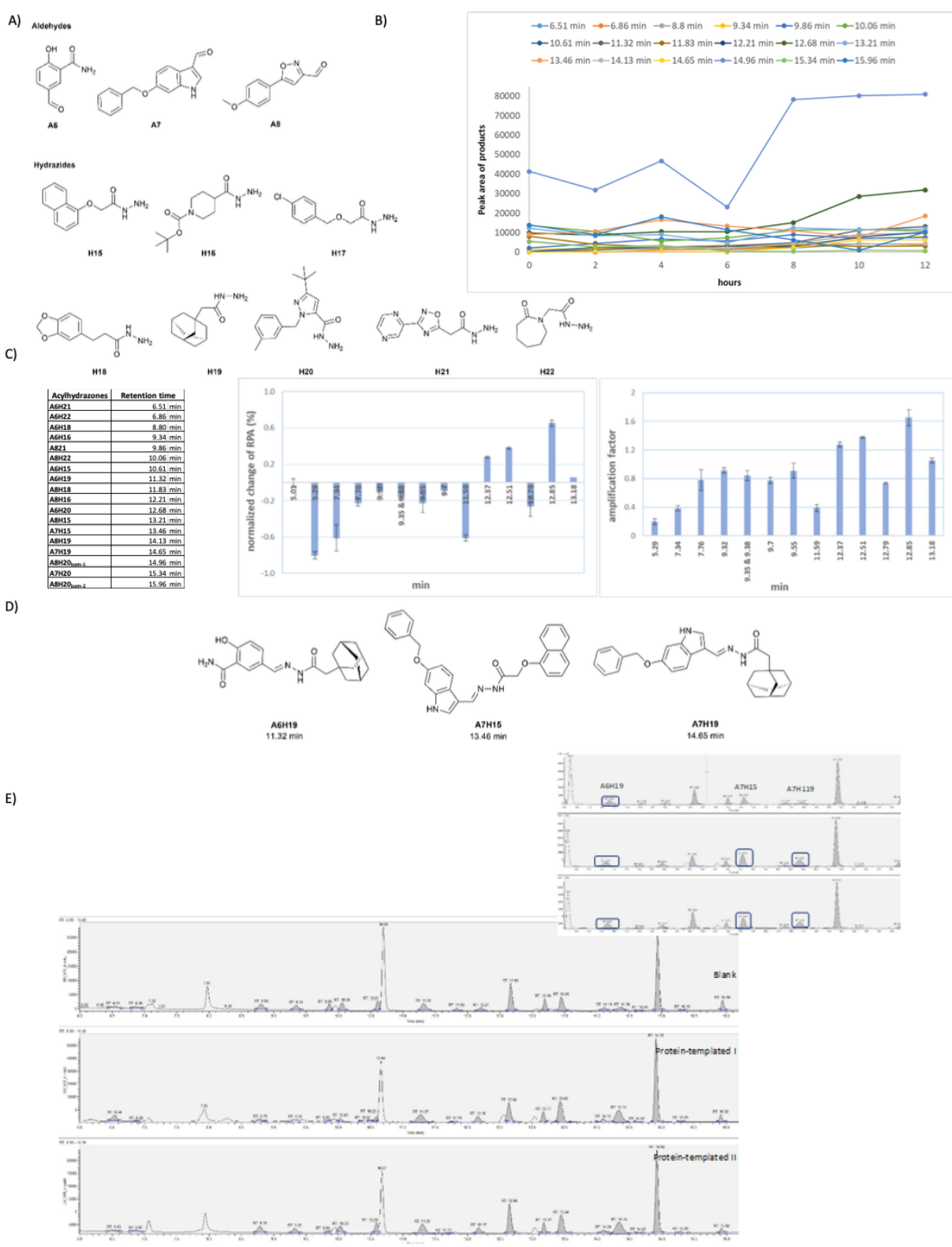


Figure S.3. A) Dynamic combinatorial library 3 (DCL-3) composition, B) evaluation of the equilibrium state in the blank DCL-3 by comparing relative peak areas (RPA) of products formed over time, C) amplification factor and normalized change of RPA of products, D) amplified

acylhydrazones in protein-templated target-directed dynamic combinatorial chemistry 3 (tdDCC-3). E) Comparison between blank and protein-templated tdDCC-3 samples at twenty-height hours.

#### General procedure for acylhydrazone formation (GP-3):

To a crimp tube equipped with a magnetic stirring bar, the hydrazide (1–1.2 equiv.) and the corresponding aldehyde (1 equiv.) were dissolved/suspended in MeOH (0. 6 M) under a nitrogen atmosphere. The reaction mixture was stirred at 65 °C until complete consumption of the starting material. After cooling the reaction to room temperature, the reaction mixture was precipitated by cooling the crimp tube to 0 °C in an ice bath. The resulting crude was purified by preparative HPLC on a reversed-phase column (C18 column, μM, Macherey-Nagel, Germany) using 15–100% gradient of MeCN (0.05% formic acid) in water (0.05%

$$R_1$$
 0 +  $R_2$  0  $R_1$  = aromatic group  $R_2$ = aromatic or aliphatic group

X= CH<sub>2</sub>, OCH<sub>2</sub>, CH<sub>2</sub>O, CH<sub>2</sub>OCH<sub>2</sub>, (CH<sub>2</sub>)<sub>2</sub>, CH<sub>2</sub>CH<sub>2</sub>, R<sub>2</sub>

Scheme 1. General conditions for the synthesis of acylhydrazones.

formic acid), affording the corresponding acylhydrazone products in 60-90% isolated yields.1

#### Characterization of acylhydrazones

Based on  $^1$ H-NMR data, the acylhydrazones reported in this work exist as a mixture of cis/trans rotamers in DMSO- $d_{\delta}$  solutions. Thus,  $^1$ H-NMR spectra for all compounds show resonances for the CO–NH group protons where the rotamers proton (cis/trans) are reported as Ha and Ha'. After reviewing the available literature, it becomes apparent that the acylhydrazones synthesized from aromatic carbaldehydes are essentially planar and exist completely in the form of geometric (E)-configuration about the C=N bond due to steric hindrance on the imine bond. Therefore, we discarded the formation of Z, cis and Z, trans isomers.  $^{4,5}$ 

#### (E)-1-(5-Chlorothiophen-2-yl)-2-((2-fluoro-4-hydroxybenzylidene)amino)ethan-1-one (A1H5)

According to GP-3, 2-fluoro-4-hydroxybenzaldehyde **A1** (60 mg, 0.43 mmol) and 2-(4-nitrophenoxy)acetohydrazide **H5** (75.6 mg, 0.42 mmol) were mixed in MeOH (0.7 mL). The crude was purified by preparative HPLC (64% CH<sub>3</sub>CN) to afford **A1H5** as a mixture of two rotamers of the amide CO–NH (76:24) as an off-white solid (92.1 mg, 0.428 mmol, 72%). <sup>1</sup>H NMR (500 MHz, DMSO- $d_6$ ) δ 11.88 (br. s, 2H, 1Ha and 1Ha´ı), 10.54 (s, 2H, 1Ha and 1Ha´ı), 8.53 (s, 1H, Ha'), 8.21 (s, 1Ha), 7.88 (d, J = 4.1 Hz, 1H, Ha), 7.83 – 7.69 (m, 3H, 1Ha and 2Ha´ı), 7.26 (d, J = 4.1 Hz, 2H, 1Ha and 1Ha´ı), 6.80 (d, J = 8.7 Hz, 1H, Ha), 6.72 (d, J = 8.1 Hz, 1H, Ha'ı), 6.65 (dt, J = 9.9, 4.9 Hz, 2H, 1Ha and 1Ha'ı). <sup>13</sup>C NMR (126 MHz, DMSO- $d_6$ ) δ 162.9, 161.3, 161.2, 160.9, 159.8, 156.5, 141.2, 138.3, 138.3, 137.6, 137.2, 134.3, 133.8, 130.7, 128.7, 128.3, 127.8, 127.8, 127.3, 126.5, 113.1, 112.9, 112.2, 112.1, 102.8, 102.6, 102.4. <sup>19</sup>F NMR (470 MHz, DMSO- $d_6$ ) δ -118.4 (s), -119.5 (s).

HRMS (ESI+): m/z calcd. for C<sub>12</sub>H<sub>8</sub>CIFN<sub>2</sub>O<sub>2</sub>S [M-H]- 296.9906, measured 296.99024.

#### (E)-5-Chloro-N'-((6-(trifluoromethyl)pyridin-3-yl)methylene)thiophene-2-carbohydrazide (A2H5)

According to GP-3, 6-(trifluoromethyl)nicotinaldehyde **A2** (60 mg, 0.34 mmol) and 5-chlorothiophene-2-carbohydrazide **H5** (60.52 mg, 0.34 mmol) were mixed in MeOH(0.52 mL). The crude was purified by preparative HPLC (70% CH<sub>3</sub>CN) to afford **A2H5** as a mixture of two rotamers of the amide CO–NH (73:27) as a white solid (102 mg, 0.34 mmol, 89%).  $^{1}$ H NMR (500 MHz, DMSO- $d_6$ )  $\delta$  12.34 (br. s, 2H, 1Ha and 1Ha'), 9.18 – 9.00 (m, 2H, 1Ha and 1Ha'), 8.48 – 8.35 (m, J = 7.5 Hz, 3H, 1Ha and 2Ha'), 8.24 (s, 1H, Ha), 8.13 – 8.02 (m, J = 7.9 Hz, 2H, 1Ha and 1Ha'), 7.83 (s, 2H, 1Ha and 1Ha'), 7.29 (d, J = 4.1 Hz, 2H, 1Ha and 1Ha').  $^{13}$ C NMR (126 MHz, DMSO- $d_6$ )  $\delta$  160.8, 149.4, 147.2, 147.2, 147.2, 146.9, 146.9, 146.9, 144.1, 144.0, 144.0, 141.2, 141.1, 138.1, 136.6, 136.1, 135.4, 133.6, 130.5, 130.0, 129.9, 129.9, 128.9, 128.9, 128.8, 127.2, 123.1, 121.70, 120.98, 120.95, 120.93.  $^{19}$ F NMR (470 MHz, DMSO- $d_6$ )  $\delta$  –66.4, –66.5.

HRMS (ESI+): m/z calcd. for  $C_{12}H_7CIF_3N_3OS$  [M-H]- 331.98777, measured 331.98724.

#### (E)-N'-(2-Fluoro-4-hydroxybenzylidene)-2-(4-nitrophenoxy)acetohydrazide (A1H6)

According to GP-3, 2-fluoro-4-hydroxybenzaldehyde **A1** (40 mg, 0.286 mmol) and 2-(4-nitrophenoxy)acetohydrazide **H6** (60.3 mg, 0.286 mmol) were mixed in MeOH (0.48 mL). The crude was purified by preparative HPLC (60% CH<sub>3</sub>CN) to afford **A1H6** as a mixture of two rotamers of the amide CO–NH (70:30) as a white solid (76 mg, 0.286 mmol, 80%).

<sup>1</sup>H NMR (500 MHz, DMSO- $d_6$ ) δ 11.59 (d, J = 13.1 Hz, 2H, 1Ha and 1Ha'), 10.48 (s, 2H, 1Ha and 1Ha'), 8.43 (s, 1H, Ha'), 8.24 (d, J = 9.2 Hz, 2H, Ha'), 8.20 (d, 9H), 8.11 (s, 5H), 7.77 (t, J = 8.7 Hz, 2H, 1Ha and 1Ha'), 7.71 (t, J = 8.7 Hz, 1H, Ha'), 7.20 (d, J = 9.3 Hz, 2H, Ha'), 7.17 – 7.09 (m, 10H), 6.70 (dd, J = 8.6, 2.2 Hz, 7H), 6.62 (dd, J = 12.7, 2.2 Hz, 7H), 5.31 (s, 2H, Ha), 4.83 (s, 2H, Ha'). <sup>13</sup>C NMR (126 MHz, DMSO- $d_6$ ) δ 167.9, 163.6, 163.1, 163.0, 162.9, 162.7, 161.0, 160.9, 160.7, 141.3, 141.3, 140.9, 137.5, 137.5, 127.5, 127.4, 127.4, 125.8, 125.7, 115.3, 115.2, 112.8, 112.7, 112.3, 112.3, 102.6, 102.6, 102.4, 102.4, 66.7, 65.4. <sup>19</sup>F NMR (470 MHz, DMSO- $d_6$ ) δ -119.45, -119.69.

HRMS (ESI+): m/z calcd. for  $C_{15}H_{12}FN_3O_5$  [M+H]+ 332.06882, measured 332.06827.

#### (E)-N'-(2-Fluoro-4-hydroxybenzylidene)thiophene-2-carbohydrazide (A1H7)

According to GP-3, 2-fluoro-4-hydroxybenzaldehyde **A1** (50 mg, 0.36 mmol) and thiophene-2-carbohydrazide **H7** (50.7 mg, 0.36 mmol) were mixed in MeOH (0.6 mL). The crude was purified by preparative HPLC (50%  $CH_3CN$ ) to afford **A1H7** as a mixture of two rotamers of the amide CO-NH (51:49) as a white solid (87 mg, 0.36 mmol, 90%).

1H NMR (500 MHz, DMSO- $d_6$ )  $\delta$  11.78 (d, 2H, 1Ha and 1Ha'), 10.48 (s, 2H, 1Ha and 1Ha'), 8.55 (s, 1, Ha'), 8.21 (s, 1H, 1Ha), 8.04 (s, 1H, Ha), 7.98 – 7.64 (m, 4H, 2Ha and 2Ha'), 7.22 (t, J = 4.2 Hz, 2H, 1Ha and 1Ha'), 6.75 (dd, J = 21.3, 8.1 Hz, 2H, 1Ha and 1Ha'), 6.64 (d, J = 12.5 Hz, 2H, 1Ha and 1 Ha'), 13C NMR (126 MHz, DMSO- $d_6$ )  $\delta$  162.86, 161.09, 160.94, 160.87, 157.51, 157.5,  $^{14}$ 0.7, 138.3, 137.4, 134.8, 134.6, 133.2, 131.8, 128.8, 128.14, 127.7, 127.6, 127.3, 126.7, 113.0, 112.8, 112.7, 112.6, 112.5, 102.7, 102.6, 102.5, 102.4.  $^{19}$ F NMR (470 MHz, DMSO- $d_6$ )  $\delta$  -118.3 (s), -119.4 (s).

HRMS (ESI+): m/z calcd. for  $C_{12}H_{18}FN_2O_2S$  [M-H]- 263.02960, measured 263.02908.

#### (E)-4-Methyl-N'-((6-methylpyridin-3-yl)methylene)benzenesulfonohydrazide (A3H8)

According to GP-, 6-methylnicotinaldehyde **A3** (80 mg, 0.66 mmol) and 4-methylbenzenesulfonohydrazide **H8** (112.42 mg, 0.34 mmol) were mixed in MeOH (1.1 mL) to afford after purification by preparative HPLC (50% CH<sub>3</sub>CN) **A3H8** as one rotamer of the amide CO–NH) as a yellow solid (183.23 mg, 0.66 mmol, 96%).

<sup>1</sup>H NMR (500 MHz, DMSO- $d_6$ ) δ 11.75 (s, 1H), 8.82 (s, 2H), 7.90 (s, 1H), 7.77 (d, J = 8.2 Hz, 2H), 7.41 (d, J = 8.1 Hz, 2H), 2.61 (s, 3H), 2.36 (s, 3H). <sup>13</sup>C NMR (126 MHz, DMSO- $d_6$ ) δ 168.0, 154.8, 143.6, 141.7, 135.9, 129.7, 127.3, 124.8, 25.6, 21.0. HRMS (ESI<sup>+</sup>): m/z calcd. for C<sub>14</sub>H<sub>15</sub>N<sub>3</sub>O<sub>2</sub>S [M+H]<sup>+</sup> 291.09913, measured 291.08968.

#### (E)-5-((2-(1-Naphthoyl)hydrazineylidene)methyl)-2-hydroxybenzoic acid (3, A4H9)

According to GP-3, 5-formyl-2-hydroxybenzoic acid, A4 (100 mg, 0.602 mmol) and 1-naphthohydrazide H9 (112.09 mg, 0.602 mmol) were mixed in MeOH (1.1 mL) to afford after preparative HPLC (70% CH<sub>3</sub>CN) (E)-5-((2-(1-Naphthoyl)hydrazineylidene)methyl)-2-hydroxybenzoic acid 3 (A4H9) as a mixture of two rotamers of the amide CO–NH (84:16) as an off-white solid (105 mg, 0.602 mmol, 92%).

<sup>1</sup>H NMR (500 MHz, DMSO- $d_6$ ) δ 11.96 (s, 2H, Ha and Ha'), 8.29 (s, 1H), 8.23 – 8.18 (m, J = 6.4, 2.8 Hz, 1H, Ha), 8.16 (d, J = 2.2 Hz, 1H, Ha), 8.09 (d, J = 8.2 Hz, 1H, Ha), 8.05 – 7.98 (m, 4H, 1Ha and 3Ha'), 7.90 (dd, J = 14.3, 7.1 Hz, 2H, 1Ha and 1Ha'), 7.74 (dd, 1H, Ha), 7.69 (d, 1H, Ha'), 7.64 – 7.50 (m, 6H, 3Ha and 3Ha'), 7.29 (dd, J = 8.7 Hz, 1H, Ha'), 7.07 (d, J = 8.6 Hz, 1H, Ha), 6.83 (d, J = 8.6 Hz, 1H, Ha'). <sup>13</sup>C NMR (126 MHz, DMSO- $d_6$ ) δ 171.4, 164.6, 163.0, 147.0, 133.4, 133.2, 133.0, 130.4, 130.0, 129.4, 128.4, 127.1, 126.5, 125.8, 125.2, 125.0, 117.9.

HRMS (ESI+): m/z calcd. for  $C_{19}H_{14}N_2O_4$  [M+H]+ 335.10263, measured 335.1007.

#### (E)-4-Bromo-N'-((5-(4-chlorophenyl)furan-3-yl)methylene)benzohydrazide (4, A5H10)

According to GP-3, 5-(4-chlorophenyl)furan-3-carbaldehyde **A5** (40 mg, 0.19 mmol) and 4-bromobenzohydrazide **H10** (41.63 mg, 0.19 mmol) were mixed in MeOH (0.32 mL) to give after purification by preparative HPLC (80% CH<sub>3</sub>CN) **4 (A5H10)** as a mixture of two rotamers of the amide CO–NH (91:9) as a yellow solid (59.2 mg, 0.194 mmol, 76%).

<sup>1</sup>H NMR (500 MHz, DMSO- $d_6$ ) δ 11.93 (brs, 2H, 1Ha and 1Ha'), 8.37 (s, 1H), 7.93 – 7.70 (m, 12H, 6Ha and Ha'), 7.54 (d, J = 8.4 Hz, 4H, 2Ha and 2Ha'), 7.15 (dd, J = 58.7, 3.2 Hz, 4H, 2Ha and 2Ha'). <sup>13</sup>C NMR (126 MHz, DMSO- $d_6$ ) δ 162.1, 153.7, 149.3, 137.5, 132.7, 132.4, 131.5, 129.7, 129.1, 128.3, 125.7, 125.6, 116.4, 109.1.

HRMS (ESI+): m/z calcd. for C<sub>18</sub>H<sub>12</sub>BrClN<sub>2</sub>O<sub>2</sub> [M+H]+ 404.98230, measured 404.98146.

#### (E)-N'-((5-(4-Chlorophenyl)furan-2-yl)methylene)-1-naphthohydrazide (5, A5H9)

According to GP-3, 5-(4-chlorophenyl)furan-3-carbaldehyde **A5** (100 mg, 0.48 mmol) and 1-naphthohydrazide **H9** (90.1 mg, 0.48 mmol) were mixed in MeOH (0.8 mL). The crude was purified by preparative HPLC (84%  $CH_3CN$ ) to afford **(A5H9)** as a mixture of two rotamers of the amide CO-NH (89:11) as a yellow solid (136mg, 0.64 mmol, 75%).

<sup>1</sup>H NMR (500 MHz, DMSO- $d_6$ ) δ 12.07 – 11.97 (m, 2H, 1Ha and 1Ha'), 8.25 (s, 1H), 8.23 – 8.19 (m, 1Ha), 8.18 – 8.06 (m, 3H, 1Ha and 2Ha'), 8.03 (dd, 3H, 1Ha and 2 Ha'), 7.91 (td, J = 16.2, 7.4 Hz, 2H, Ha'), 7.84 (d, J = 8.5 Hz, 2H, Ha), 7.75 (d, J = 6.9 Hz, 1H, Ha), 7.64 – 7.59 (m, 6H, 3Ha and 3Ha'), 7.55 (d, J = 8.5 Hz, 4H, 2Ha and 2Ha'), 7.22 (d, J = 3.6 Hz, 1H, Ha), 7.09 (d, J = 3.6 Hz, 1H, Ha'), 6.72 (d, 1H, Ha'). <sup>13</sup>C NMR (126 MHz, DMSO- $d_6$ ) δ 164.6, 153.7, 149.3, 137.1, 133.2, 132.8, 132.7, 130.6, 129.9, 129.16, 128.4, 127.2, 126.5, 125.9, 125.7, 125.0, 125.0, 116.3, 109.1.

HRMS (ESI<sup>+</sup>): m/z calcd. for  $C_{22}H_{15}CIN_2O_2$  [M+H]<sup>+</sup> 375.08948, measured 375.0890.

#### 5-((E)-(2-(2-((3R,5R,7R)-adamantan-1-yl)acetyl)hydrazineylidene)methyl)-2-hydroxybenzamide (6, A6H19)

$$H_2N$$

According to GP-3, 5-formyl-2-hydroxybenzamide **A6** (50 mg, 0.30 mmol) and adamantane-1-yl-acetic acid hydrazide **H19** (67.3 mg, 0.30 mmol) were mixed in MeOH (0.5 mL). The crude was purified by preparative HPLC (75%  $CH_3CN$ ) to afford **6** (**A6H19**) as a mixture of two rotamers of the amide CO-NH (57:43) as an off-white solid (78 mg, 0.3 mmol, 72%).

<sup>1</sup>H NMR (500 MHz, DMSO- $d_6$ )  $\delta$  13.29 (s, 2H, 1Ha and 1Ha'), 11.16 (d, J = 10.8 Hz, 2H, 1Ha and 1Ha'), 8.53 (d, J = 9.3 Hz, 2H, 1Ha and 1 Ha'), 8.09 (s, 1H), 8.04 (dd, J = 27.2, 1.6 Hz, 1H), 7.99 (s, 1H), 7.87 (s, 1H), 7.78 (ddd, J = 18.4, 8.7, 1.7 Hz, 2H, 1Ha and 1Ha'), 6.96 (t, J = 9.2 Hz, 2H, 1Ha and 1Ha'), 1.92 (d, J = 15.7 Hz, 8H), 1.74 – 1.42 (m, 25H).

 $^{13}$ C NMR (126 MHz, DMSO- $d_6$ )  $\delta$  172.6, 172.0, 171.9, 166.6, 162.8, 145.5, 141.5, 132.1, 131.0, 128.8, 128.5, 125.7, 125.6, 119.0, 118.6, 115.8, 115.2, 115.2, 114.9, 49.1, 45.3, 42.9, 42.6, 36.9, 33.4, 33.2, 28.5.

HRMS (ESI+): m/z calcd. for  $C_{20}H_{25}N_3O_3$  [M+H]+ 356.19687, measured 356.19603.

#### (E)-N'-((6-(Benzyloxy)-1H-indol-3-yl)methylene)-2-(naphthalen-1-yloxy)acetohydrazide (A7H15)

According to GP-3, 6-(benzyloxy)-1H-indole-3-carbaldehyde **A7** (50 mg, 0.2 mmol) and 2-(naphthalen-1-yloxy)acetohydrazide **H15** (172 mg, 0.8 mmol) were mixed in MeOH (0.33 mL) to give after purification by preparative HPLC (78% CH<sub>3</sub>CN) **A7H15** as a mixture of two rotamers of the amide CO–NH (67:33) as an off-white solid (63 mg, 0.2 mmol, 70%).

<sup>1</sup>H NMR (500 MHz, DMSO- $d_6$ ) δ 11.41 (s, 2H, 1Ha and Ha'), 11.38 (s, 1H, Ha), 11.34 (s, 1H, Ha'), 8.43 (s, 1H, Ha'), 8.37 – 8.31 (m, 1H, Ha'), 8.30 – 8.25 (m, 1H, Ha), 8.16 (s, 1H, Ha), 8.09 (d, J = 8.7 Hz, 1H, Ha'), 8.01 (d, J = 8.7 Hz, 1H, Ha), 7.92 – 7.86 (m, 2H, 1Ha and 1Ha'), 7.69 (dd, J = 7.5, 2.6 Hz, 2H, 1Ha and 1Ha'), 7.59 – 7.36 (m, 14H, 7Ha and 5Ha'), 7.32 (dt, J = 11.8, 5.8 Hz, 2H, 1Ha and 1Ha'), 7.00 (d, J = 1.8 Hz, 2H, 1Ha and 1Ha'), 6.97 (d, J = 7.6 Hz, 1H, Ha'), 6.92 – 6.85 (m, 3H, 1Ha and 2Ha'), 6.85 (d, J = 2.2 Hz, 1H,

Ha'), 5.39 (s, 2H, Ha), 5.13 (s, 3H, 2Ha and 1Ha'), 4.84 (s, 2H, Ha').  $^{13}$ C NMR (126 MHz, DMSO- $d_6$ )  $\delta$  168.40, 155.8, 155.8, 154.26, 154.0, 145.6, 141.8, 138.3, 138.2, 137.9, 134.6, 134.6, 130.2, 128.9, 128.2, 128.1, 128.0, 127.9, 127.0, 126.9, 126.6, 126.5, 125.8, 125.7, 125.4, 125.4, 123.0, 122.8, 122.5, 122.2, 121.1, 120.6, 119.1, 118.9, 112.0, 111.9, 111.6, 111.4, 106.1, 105.7, 96.8, 96.7, 69.9, 69.9, 67.6, 65.7.

HRMS (ESI+): m/z calcd. for  $C_{28}H_{23}N_3O_3$  [M+H]+ 450.18122, measured 450.18049.

## 2-((3R,5R,7R)-Adamantan-1-yl)-N'-((E)-(6-(benzyloxy)-1H-indol-3-yl)methylene) acetohydrazide (A7H19)

According to GP-3, 6-(benzyloxy)-1H-indole-3-carbaldehyde **A7** (50 mg, 0.2 mmol) and adamantane-1-yl-acetic acid hydrazide **H19** (41.45 mg, 0.2 mmol). Were mixed in MeOH (0.33 mL). The crude was purified by preparative HPLC (80% CH<sub>3</sub>CN) to afford **A7H19** as a mixture of two rotamers of the amide CO–NH (46:44) as a yellow solid (80 mg, 0.24 mmol, 77%).

<sup>1</sup>H NMR (500 MHz, DMSO- $d_6$ ))  $\delta$  11.29 (dd, J = 12.8, 2.0 Hz, 2H, 1Ha and 1Ha'), 8.88 (s, 2H, 1Ha and 1Ha'), 8.25 (s, 1H), 8.06 (dd, J = 12.9, 8.6 Hz, 3H, 2Ha and 1Ha'), 7.56 (dt, J = 17.3, 8.6 Hz, 2H, 1Ha and 1Ha'), 7.45 (dt, J = 15.4, 7.8 Hz, 4H, 2Ha and 2Ha'), 7.38 (td, J = 7.5, 1.8 Hz, 4H, 2Ha and 2Ha'), 7.34 – 7.28 (m, 2H, 1Ha and 1Ha'), 7.00 (dd, J = 6.5, 2.2 Hz, 2H, 1Ha and 1Ha'), 6.86 (ddd, J = 13.0, 8.7, 2.2 Hz, 2H, 1Ha and 1Ha'), 5.12 (d, J = 5.7 Hz, 4H, 2Ha and 2Ha'), 1.94 – 1.85 (m, 5H), 1.53 (t, J = 10.2 Hz, 47H). <sup>13</sup>C NMR (126 MHz, DMSO- $d_6$ )  $\delta$  172.14, 170.09, 155.72, 143.32, 139.80, 138.30, 138.18, 137.83, 137.82, 129.47, 129.37, 128.88, 128.20, 128.08, 128.00, 123.08, 122.41, 121.38, 119.06, 118.92, 112.20, 111.24, 96.98, 96.88, 96.65, 69.93, 48.35, 42.97, 42.48, 36.85, 33.57, 33.09, 32.59, 28.46.

HRMS (ESI+): m/z calcd. for  $C_{28}H_{31}N_3O_2$  [M+H]+ 442.24890, measured 442.24831.

## Biological evaluation of synthesized compounds

#### Protein homology sequence and structure identity determination of the entire complex of ECF-PanT

The NCBI BLAST program was utilized to conduct the BLAST analysis with specific parameters, including BLASTp and an E-value threshold of 0.05. The query protein under examination was *S. pneumoniae* ECF-PanT with UniProtKB database ID of EcfS: A0A064C5C4, EcfT: A0A4L7ULF4, EcfA1: Q04HV7, and EcfA2: Q97N51, while the subject protein was *L. delbrueckii* ECF PanT with PDB ID of 6ZG3 and UniProtKB ID of EcfS: Q1GBG0, EcfT: Q1GBI8, EcfA1: Q1GBJ0, and EcfA2: Q1GBI9. The resulting values obtained from the analysis were an E-value of 0 and a percentage identity of 40.80 %.<sup>6, 7</sup>

In this study, the multiple sequence alignment with both the query and subject proteins was produced by T-Coffee<sup>8,9</sup> and nimBOXshade was utilized to enhance the presentation of the sequence alignments in shade (Figure S4).<sup>10</sup>

S.ECF-PanT L.ECF-PanT		MKKRSNIAPIAIFFATMLVIHFLSSLIFNLFPFPIKPTIVHIPVIIASIIYG MYDSEARQKTLNLTVSAVFVAILLLEAFIPNVGY-ITILPGLPAITTIPLTVAVFASLRG
S.ECF-PanT L.ECF-PanT		:70:80:90:100:110:120 PRVGVTLGFLMGLLSLTVNTITILPTSYLFSPFVPNGNIYSAIIAIVPRILIGLT PKAGAAFGLVWGLTSLLRA
S.ECF-PanT L.ECF-PanT		:130:140:150:160:170:180 PYLVYKLMKNKTGLILAGALGSLTNTIFVLGGIFFLFGNVYN AGLAGQLADKWEKESRKPLAYALSGLLASAVNTLIVILLSDLVYFIHPQKLALALGAKSG
S.ECF-PanT L.ECF-PanT	150 168	:190:200:210:220:230:240 GNIQLLLATVISTNSIAELVISAILTLAIVP-RLQTL-KKMDSMILGRYIPGDSIVHRLD QSLLVILFTALAVNGILEAVFSGLITPLITAPLKKRLKRRMSKIIIGRYLPGTTFVYRVD
S.ECF-PanT L.ECF-PanT		:250:260:270:280:290:300 PRSKLLAMMLLILIVFWANNPLTNLILFIATGIFIALSGVSLSFFIQGLKSIFFLIAFTT PRAKLLTTFYFIIMIFLANNWVSYLVISIFGLAYVFATGLKARVFWDGVKPMIWMIVFTS
S.ECF-PanT L.ECF-PanT		:310:320:330:340:350:360 IFQLFFISNGNVLFEFSFVRITDYALQQAGIIFCRFVLIIFFSTLLTLTTMPLSLASAVE LLQTFFMAGGKVYWHWWIFTLSSEGLINGLYVFIRFAMIILVSTVMTVTTKPLEIADAME
S.ECF-PanT L.ECF-PanT		:370:380:390:400:410:420 ALLAPLKRVKVPVHEIGLMLSMSLRFVPTLMDDTTRIMNAQKARGVDFGEGSIVQKVKAM WMLTPLKLFKVNVGMISLVISIALRFVPTLFDQTVKIMNAQRSRGADFNDGGLVKRAKSV
S.ECF-PanT L.ECF-PanT		:430:440:450:460:470:480 IPILIPLFATSLKRADSLAIAMEARGYQGGKGRSQYRQLKWTLKDTLTILVILVLGCCLF VPMLVPLFIDSLEVALDLSTAMESRGYKGSEGRTRYRILEWSKVDLIPVAYCLLLTILMI
S.ECF-PanT L.ECF-PanT		:490:500:510:520:530:540 -FLKSMGIALENVNFTYQEGTPLASAALSDVSLTIEDGSYTALIGHTGSGKSTILQLLNG TTRKHMAIKFENVSYVYSPGSPLEAIGLDQLNFSLEEGKFIALVGHTGSGKSTLMQHFNA
S.ECF-PanT L.ECF-PanT		:550:560:.570:.580:.590:600 LLVPSQGSVRVFDTLITSTSKNKDIRQIRKQVGLVFQFAENQIFEETVLKDVAFGPQNFG LLKPTSGKIEIAGYTITPETGNKGLKDLRRKVSLAFQFSEAQLFENTVLKDVEYGPRNFG
S.ECF-PanT L.ECF-PanT		:610:620:630:640:650:660 VSEEDAVKTAREKLALVGIDESLFDRSPFELSGGQMRRVAIAGILAMEPAILVLDEPTAG FSEDEAREAALKWLKKVGLKDDLIEHSPFDLSGGQMRRVALAGVLAYEPEIICLDEPAAG
S.ECF-PanT L.ECF-PanT		:670:680:690:700:710:720 LDPLGRKELMTLFKKLHQSGMTIVLVTHLMDDVAEYANQVYVMEKGRLVKGGKPSDVFQD LDPMGRLEMMQLFKDYQAAGHTVILVTHNMDDVADYADDVLALEHGRLIKHASPKEVFKD
S.ECF-PanT L.ECF-PanT		:730:740:750:760:770:780  VVFMEEVQLGVPKITAFCKRLADRGVSFKRLPIKIEEFKESLNGMKSIIDV SEWLQKHHLAEPRSARFAAKLEAAGLKLPGQPLTMPELADAIKQSLKGGEHEMSDNIISF
S.ECF-PanT L.ECF-PanT		:790:800:810:820:830:840 KNLSFRYKENQNYYDVKDITFHVKRGEWLSIVGHNGSGKSTTVRLIDGLLEAESGEI DHVTFTYPDSPR-PALSDLSFAIERGSWTALIGHNGSGKSTVSKLINGLLAPDDLDKSSI
S.ECF-PanT L.ECF-PanT		:850:860:870:880:.890:900 VIDGQRLTEENVWNIRRQIGMVFQNPDNQFVGATVEDDVAFGLENQGLSRQEMKKRVEEA TVDGVKLGADTVWEVREKVGIVFQNPDNQFVGATVSDDVAFGLENRAVPRPEMLKIVAQA
S.ECF-PanT L.ECF-PanT		:910:920:930:940:950:960 LALVGMLDFKKREPARLSGGQKQRVAIAGVVALRPAILILDEATSMLDPEGRRELIGTVK VADVGMADYADSEPSNLSGGQKQRVAIAGILAVKPQVIILDESTSMLDPEGKEQILDLVR
S.ECF-PanT L.ECF-PanT		:970:.980:.990:.1000:.1010:.1020 GIRKDYDMTVISITHDLEEVAMSDRVLVMKKGEIESTSSPRELFSRND-LDQIGLDDPFA KIKEDNNLTVISITHDLEEAAGADQVLVLDDGQLLDQGKPEEIFPKVEMLKRIGLDIPFV

```
S.ECF-PanT 974 NQLKKSLSQNGYDLPENYLTESELEDKLWELL---
L.ECF-PanT 1007 YRLKQLLKERGIVLPDEIDDDEKLVQSLWQLNSKM
```

Figure S4. The fraction of sequences that must agree for a consensus (0–1) was set to 0.5. The foreground color for both identical and similar residues was set to black. The background color for identical and similar residues was set to green and yellow, respectively.

#### Uptake assay into proteoliposome

To assess the effectiveness of the tDCC compounds inhibiting the ECF proteins, we performed an uptake assay inspired by Swier et al.<sup>11</sup> In this assay, the ECF transporter for folate (ECF-FoIT2) from L. delbrueckii was used and reconstituted into lipid vesicles known as proteoliposomes. For our purposes, we utilized the ECF transporter for pantothenate (ECF-PanT) from L. delbrueckii. This choice was made for two reasons: firstly, it originates from the same organism for which the assay was initially designed, and secondly, it exhibits homology to S. pneumoniae ECF-PanT as confirmed through BLASTp analysis (Figure S4), demonstrating a sufficient sequence similarity of 34%. This similarity allows us to use L. delbrueckii ECF-PanT as a representative model, enabling meaningful comparisons and insights applicable to both proteins and their respective organisms. Figure S5 exhibits the percentage of inhibition for each compound at 250 µM. In Figures S6A and S6B, pantothenate uptake traces are shown. Mg-ATP and Mg-ADP were used as positive and negative controls, respectively. The differences in the uptake patterns for the 5 mM Mg-ATP control can be explained by how recently we purified the protein, as over time, the protein tends to lose its activity.

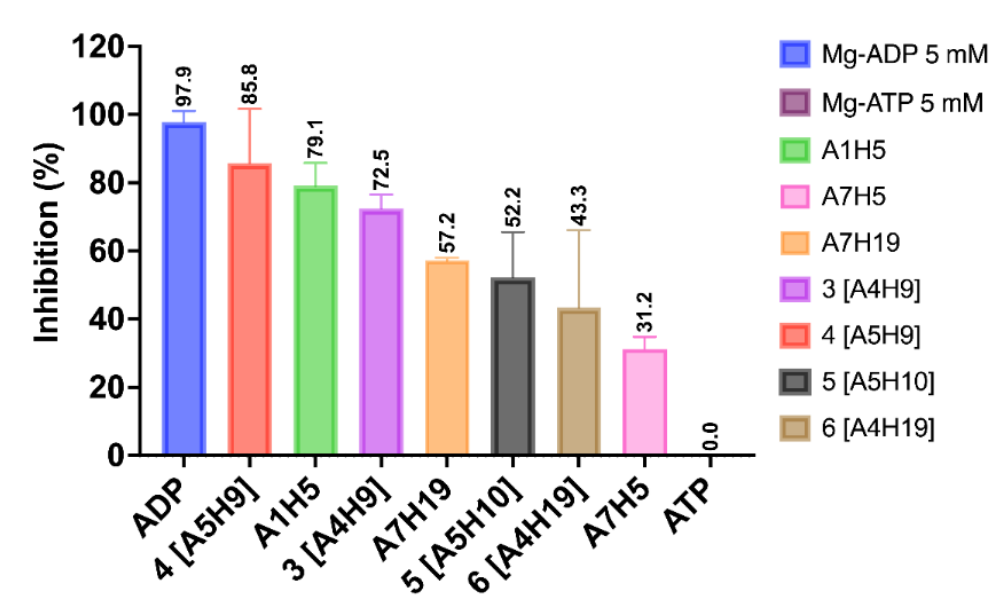


Figure S5. The graph displays inhibition percentages for individual target-directed combinatorial chemistry (td-DCC) product compounds at a concentration of 250  $\mu$ M, obtained through the proteoliposome uptake assay, and is presented in column format.

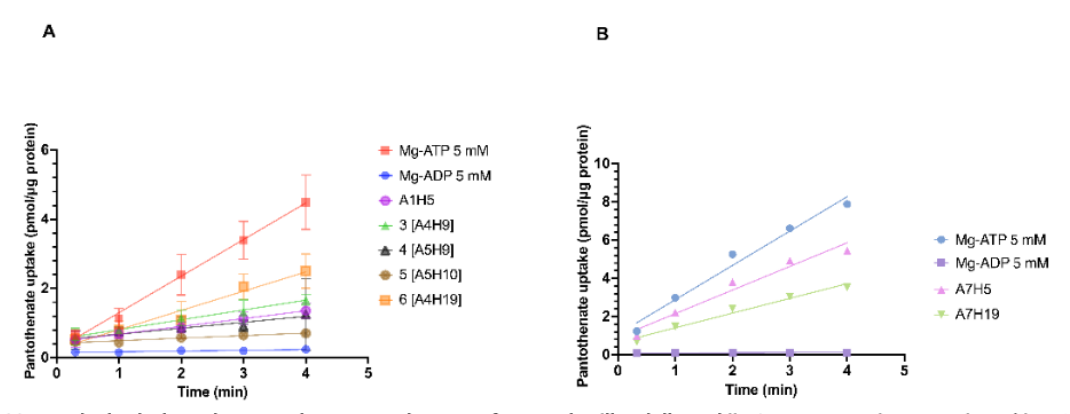


Figure S6. A and B both show the pantothenate uptake traces for Lactobacillus delbrueckii ECF-PanT protein reconstituted in a 1:125 ratio. The corresponding line for each compound is between Mg-ATP as a positive control and Mg-ADP as a negative control. Figure 6. A depicts the results of the assay conducted with three technical replicates, each of which was performed as a duplicate biological assay. Figure 6. B illustrates the results obtained from a single biological and technical replicate assay. Whole-cell bacterial uptake assay (ECF-T assay)

The ECF inhibitors and their inhibitory effect on folate uptake in the Gram-positive model organism L. casei were studied in a whole-cell uptake assay as recently published in our group. This purpose, 20  $\mu$ L of inhibitor, was added to the wells of a MultiScreen HTS Filter Plate containing 175  $\mu$ L of L. casei culture diluted in citrate buffer. The blank was determined with 185  $\mu$ L citrate buffer and 10  $\mu$ L of DMSO. 5  $\mu$ L of radiolabeled folic acid was added to each well (2  $\mu$ M, Moravek Biochemicals, Brea, CA). Using this method, we determined the percentage of inhibition at 200  $\mu$ M for the building blocks and the amplified compounds (Figure S7) and the IC50 values for our best compounds. The assay was done in both technical and biological duplicate ensuring the reliability and consistency of the data. Subsequently, the gathered data were analyzed using GraphPad Prism, a robust statistical software tool.

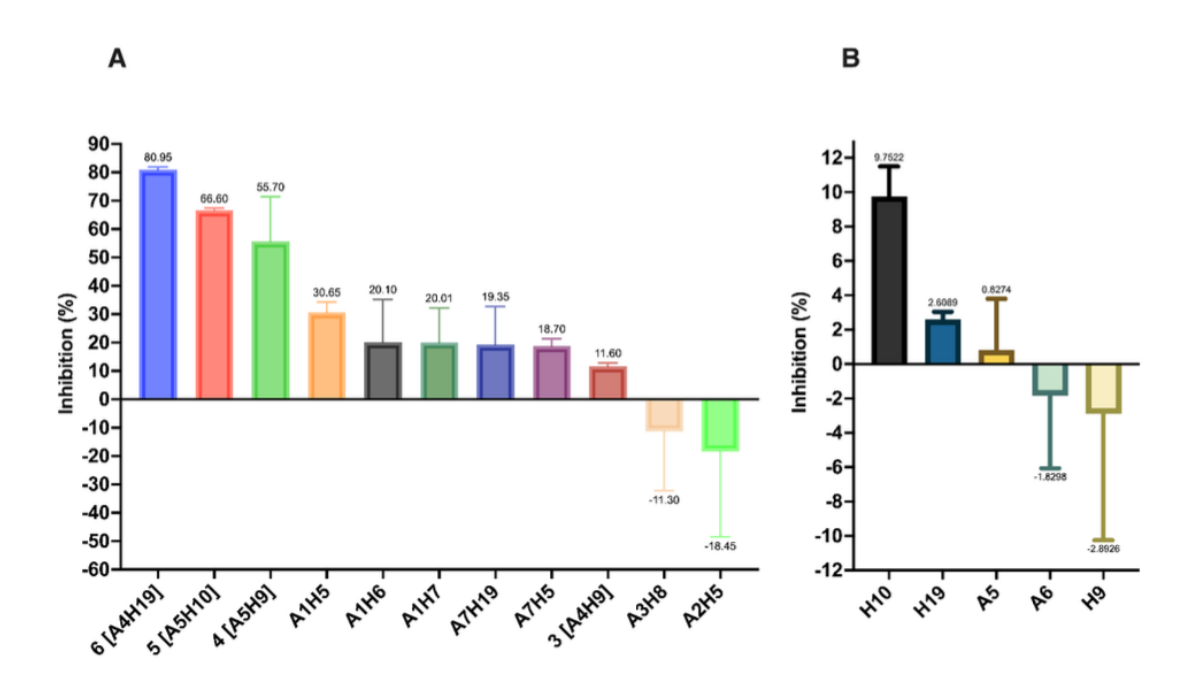


Figure S7. The figure depicts the percentage of inhibition of A) target-directed combinatorial chemistry (tdDCC) product compounds and B) building blocks at a concentration of 200  $\mu$ M, as determined through the whole-cell-based uptake assay.

## Cytotoxicity assays

To obtain information regarding the cytotoxicity of our compounds, their impact on the viability of human cells was investigated. HepG2, HEK293 and A549 cells ( $2x10^5$  cells per well) were seeded in 24-well, flat-bottomed culture plates. Twenty-four hours after seeding the cells, the incubation was started by the addition of compounds in a final DMSO concentration of 1%. Duplicates were prepared for each compound concentration. Epirubicin and doxorubicin were used as positive controls (each at 1  $\mu$ M), and rifampicin was used as a negative control (at 100  $\mu$ M). The living cell mass was determined 48 h after treatment with compounds by adding 0.1 volumes of 3-(4,5-dimethylthiazol-2-yl)-2,5-diphenyltetrazolium bromide (MTT) solution (5 mg per mL sterile PBS) (Sigma, St. Louis, MO) to the wells. After incubating the cells at 37 °C for 30 min (atmosphere containing 5% CO2), MTT crystals were dissolved in a solution containing 10% SDS and 0.5% acetic acid in DMSO. The optical density (OD) of the samples was determined photometrically at 570 nm in a FLUOstar Omega plate reader (BMG labtech, Ortenberg, Germany). To obtain percent inhibition values for each sample, their ODs were related to those of DMSO controls. At least two independent measurements were performed for each compound.<sup>13</sup>

Table 4. Antibacterial activity and cytotoxicity results for compounds 4, 5 and 6 in three different cell lines.

Compound	Cytotoxicit	y % Inh. @ 10	00 μΜ	Antibacterial profile ( μM)		
	HepG2	A549	HEK293	Streptococcus pneumoniae DSM-20566	Streptococcus pneumoniae DSM-11865 (PRSP)	
	4	<10	<10	<10	>64	>64
	5	<10	<10	<10	>64	>64
	6	<10	20 ± 3	<10	>64	>64

#### **Computational Modeling**

#### Methods:

Data sets: From the coarse-grained MD simulation of *L. delbrueckii* ECF-PanT transporter X-ray crystal structure (PDB ID: 6ZG3) with hit compound **1**, two snapshots with the best calculated free energies were selected. These snapshots provided two distinct binding pockets, P11, a cavity in the S-component, and P9, a hidden pocket at the interface between ECF-T and the S-component, as described in Diamanti *et al.* Three potent inhibitors, two compounds from the hit **2** series (**4** and **5**) and compound **6** from the hit **1** series, were chosen to examine the binding mode commonalities and differences between both different hit series. Distinct isomers were used as input for the docking study for compounds that contain an acylhydrazone moiety (**4**, **5** and **6**) to be able to pick the enantiomer that fits better to the binding site for the downstream studies.

Docking: As in the previous study, <sup>14</sup> we used FlexX for protein–ligand docking from SeeSAR version 13.0.1<sup>15</sup> to generate docking poses for the selected three compounds. The CG-MD snapshot with hit1 compound bound to pocket P9 was used as input, and the bound ligand, 1, served to define the binding site. Thirty poses for every compound were generated using the default parameters. All poses were evaluated using the built-in HYDE scoring function. <sup>16</sup>

Manual pose selection: We selected poses with favorable estimated affinity that mimic the key interactions of hit compound 1, contained in pocket P9 in the CG-MD snapshot. Thus, for 6, the pose was chosen that most closely overlapped with the salicylic acid moiety of 1. In both series, poses forming hydrogen-bond interactions with the side chain of ARG77-C were preferred. Note that for 4, 5 and 6 the *E*-enantiomers were selected for analysis and for MD simulations due to their better fit.

MD Simulations: MD simulations were performed to answer different questions, the general set-up has been the same, only the chosen poses differ.

First, the protein structure was prepared using PDBFixer from OpenMM.<sup>17</sup> Missing hydrogen atoms were added, and missing residues were ignored. Selected poses were prepared using RDKit<sup>18</sup> to protonate the compounds and to assign the bond order correctly. The system was then prepared for the MD simulations: Parameters for the protein were generated from the amber14-all force field within OpenMM; for the compound parameters, we used the General AMBER Force Field (GAFF).<sup>19</sup> The complex was embedded in a cubic box, the dimensions of the box were set based on the largest dimension of the complex, including padding. The system has been solvated using the standard three-site water model TIP3P.<sup>20</sup> Langevin integrator<sup>21</sup> was the method of choice for simulating the created system by integrating the equations of motion. The starting position was set by minimizing the energy of the system first to decrease the probability of simulation failures. We simulated 60 picoseconds of MD corresponding to 30,000 steps of 2 femtosecond each. Snapshots were saved every 2000 steps (4 picoseconds), having 150 snapshots at the end of each MD simulation.

I) MD simulations to select pocket: To confirm the selected binding pocket, we performed an MD simulation using the three potent compounds (4, 5 and 6) for both binding pockets P11 and P9. The highest-scoring poses were selected for each binding pocket from the FlexX docking using HYDE scoring function (see docking section).

II) MD simulations to test stability: To support the docking hypothesis, the selected poses for compounds **4**, **5** and **6** were tested for their stability in pocket P9. Furthermore, the interaction of selected poses with ARG77-C was determined for every frame.

Analysis: For the analysis of the MD simulation, the trajectory was aligned based on the protein. The root mean square deviation (RMSD) was calculated to assess the deviation of atom positions compared to the starting pose over time. Furthermore, distances between the interacting protein and ligand atoms for the hydrogen bond were tracked over the whole trajectory.

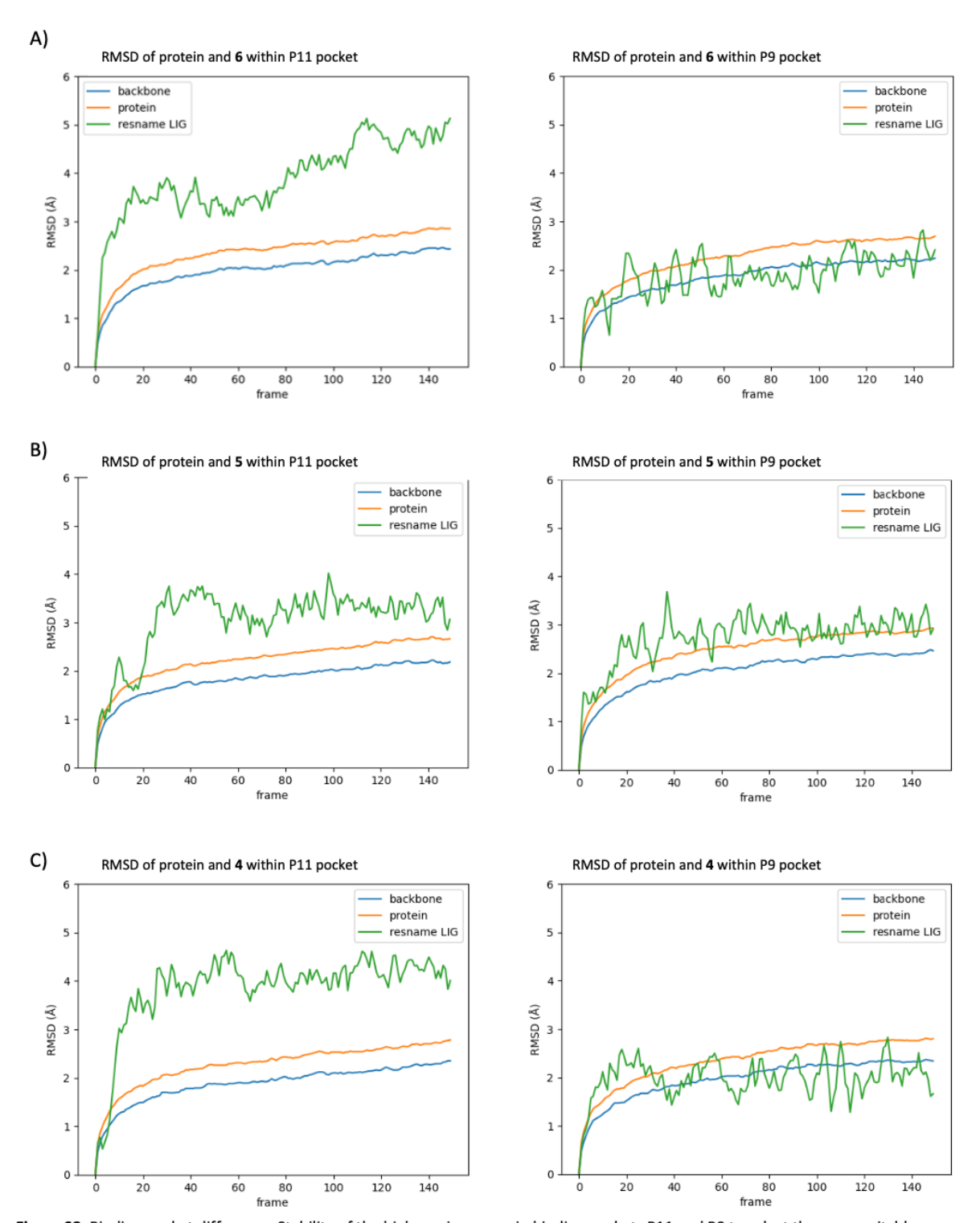


Figure S8. Binding pocket difference: Stability of the high scoring poses in binding pockets P11 and P9 to select the more suitable starting structure for this study. Results are shown for the three compounds: A) 6, B) 5 and C) 4. Left: Results for pocket P11, right results for pocket P9.

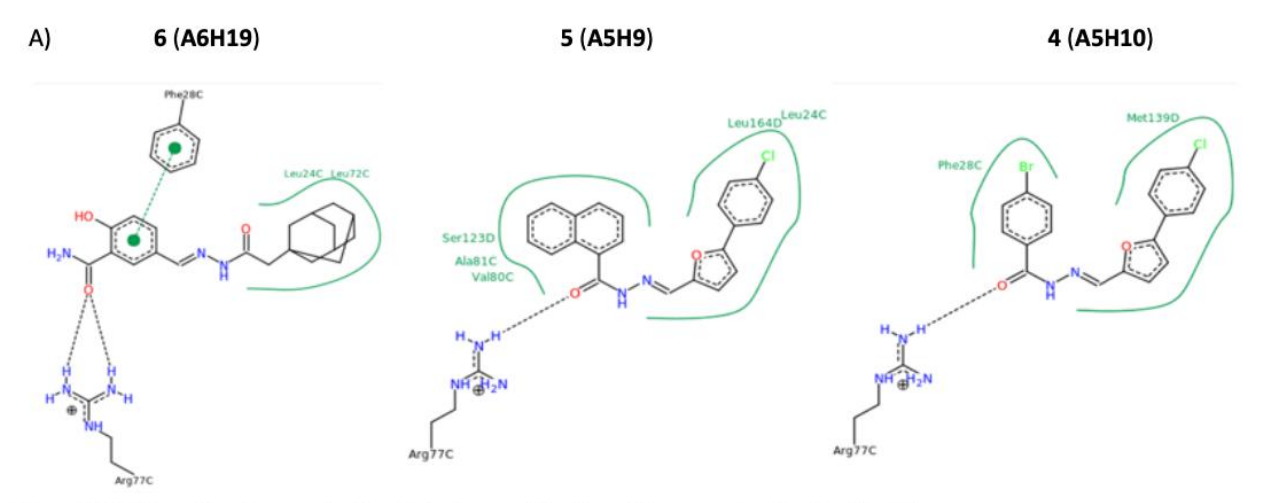


Figure S9. 2D interaction diagrams for the selected poses of the three hit compounds using PoseView.<sup>22</sup>

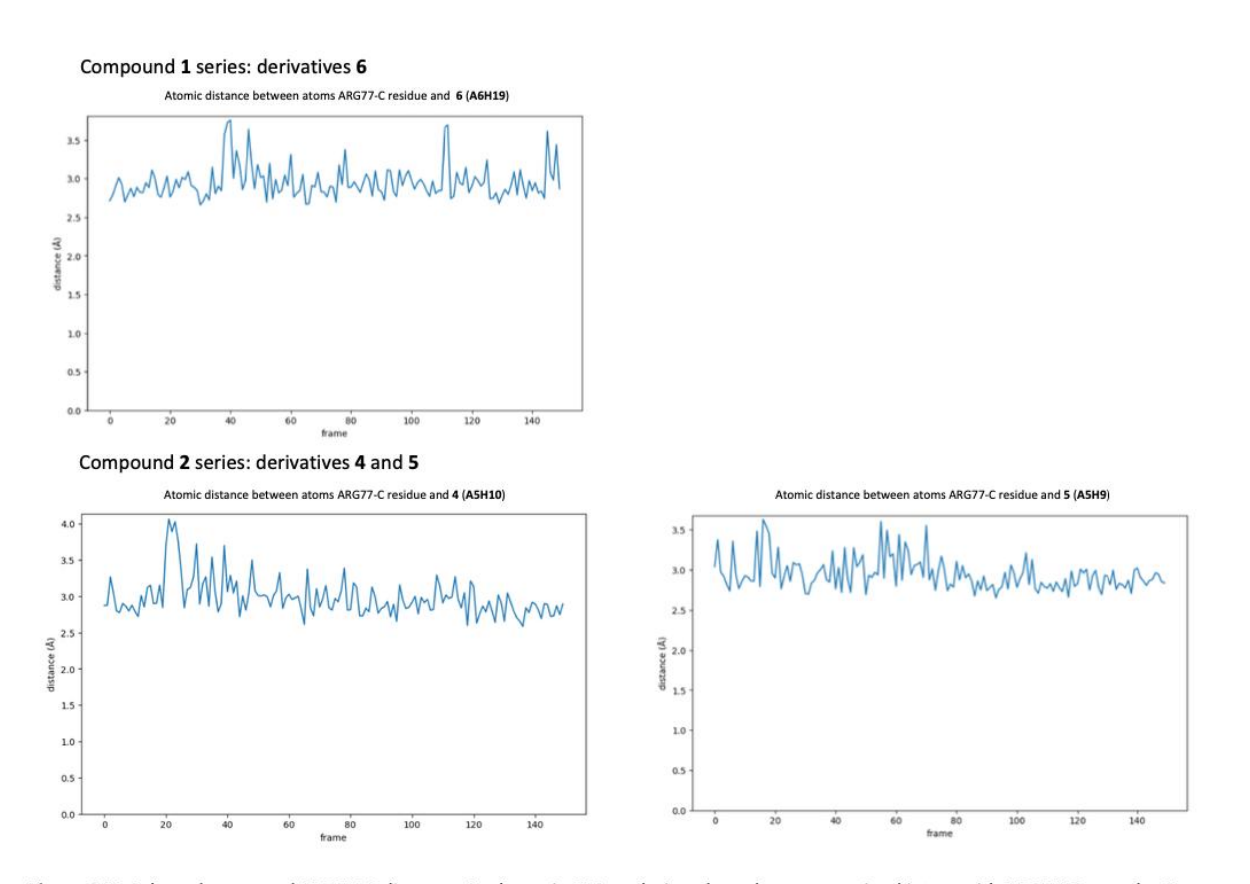


Figure S10. Selected poses and ARG77-C distance: As shown in MD analysis, selected poses remained intact with ARG77-C over the 6 picoseconds.

#### **SUPPLEMENTARY FIGURES**

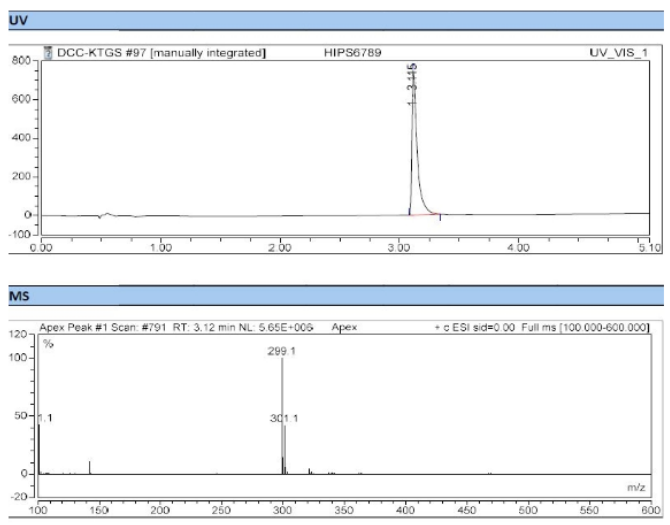


Figure S11. HPLC purity analysis of A1H5.

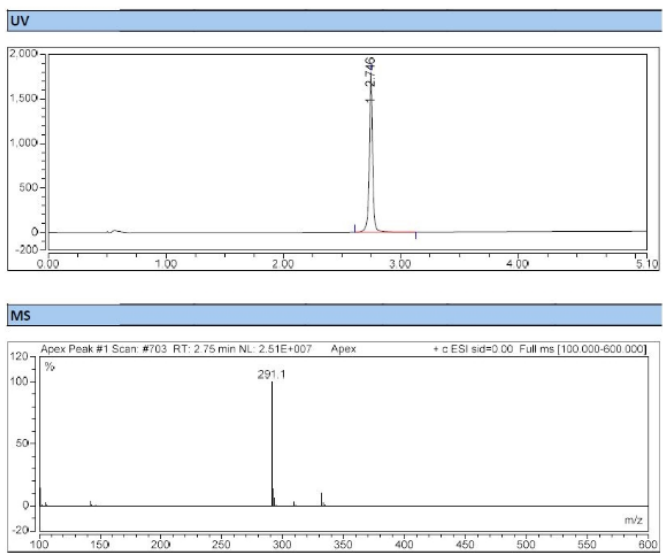


Figure S12. HPLC purity analysis of A3H8.

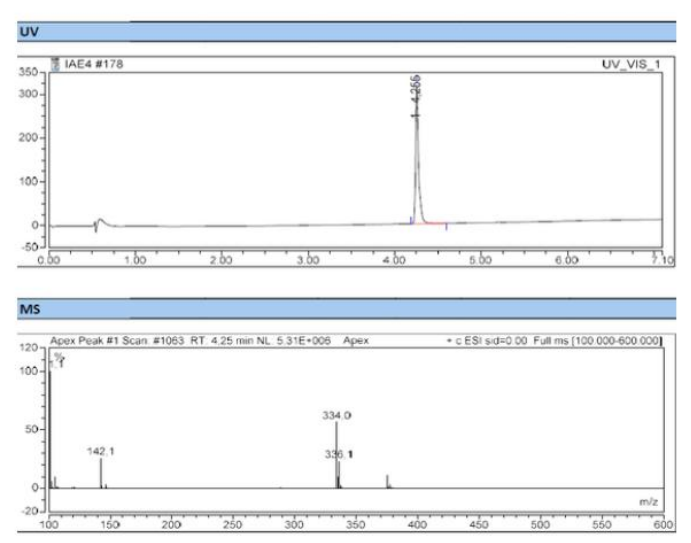


Figure S13. HPLC purity analysis of A2H5.

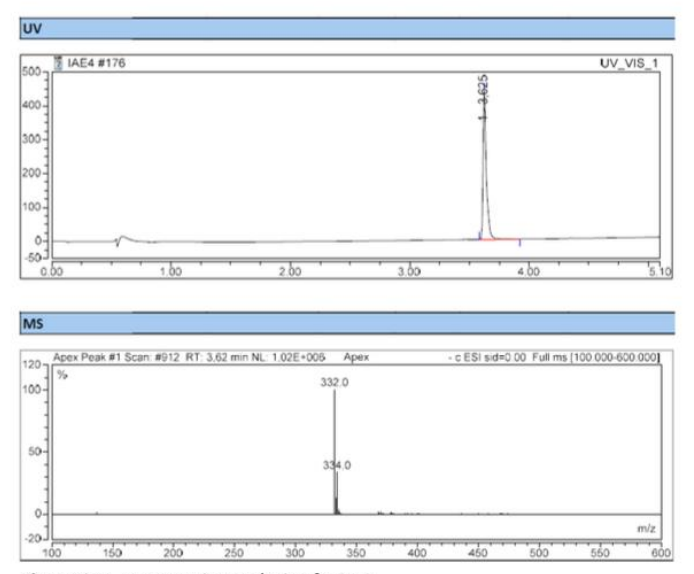
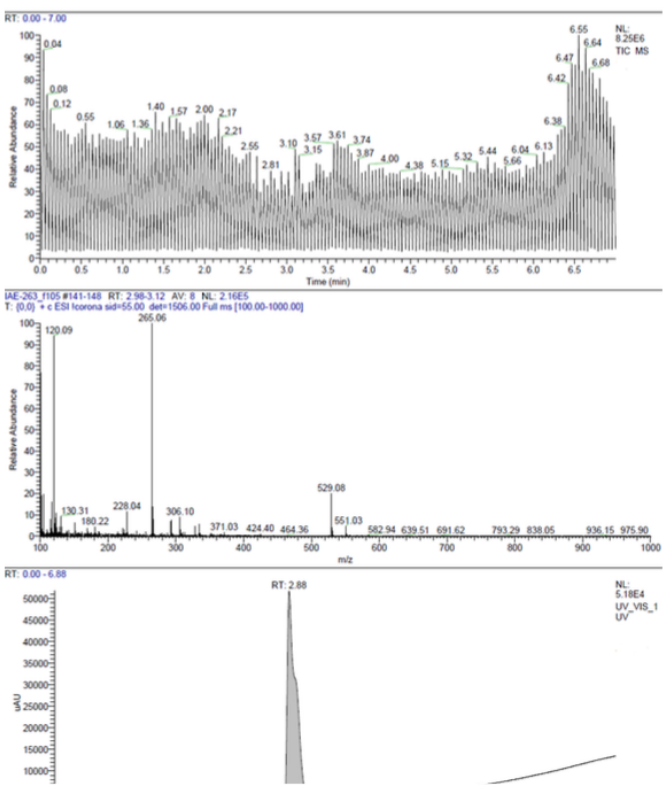


Figure S14. HPLC purity analysis of A2H6.



**Figure S15.** HPLC purity analysis of compound **A1H7** as a mixture of both rotamers.

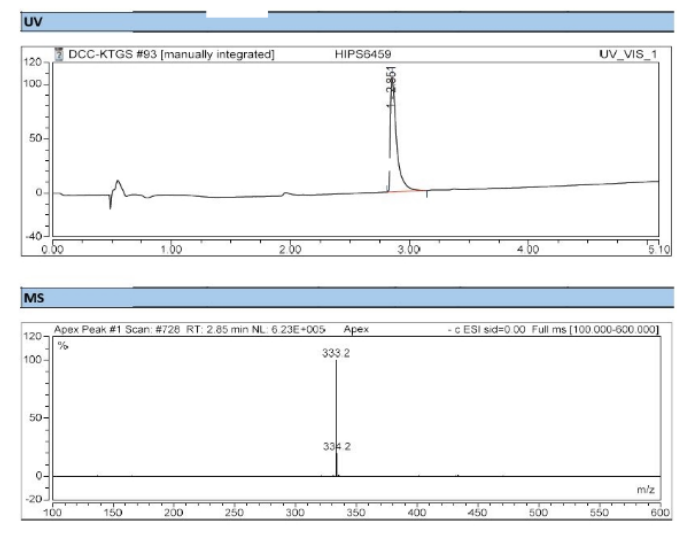
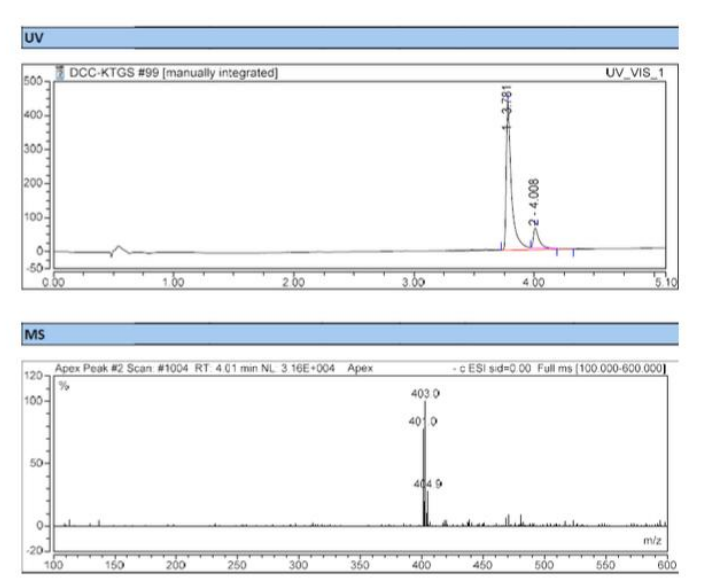
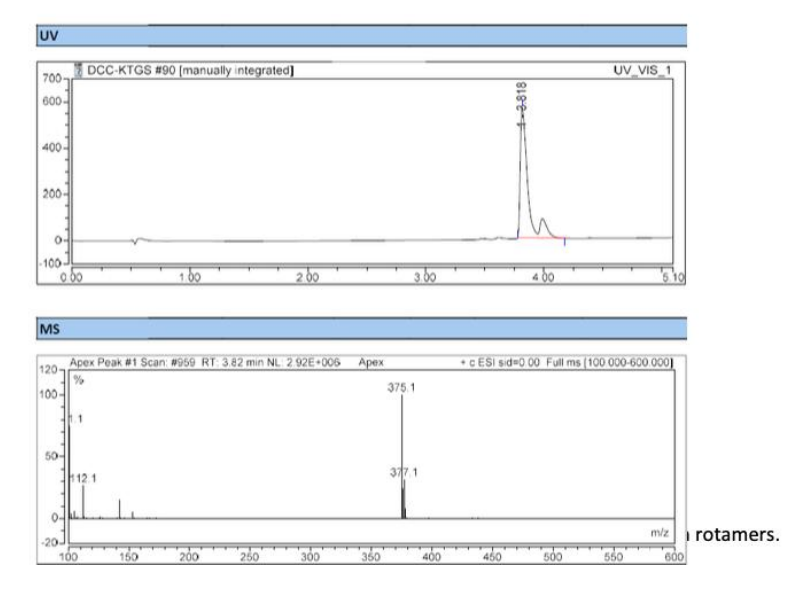


Figure S16. HPLC purity analysis of compound 3 (A4H9).



 $\textbf{Figure S17}. \ \textbf{HPLC purity analysis of compound 4 (A5H10)} \ as \ a \ mixture \ of \ both \ rotamers.$ 



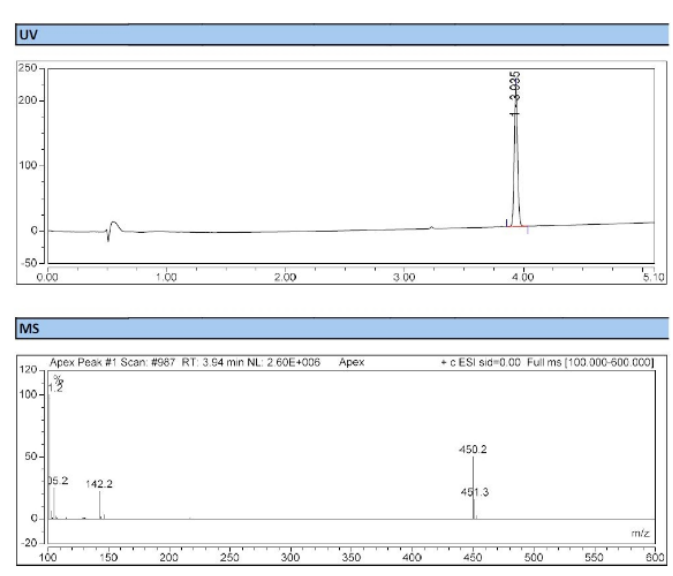


Figure \$19. HPLC purity analysis of A7H15.

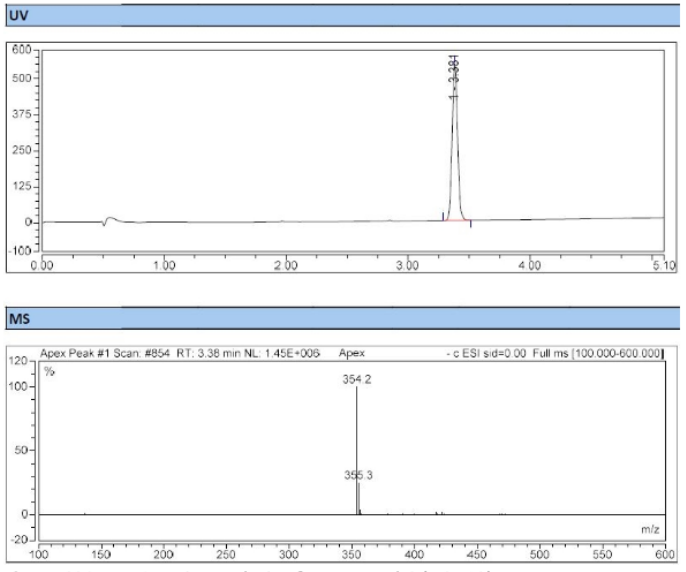


Figure S20. HPLC purity analysis of compound 6 (A6H19).

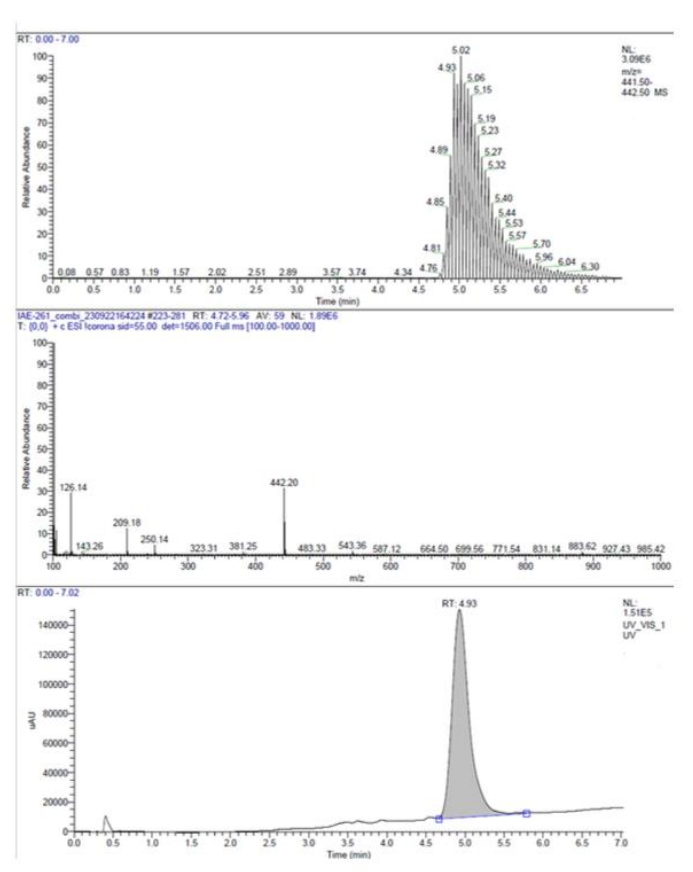


Figure S21. HPLC purity analysis of compound A7H19.

#### **Supplementary References**

- 1 R. P. Jumde, M. Guardigni, R. M. Gierse, A. Alhayek, D. Zhu, Z. Hamid, S. Johannsen, W. A. M. Elgaher, P. J. Neusens, C. Nehls, J. Haupenthal, N. Reiling and A. K. H. Hirsch, *Chem. Sci.*, 2021, **12**, 7775–7785.
- 2 A. Shams, unpublished work.
- 3 O. Ramström and J. M. Lehn, *Nat. Rev. Drug Discov.*, 2022, **1**, 26–36.
- 4 M. Durgun, H. Turkmen, M. Ceruso and C. T. Supuran, Bioorg Med Chem, 2016, 24, 982-988.
- 5 S. N. P. V. V. Syakaev, B. I. Buzykin, S. K. Latypov, W. D. Habicher, A. I. Konovalov, *J. Mol. Struct.*, 2006, **788**, 55-62.
- T. L. M. S. F. Altschul, A. A. Schäffer, J. Zhang, Z. Zhang, W. Miller and D. J. Lipman, Nucleic Acids Res. 1997, 25, 3389–3402
- J. C. W. S. F. Altschul, E. M. Gertz, R. Agarwala, A. Morgulis, A. A. Schäffer, Yi. K. Yu, FEBS J., 2005, 272, 5101
   5109
- 8 P. Di Tommaso, S. Moretti, I. Xenarios, M. Orobitg, A. Montanyola, J. M. Chang, J. F. Taly and C. Notredame, *Nucleic Acids Res.*, 2011, **39**, W13–W17.
- 9 C. Notredame, D. G. Higgins and J. Heringa, J. Mol. Biol., 2000, 302, 205-217.
- 10 Tutorial: How to generate a publication-quality multiple sequence alignment, https://labs.mcdb.ucsb.edu/weimbs/thomas/sites/labs.mcdb.ucsb.edu.weimbs.thomas/files/docs/multiplesequencealignmenttutorial.pdf.
- 11 L. J. Swier, A. Guskov and D. J. Slotboom, *Nat. Commun.*, 2016, **7**, 11072.
- 12 S. Bousis, S. Winkler, J. Haupenthal, F. Fulco, E. Diamanti and A. K. H. Hirsch, Int. J. Mol. Sci., 2022, 23.
- 13 J. Haupenthal, C. Baehr, S. Zeuzem and A. Piiper, Int. J. Cancer., 2007, 121, 206-210.
- 14 E. Diamanti, P. C. T. Souza, I. Setyawati, S. Bousis, L. M. Gómez, L. J. Y. M. Swier, A. Shams, A. Tsarenko, W. K. Stanek, M. Jäger, S. J. Marrink, D. J. Slotboom and A. K. H. Hirsch, *Communications Biology*, 2023, **6**, 1182.
- 15 SeeSAR version 13.0.3 BioSolvelT GmbH, Sankt Augustin, Germany, 2023.
- 16 N. Schneider, G. Lange, S. Hindle, R. Klein and M. Rarey, J. Comput. Aided Mol. Des., 2013, 27, 15-29.
- 17 P. Eastman ,J. Swails, J. D. Chodera, R. T. McGibbon, Y. Zhao, K. A. Beauchamp, L. P. Wang, A. C. Simmonett, M. P. Harrigan, C. D. Stern, R. P. Wiewiora, B. R. Brooks and V. S. Pande, *PLoS Comput. Biol.*, 2017, 13, e1005659.
- 18 Landrum, G. 2010. "RDKit." Q2. https://www.rdkit.org/.
- 19 J. Wang, R. M. Wolf, J. W. Caldwell, P. A. Kollman and D. A. Case, J. Comput. Chem., 2004, 25, 1157-1174.
- W. L. Jorgensen, J. Chandrasekhar, J. D. Madura; R. W. Impey and M. L. Klein, J. Chem. Phys., 1983, 79, 926–935
- 21 J. A. Izaguirre C. R. Sweet and V. S. Pande, Pac Symp Biocomput., 2010, 240–251.
- 22 K. Stierand and M. Rarey, ACS Med. Chem. Lett., 2010, 1, 540–545.

# 3.3 Chapter C: Investigation of the rescue effect of energy coupling factor inhibitors against roseoflavin toxicity in *Streptococcus pneumoniae*

Shams A.; Zeimetz L., Haupenthal J.; Bousis S.; Hirsch Anna K. H: Investigation of the rescue effect of energy coupling factor inhibitors against roseoflavin toxicity in *Streptococcus pneumoniae*. The manuscript and experimental protocol are currently in preparation.

The authors would like to thank Simone Amann, a technical assistant of the department DDOP, for her support and assistance in performing the assay.

#### **Abstract**

This chapter describes the optimization of antimicrobial assays focusing on the interaction between roseoflavin (RoF), a toxic riboflavin analog, and energy-coupling factor (ECF) transporters in *Streptococcus pneumoniae*. The study investigates the minimum inhibitory concentrations of RoF and various test compounds, both individually and in combination, to assess potential synergistic or antagonistic effects on bacterial growth. The findings aim to elucidate the mechanisms by which ECF transporter inhibitors influence RoF uptake and efficacy.

#### Introduction

Vitamins are essential organic compounds that serve as enzymatic cofactors across all living organisms. Riboflavin, also known as vitamin B<sub>2</sub>, is a water-soluble vitamin essential for various cellular processes, including energy production and the metabolism of fats, drugs, and steroids. Riboflavin is particularly important as a precursor to the critical redox cofactors flavin mononucleotide (FMN) and flavin adenine dinucleotide (FAD). Interestingly, certain human pathogens, including *Listeria*, *Streptococcus*, and *Enterococcus*, lack the necessary enzymes for synthesizing riboflavin *de novo*. Instead, these bacteria rely on energy-coupling factor (ECF) transporters, specifically the RibU subunit, to acquire riboflavin from their environment. As a result, the ECF-RibU system appears to be the primary or exclusive means of riboflavin uptake in these pathogens<sup>56</sup>.

Roseoflavin (RoF) is a structural analog of riboflavin and its phosphorylated derivative, FMN. Isolated from the Gram-positive bacterium *Streptomyces davawensis*, RoF exhibits antibiotic activity against various Gram-positive bacteria, including *Bacillus subtilis* and *Staphylococcus aureus*. Riboswitches are gene-regulating elements that modulate gene expression upon binding specific metabolites. In *B. subtilis*, the FMN riboswitch regulates genes responsible for riboflavin biosynthesis and transport by binding to FMN. Notably, RoF can bind directly to FMN riboswitches, leading to downregulation of associated genes. This interaction suggests that RoF may exert its antimicrobial effects by targeting FMN riboswitches, thereby disrupting essential metabolic processes in bacteria<sup>57</sup>.

### Aim of the assay

RoF, as a riboflavin analog, is presumed to require binding to riboflavin-specific ECF transporters for uptake. Given this, the present study aims to investigate the impact of our test compounds on bacterial growth in combination with RoF. Depending on their mode of action, the compounds may exhibit one of two potential effects: (i) growth inhibition or a synergistic interaction if the compounds amplify RoF's antimicrobial activity and work in concert with it; or (ii) a rescue effect, where the compounds counteract RoF toxicity and restore bacterial growth by inhibition of the corresponding ECF transporter.

Based on the hypothesized mechanism of action, the tested compounds are expected to exhibit a rescue effect. This assumption is based on the idea that the compounds function as inhibitors of the ECF transport group II by binding to the ECF module, thereby disrupting the transport cycle of various S-components, including RibU<sup>50</sup>. If RibU-mediated riboflavin uptake is inhibited, RoF, which is a structurally similar antimicrobial, would also be unable to enter bacterial cells. As a result, bacteria would evade RoF-induced toxicity, leading to a rescue rather than inhibitory effect. This study aims to experimentally confirm this hypothesis by assessing bacterial growth under different treatment conditions.

#### **Materials and Methods**

This assay was first developed for *B. subtilis* and then adapted and optimized for *S. pneumoniae*.

## 1. Determination of Minimum Inhibitory Concentration (MIC):

MICs for RoF and selected compounds were determined. The MIC assay was performed based on a previously published protocol<sup>58</sup>.

## 2. Rescue or inhibition effect studies using RoF:

To prepare Todd–Hewitt Medium (THM) with 0.1% choline, the medium was sterilized in an appropriate flask by autoclaving. Under sterile conditions, 0.1% choline was added to the autoclaved medium, with the final mixture remaining stable for 20 days. For culture preparation, *S. pneumoniae (DSM20566)* was inoculated in 15 mL of THM and incubated at 37 °C with 5% CO<sub>2</sub> for 24 hours or more without shaking, with the Erlenmeyer covered using a breathable seal. After 24 hours, the Optical Density (OD<sub>600</sub>) was measured, aiming for a target OD of 0.6–1. The culture was then diluted to an OD of 0.06 in THM before being added to the assay plate, ensuring a final concentration of 0.03 in the well plate. For the assay, a plate layout was prepared, and the stock concentrations of each compound and RoF were calculated. A total of 2  $\mu$ L of DMSO or test compounds was added to each well, or 1  $\mu$ L from each compound and RoF was used for combinations. Then, 98  $\mu$ L of diluted culture (OD 0.06) and 100  $\mu$ L of THM were added to each well. The contents in each well were gently mixed before being placed in a Fluostar plate reader. The plate reader was set to 37 °C with 5% CO<sub>2</sub>, and measurements were run for 24 hours without shaking, with absorbance data collected every 10 min from the center of each well. Finally, the data were analyzed using Excel or GraphPad Prism.

The assay included control groups consisting of RoF only, compounds only, DMSO only, and medium without additives. The test groups included combinations of RoF and compounds at sub-MIC concentrations to better observe the effect.

#### Results and discussion

The MICs for RoF and the selected compounds were successfully determined (Table 2).

**Table 2:** Minimum inhibitory concentration (MIC) values for the selected ECF inhibitors and roseoflavin, a toxic analogue of riboflavin, are presented. MIC values provide essential information on the lowest concentration of

each compound required to inhibit bacterial growth.

Compound name	MIC value (μM)
HIPS 6989	$2.5 \pm 0.1$
HIPS 8231	$5.2 \pm 0.3$
HIPS 8235	$3.4 \pm 1.1$
Roseoflavin (RoF)	$22.0 \pm 6.6$

In this assay, these selected compounds supposed to exhibit a rescue effect, mitigating the inhibitory impact of RoF on bacterial growth. This would align with the hypothesis that inhibition of the ECF module by these compounds prevents RoF from entering the cells, thereby reducing its antimicrobial efficacy.

The concentrations that were used in the assay were lower than their MIC values and at 1, 2, and 1 µM for 6989, 8231 and 8235, respectively. The compounds were tested at sub-MIC concentrations to assess their potential for inhibiting the ECF transporter without directly killing the bacteria. Even at these lower concentrations, the compounds may still partially inhibit the transporter. When combined with RoF (or acting against it), due to the expected rescue effect, their effect should not be the sum of their individual antibacterial effects. This approach allows for testing whether the compounds can block RoF uptake without causing bacterial death. Higher concentrations close to the MIC would likely result in bactericidal effects, making it difficult to differentiate between transporter inhibition and bacterial killing. By using sub-MIC concentrations, the study focuses specifically on transporter inhibition, ensuring that any observed effect is due to blocking RoF uptake rather than outcompeting RoF's toxicity. This method helps isolate the transporter-inhibiting potential of the compounds, rather than their bactericidal activity.

In **Figure 5**, the concentration of compound **HIPS 6989** in both conditions **A** and **B** was 1  $\mu$ M, while the RoF concentrations were at 1 and 5  $\mu$ M, respectively. In **5A**, the combination of RoF and the compound at 1  $\mu$ M resulted in the same OD as the compound alone, suggesting no synergy between them. This indicates that RoF does not enhance the compound's effect, and the compound's action dominates, with RoF not contributing significantly to the outcome at this concentration.

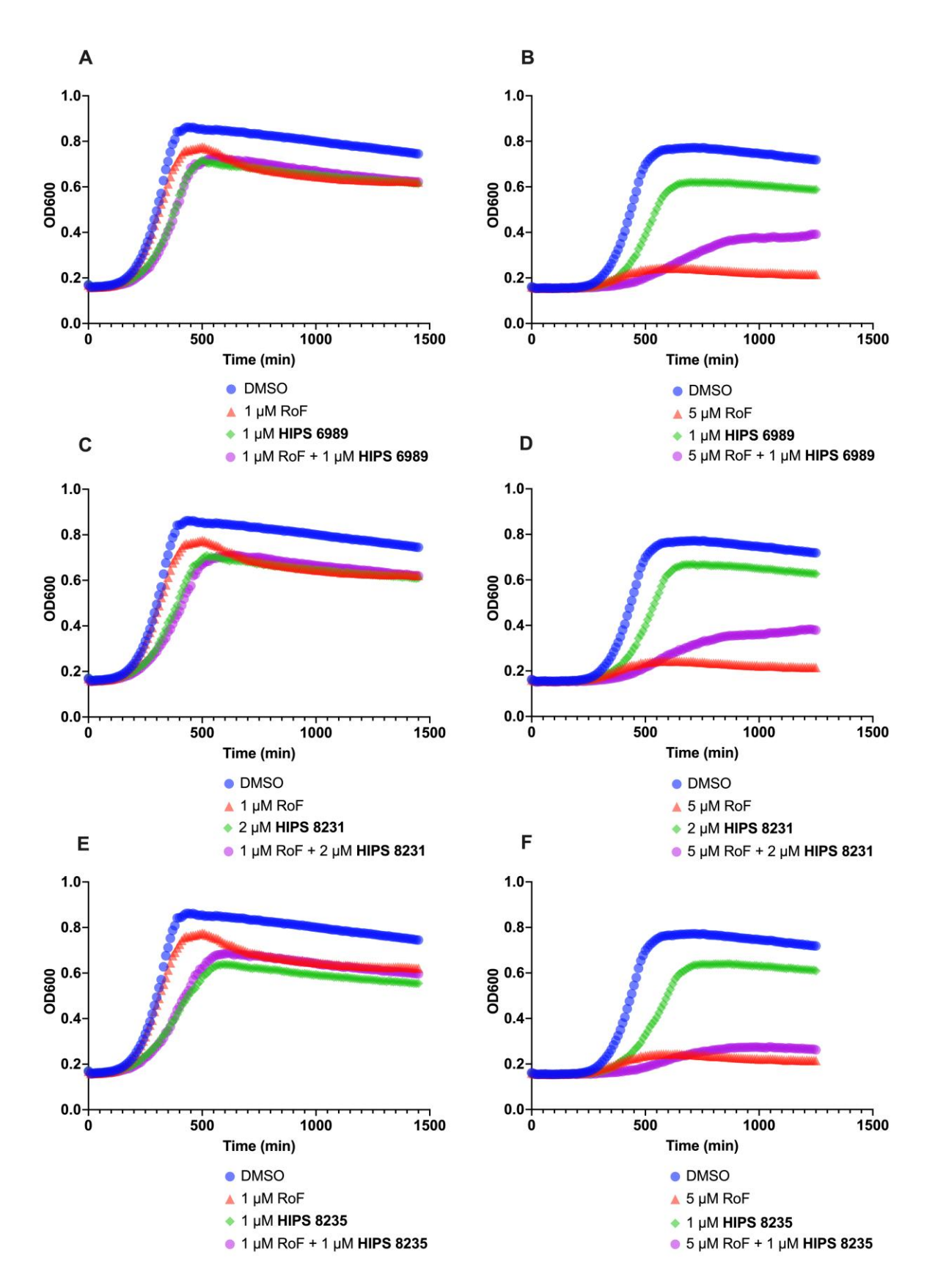


Figure 5: Rescue effect studies against roseoflavin (RoF) toxicity using *Streptococcus pneumoniae*. Figures A and B shows 1  $\mu$ M of HIPS 6989 with 1  $\mu$ M and 5  $\mu$ M of RoF, respectively. Figures C and D shows 2  $\mu$ M of

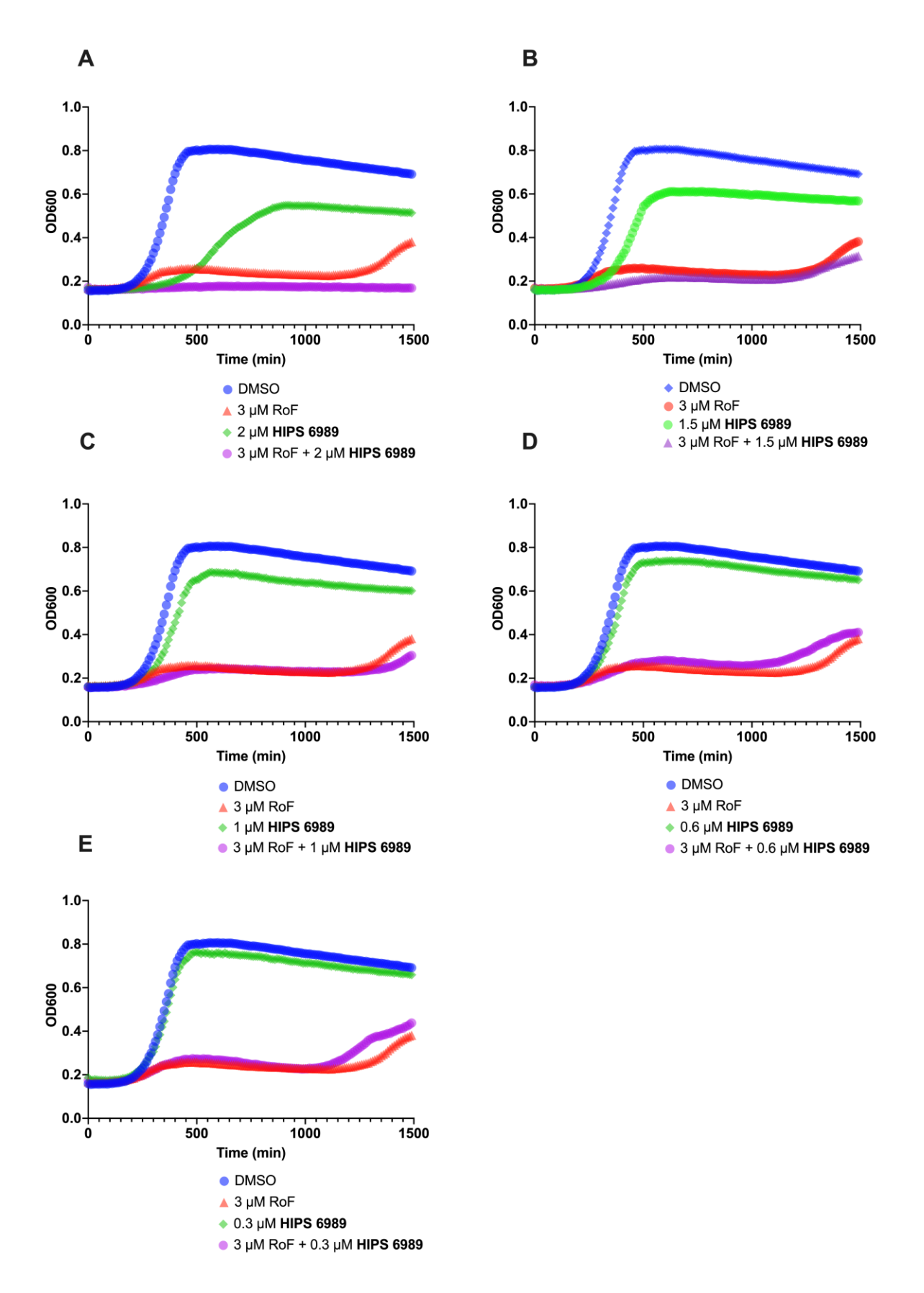
HIPS 8231 with 1  $\mu$ M and 5  $\mu$ M of RoF, respectively. Figures E and F shows 1  $\mu$ M of HIPS 8235 with 1  $\mu$ M and 5  $\mu$ M of RoF, respectively.

Figure **5B** exhibits that the OD for DMSO remains the same, while RoF at 5  $\mu$ M almost completely inhibits the growth. The compound at 1  $\mu$ M is close to the DMSO level, and initially, the combination of RoF and the compound results in a higher OD than RoF alone for the first 500 minutes. However, after this time, the OD of the combination treatment surpasses that of RoF alone, suggesting a delayed effect especially on the growth log phase. This could indicate that the compound is partially mitigating the inhibitory effect of RoF, but not to the full extent as when the compound is used alone. The combination seems to reduce RoF's impact, but it is not completely overcoming it, which could suggest a partial rescue effect or a modulatory interaction rather than a full rescue.

The same observation also applies to compound HIPS 8231, in both conditions C and D in Figure 5.

**Figure 5E** shows that the OD for RoF at 1  $\mu$ M alone is near to the DMSO control, while the compound alone results in a lower OD. The combination of RoF and the compound shows a similar OD to the compound alone, with only a slight increase. In Figure **5F**, RoF at 5  $\mu$ M shows the same effect as the other compounds, with the difference being that the rescue effect is slightly less pronounced.

In Figure 6, we selected one of the compounds to explore the effect of different concentrations on bacterial growth. The RoF concentration was set to 3  $\mu$ M, while compound HIPS 6989 was tested at concentrations of 0.3, 1, 1.5, and 2  $\mu$ M shown in Figure 6, A–E, respectively. As the concentration of the compound increased, a more pronounced inhibition of bacterial growth was observed. Interestingly, at lower concentrations, a better rescue effect was seen in the combination of compound and RoF test group. This could potentially be due to a reduced bactericidal effect at lower compound concentrations, which might allow the compound to focus more on inhibiting RoF uptake or lessening RoF's inhibitory impact, thereby promoting bacterial survival. At higher concentrations, the compound's bactericidal activity may overshadow these effects, making it less effective in mitigating RoF's impact. However, this is speculative and would require further investigation to fully understand the mechanism.



**Figure 6: rescue–effect studies.** Roseoflavin (RoF) toxicity was evaluated in *Streptococcus pneumoniae* in combination with **HIPS 6989** at different concentrations and 3 µM RoF.

The next step was to assess the competition between RoF at 1  $\mu$ M and three standard antibiotics with different mechanisms of action namely levofloxacin, ampicillin, and meropenem at 0.7, 0.025, 0.008  $\mu$ M, respectively (**Figure 7**).

Roseoflavin primarily targets FMN riboswitches, and its mode of action differs significantly from the three antibiotics mentioned:

Levofloxacin (fluoroquinolone) inhibits bacterial DNA gyrase and topoisomerase IV, enzymes crucial for DNA replication, transcription, repair, and recombination<sup>59</sup>. It acts as a bactericide by preventing DNA separation and supercoiling, ultimately stopping bacterial cell division<sup>60</sup>.

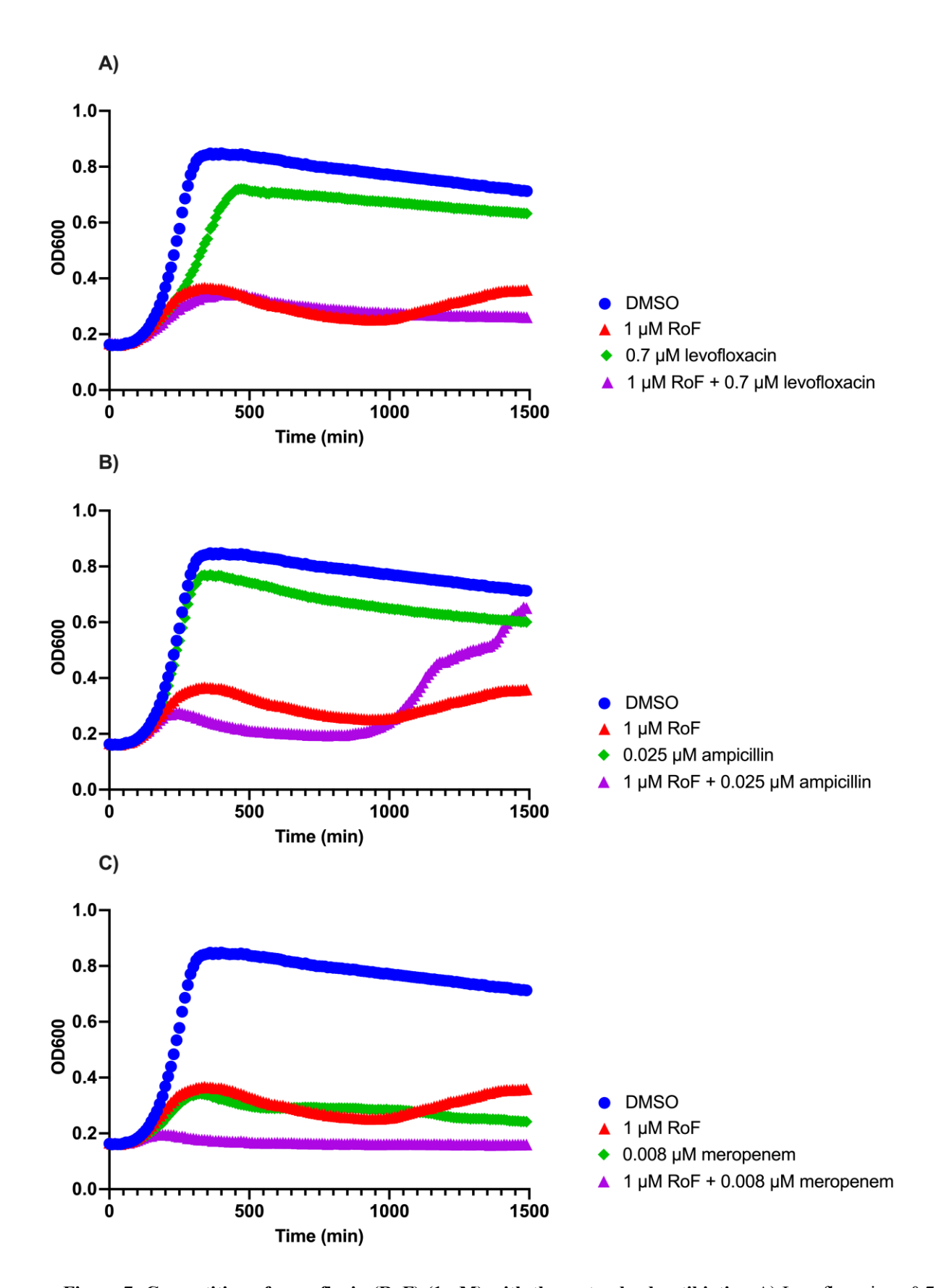


Figure 7: Competition of roseoflavin (RoF) (1  $\mu$ M) with three standard antibiotics. A) Levofloxacin at 0.7  $\mu$ M, B) Ampicillin at 0.025  $\mu$ M, and C) Meropenem at 0.008  $\mu$ M tested alone and in combination with RoF.

As a  $\beta$ -lactam antibiotic, ampicillin inhibits bacterial cell-wall synthesis by interfering with the cross-linking of peptidoglycan chains, leading to bacterial cell lysis  $^{61}$ .

Meropenem, a carbapenem antibiotic, is bactericidal and inhibits bacterial cell–wall synthesis. It penetrates bacterial cells and interferes with vital cell–wall component synthesis, causing cell death<sup>62</sup>. Meropenem is highly resistant to degradation by many  $\beta$ -lactamases<sup>63</sup>.

While direct competition between these antibiotics and roseoflavin is unlikely due to their different targets, testing them together could reveal interesting interactions and potential synergies (due to their different mechanisms of action) in their antimicrobial effects. Also, the antibiotics might affect the uptake of roseoflavin by altering membrane permeability or transport systems, potentially leading to apparent competition.

The growth curves reveal a synergistic effect when combining RoF with different antibiotics. Individually, 1 µM RoF significantly inhibits bacterial growth compared to the DMSO control. However, when combined with either 0.7 µM levofloxacin (**Figure 7A**), 0.025 µM ampicillin (**Figure 7B**), or 0.008 µM meropenem (**Figure 7C**), the growth inhibition is slightly increased, enhancing the overall antibacterial activity. Specifically, the ampicillin combination initially shows some suppression, then recovery, which suggests that the antibiotic might interfere with the mechanism of RoF by disrupting its uptake or activity within the bacterial cell, rather than acting synergistically to enhance growth inhibition.

#### **Conclusions**

The observed rescue effects support the proposed mechanism wherein ECF transporter inhibitors impede RoF uptake. Given that RoF relies on ECF transporters, such as ECF-RibU, for cellular entry, inhibiting these transporters prevents RoF's intracellular accumulation and can effectively reduce its antimicrobial activity. This finding underscores the importance of considering transporter-mediated uptake mechanisms when developing and evaluating antimicrobial agents.

#### **Key questions and challenges**

While this study demonstrates the potential of the assay in evaluation of our ECF inhibitors, several key questions and challenges remain. One important consideration is whether the current experimental controls are sufficient. Although they provide a solid foundation, including riboflavin-supplemented controls could further confirm roseoflavin competition and validate transporter specificity. Additionally, ensuring effective roseoflavin uptake requires confirmation of RibU expression under experimental conditions, which could be assessed through qPCR analysis. Another challenge is determining whether THB contains riboflavin, as trace amounts from complex components may influence experimental outcomes. Addressing

these questions will refine our understanding of ECF transporters and their role in bacterial metabolism, ultimately improving the development of targeted antimicrobial strategies.

## 4 Final Discussion

## 4.1 ECF transporter protein and its characterization

In Chapter A, the study explores the potential of ECF transporters as promising anti-infective targets to address antimicrobial resistance, specifically focusing on the ECF transporter for pantothenate in S. pneumoniae. It assesses the stability, binding affinities, and inhibitory effects of ECF transporter inhibitors in both in vitro and in vivo settings. The study's characterization of pantothenate ECF transporters offers key insights into their potential as antimicrobial targets. Through successful heterologous expression and purification of these transporters, the study establishes a foundation for further structural and functional investigations, including the complete ECF transporter complex for pantothenate (ECF-PanT) from S. pneumoniae, the ECF module from S. pneumoniae, and the full ECF transporter complex for folic acid (ECF-FoIT2) from Lactobacillus delbrueckii. The thermal stability of these proteins was examined, and optimal buffer conditions were identified to preserve their stability for subsequent assays. Binding affinities and inhibitory activities of six ECF inhibitors against the three ECF transporter proteins were evaluated using surface plasmon resonance (SPR). Both in vitro and in vivo assays confirm the inhibitory effects of these inhibitors, supporting their potential as drug targets. In conclusion, this study provides a comprehensive understanding of pantothenate ECF transporters and their crucial role in bacterial survival. These findings pave the way for future antimicrobial drug discovery, particularly in the fight against multidrug-resistant pathogens. Ongoing research into these transporters may lead to novel strategies to combat the growing threat of antibiotic resistance.

## 4.2 Targeting ECF protein by specifically designed compounds

In this study, we demonstrated the power of dynamic combinatorial chemistry as an effective tool for identifying and optimizing hit compounds targeting the ECF-PanT transporter of *S. pneumoniae*. By applying this method, we were able to identify high-affinity inhibitors that specifically block the transporter's activity, showing promising potential as antimicrobial agents. The use of biophysical assays like SPR and molecular modeling allowed us to refine the interactions between the ligands and the target, ensuring that the inhibitors were both potent and selective.

One significant advantage of DCC is its ability to generate diverse libraries of compounds with minimal synthesis time, which is crucial for hit optimization in drug discovery. This method enabled us to identify potential hits that could be further developed into lead compounds for treating infections caused by *S. pneumoniae* and possibly other bacteria with similar transporters. Furthermore, the SAR studies conducted in parallel helped in understanding the key features necessary for optimal binding and inhibition of the transporter, which can guide further optimization efforts.

Our findings suggest that selective inhibition of ECF transporters could offer a promising strategy to combat AMR. The transporter's role in nutrient uptake means its inhibition can interfere with bacterial growth without affecting human cells, potentially minimizing side effects. However, additional testing will be important to further evaluate the therapeutic potential and toxicity profile of these compounds.

In conclusion, dynamic combinatorial chemistry proves to be a powerful strategy in the quest for novel antimicrobial agents. The compounds identified in this study were effectively inhibiting the ECF-PanT, and with further optimization and preclinical testing, they could lead to the development of a new class of antibiotics targeting essential bacterial transporters.

## 4.3 Evaluation of binding, inhibitory Effect, and selectivity of ECF inhibitors

Recent research has investigated ECF transporters as promising targets for anti-infective therapies. Various *in vitro* assays, such as SPR and transport-activity tests, have been employed to evaluate the binding affinities and inhibitory effects of ECF-transporter inhibitors<sup>55</sup>. A new whole-cell screening assay utilizing *Lactobacillus casei* has been introduced as a fast and cost-effective approach to identify ECF transporter inhibitors in a native biological context<sup>58</sup>. The proteoliposome uptake assay also plays a critical role in the investigation of inhibitors throughout the drug-discovery process<sup>64</sup>. Additionally, coarse-grained molecular dynamics simulations have been used to investigate the binding modes and inhibition mechanisms of a promising class of ECF transporter inhibitors<sup>50</sup>. Together, these studies highlight the potential of ECF transporters as drug targets and the diverse *in vitro* and *in silico* techniques employed to assess inhibitor binding and effectiveness.

Recent studies have identified promising inhibitors targeting energy-coupling factor (ECF) transporters<sup>50,51,65</sup>. These transporters are attractive antibacterial targets due to their absence in humans and crucial role in bacterial metabolism<sup>50</sup>. Through virtual screening, design, and synthesis, we have developed a novel chemical class that effectively inhibit ECF transporters<sup>50,65</sup>.

The study of Diamanti et al. 2023 <sup>50</sup> demonstrates that **hit 1** compound selectively inhibits the transport of both folate via ECF-FolT2 and pantothenate via ECF-PanT, while showing no effect on the ABC transporter OpuA. The compound does not disrupt ATP hydrolysis or the lipid bilayer, confirming its selectivity for ECF transporters. Both ECF transporters share the same ECF module but use different S-components for substrate specificity. Despite the structural differences between ECF-FolT2 and ECF-PanT, the compound binds to a similar pocket at the interface of the S-component and ECF module. Site-directed mutagenesis experiments targeting Lys102 resulted in a loss of transport activity, suggesting the functional importance of this region, which is likely targeted by **hit 1** compound. However, the loss of activity prevented validation of the binding pocket. Coarse-grained molecular dynamics (CGMD) simulations revealed that **hit 1** interacts with polar residues in both transporters, reinforcing its inhibitory

effect. The absence of activity against the ABC transporter, combined with the mutagenesis and MD findings, conclusively supports the specificity of this compound for ECF transporters.

## 4.4 Qualitative mode of action in pathogens

The qualitative mode of action of ECF transporters in pathogens is an important area of study, particularly considering their role in the pathogen's ability to acquire essential nutrients. In *S. pneumoniae*, for example, the bacterium lacks the biosynthesis pathways to produce pantothenate and must rely on external sources to acquire it. Pantothenate is vital for synthesizing coenzyme A, which is necessary for a variety of key metabolic processes, including fatty acid synthesis, amino acid metabolism, and energy production<sup>66,67</sup>.

Given that *S. pneumoniae* cannot produce pantothenate, it depends heavily on its ability to uptake the vitamin from the environment. The energy-coupling factor (ECF) transporters responsible for this uptake are crucial for the bacterium's survival<sup>20</sup>, especially under nutrient-limited conditions such as those found within the human host. If the uptake of pantothenate is disrupted, it could have severe consequences for the pathogen's metabolism. Without an adequate supply of pantothenate, the bacterium would be unable to synthesize CoA, leading to metabolic blockages in essential pathways. The inhibition of pantothenate uptake could specifically impair the Krebs cycle, fatty acid synthesis, and other CoA-dependent processes. These metabolic disruptions could effectively prevent the bacterium from growing and replicating, making ECF transporters an attractive target for therapeutic intervention.

Disrupting group II ECF transporters could impair the uptake of multiple essential vitamins, potentially exerting a broad-spectrum effect on pathogens that rely on these nutrients. While this approach may significantly hinder pathogen metabolism by blocking the acquisition of key vitamins, its effectiveness is not guaranteed due to the high adaptability of bacteria. For instance, pathogens like *Streptococcus pneumoniae* may develop compensatory mechanisms, such as upregulating alternative transporters or acquiring new genes via horizontal gene transfer to re-establish vitamin biosynthesis pathways, thereby bypassing the need for external uptake. Moreover, some pathogens already possess the genetic machinery to synthesize their own vitamins, making them less susceptible to strategies that target nutrient acquisition systems like ECF transporters. However, biosynthesis is likely more energy-intensive than uptake, which suggests that even pathogens capable of producing their own vitamins could still be affected, albeit to a lesser extent. Therefore, it is hypothesized that ECF transporter inhibitors could impact most bacteria, with those relying solely on uptake being more vulnerable than those with endogenous biosynthesis capabilities. Consequently, targeting ECF transporters alone may not be sufficient as a universal antimicrobial strategy. A more comprehensive approach, which considers the specific metabolic requirements and capabilities of individual pathogens and potentially combines ECF transporter inhibition with the disruption of other

metabolic pathways or transporter systems, may be necessary to effectively counteract bacterial adaptability and ensure broad-spectrum efficacy.

To experimentally monitor adaptation in response to disrupted pantothenate uptake in S. pneumoniae, several strategies can be employed. Transcriptomic analyses, such as RNA sequencing, can be used to observe changes in gene expression over time, particularly the upregulation of alternative transporters or pathways involved in vitamin biosynthesis. In addition, whole-genome sequencing of bacterial populations exposed to the inhibitor over time could reveal genetic adaptations, such as the acquisition of new genes through horizontal gene transfer that restore pantothenate biosynthesis. Proteomic approaches can complement this by identifying changes in protein expression profiles, while metabolomic analyses may help detect shifts in metabolite levels that indicate the activation of compensatory metabolic pathways. Finally, functional assays such as testing whether overexpression of specific genes or supplementation with alternative pantothenate sources restores growth can be used to confirm the physiological relevance of observed changes. Together, these methods would provide a comprehensive view of adaptation to nutrient stress caused by ECF transporter inhibition.

In conclusion, while the disruption of vitamin uptake through targeting ECF transporters presents a promising avenue for therapeutic intervention in pathogens like *S. pneumoniae*, the approach is not without its challenges. The pathogens' ability to adapt and their varying requirements for vitamin uptake or biosynthesis will require a deeper understanding of the specific nutrient dependencies of pathogens and the potential for resistance mechanisms, ensuring that therapeutic strategies remain effective across a broad range of bacterial species.

## 5 Outlook

#### **Advancement in Structural and Functional Studies**

Further structural elucidation of complete ECF transporter complexes is essential to guide rational inhibitor design. Ongoing efforts, such as the cryo-EM analysis of the ECF-PanT structure, aim to provide deeper insights into complex architecture. In addition, investigating the dynamic conformational changes of ECF transporters during substrate binding and transport will enhance our understanding of their functional mechanisms.

#### **Optimization of ECF Inhibitors**

To improve potency and selectivity, dynamic combinatorial chemistry approaches should be expanded for the refinement of initial hit compounds. SAR studies will be critical to optimizing efficacy and reducing potential off-target effects.

## In Vivo Validation and Preclinical Development

Comprehensive in vivo studies are necessary to assess the pharmacokinetics, bioavailability, and toxicity of optimized inhibitors in animal models. The development of infection models relevant to disease conditions will facilitate evaluation of therapeutic efficacy in a physiological context.

## **Mechanistic Insights into ECF Transporters**

Understanding the transport mechanisms of ECF proteins under physiological conditions remains a priority. MD simulations and targeted mutagenesis studies will aid in identifying key residues involved in substrate transport and inhibitor binding.

#### **Broader Antimicrobial Targeting Strategies**

Beyond *S. pneumoniae*, the potential of targeting ECF transporters in other clinically relevant bacterial pathogens should be explored. Combinatory approaches with existing antibiotics may offer synergistic effects, improving therapeutic outcomes and reducing the likelihood of resistance development.

#### **Overcoming Potential Resistance Mechanisms**

It is crucial to investigate how bacteria might adapt to ECF-targeted therapies, including the emergence of alternative transport pathways and the role of horizontal gene transfer. These insights will help in designing robust strategies to prevent or overcome resistance.

#### **Clinical Translation Potential**

To realize the clinical potential of ECF inhibitors, further studies should evaluate formulation strategies for effective drug delivery. Collaboration with pharmaceutical partners will be essential for advancing lead compounds into preclinical and clinical development phases.

## 6 References

- (1) Mancuso, G.; Midiri, A.; Gerace, E.; Biondo, C. Bacterial Antibiotic Resistance: The Most Critical Pathogens. Pathogens. MDPI October 1, 2021. https://doi.org/10.3390/pathogens10101310.
- (2) Salam, M. A.; Al-Amin, M. Y.; Salam, M. T.; Pawar, J. S.; Akhter, N.; Rabaan, A. A.; Alqumber, M. A. A. Antimicrobial Resistance: A Growing Serious Threat for Global Public Health. *Healthcare (Switzerland)*. Multidisciplinary Digital Publishing Institute (MDPI) July 1, 2023. https://doi.org/10.3390/healthcare11131946.
- (3) Ferraz, M. P. Antimicrobial Resistance: The Impact from and on Society According to One Health Approach. *Societies*. Multidisciplinary Digital Publishing Institute (MDPI) September 1, 2024. https://doi.org/10.3390/soc14090187.
- Munita, J. M.; Arias, C. A. Mechanisms of Antibiotic Resistance. *Microbiol Spectr* 2016,
   4 (2). https://doi.org/10.1128/microbiolspec.VMBF-0016-2015.
- (5) Kurihara, M. N. L.; Sales, R. O. de; Silva, K. E. da; Maciel, W. G.; Simionatto, S. Multidrug-Resistant Acinetobacter Baumannii Outbreaks: A Global Problem in Healthcare Settings. *Revista da Sociedade Brasileira de Medicina Tropical*. NLM (Medline) 2020, p e20200248. https://doi.org/10.1590/0037-8682-0248-2020.
- (6) Power, E. REVIEW Impact of Antibiotic Restrictions: The Pharmaceutical Perspective.
- (7) Bankar, N. J.; Ugemuge, S.; Ambad, R. S.; Hawale, D. V; Timilsina, D. R. Implementation of Antimicrobial Stewardship in the Healthcare Setting. *Cureus* **2022**. https://doi.org/10.7759/cureus.26664.
- (8) Essack, S. Water, Sanitation and Hygiene in National Action Plans for Antimicrobial Resistance. *Bull World Health Organ* **2021**, *99* (8), 606–608. https://doi.org/10.2471/BLT.20.284232.
- (9) Lin, D. M.; Koskella, B.; Lin, H. C. Phage Therapy: An Alternative to Antibiotics in the Age of Multi-Drug Resistance. *World J Gastrointest Pharmacol Ther* **2017**, *8* (3), 162. https://doi.org/10.4292/wjgpt.v8.i3.162.
- (10) Kaprou, G. D.; Bergšpica, I.; Alexa, E. A.; Alvarez-Ordóñez, A.; Prieto, M. Rapid Methods for Antimicrobial Resistance Diagnostics. *Antibiotics*. MDPI AG February 1, 2021, pp 1–30. https://doi.org/10.3390/antibiotics10020209.
- (11) Bhat, M. J.; Al-qahtani, M.; Badawi, A. S.; Asiri, G. B.; Alhmare, A. M.; Rashid, A.; Altalhiyyah, K. S.; Alwimny, A. A. Awareness and Knowledge of Antibiotic Resistance and Risks of Self-Medication With Antibiotics Among the Aseer Region Population, Saudi Arabia, 2023. *Cureus* 2023. https://doi.org/10.7759/cureus.40762.
- (12) Ahmed, S. K.; Hussein, S.; Qurbani, K.; Ibrahim, R. H.; Fareeq, A.; Mahmood, K. A.; Mohamed, M. G. Antimicrobial Resistance: Impacts, Challenges, and Future Prospects.

- Journal of Medicine, Surgery, and Public Health **2024**, 2, 100081. https://doi.org/10.1016/j.glmedi.2024.100081.
- (13) Semba, R. D. The Discovery of the Vitamins. *International Journal for Vitamin and Nutrition Research* **2012**, 82 (5), 310–315. https://doi.org/10.1024/0300-9831/a000124.
- (14) Darnton-Hill, I. Public Health Aspects in the Prevention and Control of Vitamin Deficiencies. *Current Developments in Nutrition*. Oxford University Press September 1, 2019. https://doi.org/10.1093/CDN/NZZ075.
- (15) Axita, V. P.; Prachi, P. K.; Payal, G. K.; Parth, M. R.; Zalak, R. R.; Meenu, S. S. Peer-Reviewed, Multidisciplinary & Multilingual Journal A REVIEW ON VITAMINS: IT'S BIOLOGICAL ROLE AND DEFICIENCIES IN HUMANS. **2022**.
- (16) LeBlanc, J. G. Introductory Chapter: B-Group Vitamins. In *B Group Vitamins Current Uses and Perspectives*; InTech, 2018. https://doi.org/10.5772/intechopen.80023.
- (17) Andrès, E.; Lorenzo-Villalba, N.; Terrade, J. E.; Méndez-Bailon, M. Fat-Soluble Vitamins A, D, E, and K: Review of the Literature and Points of Interest for the Clinician. *Journal of Clinical Medicine*. Multidisciplinary Digital Publishing Institute (MDPI) July 1, 2024. https://doi.org/10.3390/jcm13133641.
- (18) Kiani, A. K.; Dhuli, K.; Donato, K.; Aquilanti, B.; Velluti, V.; Matera, G.; Iaconelli, A.; Connelly, S. T.; Bellinato, F.; Gisondi, P.; Bertelli, M. Main Nutritional Deficiencies. *Journal of preventive medicine and hygiene*. NLM (Medline) June 1, 2022, pp E93–E101. https://doi.org/10.15167/2421-4248/jpmh2022.63.2S3.2752.
- (19) Jaehme, M.; Slotboom, D. J. Diversity of Membrane Transport Proteins for Vitamins in Bacteria and Archaea. *Biochimica et Biophysica Acta General Subjects*. Elsevier 2015, pp 565–576. https://doi.org/10.1016/j.bbagen.2014.05.006.
- (20) Bousis, S.; Setyawati, I.; Diamanti, E.; Slotboom, D. J.; Hirsch, A. K. H. Energy-Coupling Factor Transporters as Novel Antimicrobial Targets. **2018**, *1800066*, 1–17. https://doi.org/10.1002/adtp.201800066.
- (21) Sambon, M.; Wins, P.; Bettendorff, L. Neuroprotective Effects of Thiamine and Precursors with Higher Bioavailability: Focus on Benfotiamine and Dibenzoylthiamine. *International Journal of Molecular Sciences*. MDPI June 1, 2021. https://doi.org/10.3390/ijms22115418.
- (22) Tittmann, K. Reaction Mechanisms of Thiamin Diphosphate Enzymes: Redox Reactions. FEBS Journal. May 2009, pp 2454–2468. https://doi.org/10.1111/j.1742-4658.2009.06966.x.
- (23) Gangolf, M.; Czerniecki, J.; Radermecker, M.; Detry, O.; Nisolle, M.; Jouan, C.; Martin, D.; Chantraine, F.; Lakaye, B.; Wins, P.; Grisar, T.; Bettendorff, L. Thiamine Status in Humans and Content of Phosphorylated Thiamine Derivatives in Biopsies and Cultured Cells. *PLoS One* **2010**, *5* (10). https://doi.org/10.1371/journal.pone.0013616.

- (24) Parkhomenko, Y.; Vovk, A.; Protasova, Z. Chapter 10 Vitamin B1 and the Pyruvate Dehydrogenase Complex. In *Molecular Nutrition*; Patel, V. B., Ed.; Academic Press, 2020; pp 185–206. https://doi.org/https://doi.org/10.1016/B978-0-12-811907-5.00012-9.
- (25) Manzetti, S.; Zhang, J.; van der Spoel, D. Thiamin Function, Metabolism, Uptake, and Transport. *Biochemistry* **2014**, *53* (5), 821–835. https://doi.org/10.1021/bi401618y.
- (26) Vitreschak, A. G.; Rodionov, D. A.; Mironov, A. A.; Gelfand, M. S. Regulation of Ribo avin Biosynthesis and Transport Genes in Bacteria by Transcriptional and Translational Attenuation. http://www.tigr.org.
- (27) Chawla, J.; Kvarnberg, D. Chapter 59 Hydrosoluble Vitamins. In *Handbook of Clinical Neurology*; Biller, J., Ferro, J. M., Eds.; Elsevier, 2014; Vol. 120, pp 891–914. https://doi.org/https://doi.org/10.1016/B978-0-7020-4087-0.00059-0.
- (28) Gazzaniga, F.; Stebbins, R.; Chang, S. Z.; McPeek, M. A.; Brenner, C. Microbial NAD Metabolism: Lessons from Comparative Genomics. *Microbiology and Molecular Biology Reviews* **2009**, *73* (3), 529–541. https://doi.org/10.1128/mmbr.00042-08.
- (29) Elischewski, F.; Pühler, A.; Kalinowski, J. Pantothenate Production in Escherichia Coli K12 by Enhanced Expression of the PanE Gene Encoding Ketopantoate Reductase. *J Biotechnol* **1999**, 75 (2), 135–146. https://doi.org/https://doi.org/10.1016/S0168-1656(99)00153-4.
- (30) Roberta, L.; Suzanne, J. Biosynthesis of Pantothenic Acid and Coenzyme A. *EcoSal Plus* **2007**, *2* (2), 10.1128/ecosalplus.3.6.3.4. https://doi.org/10.1128/ecosalplus.3.6.3.4.
- (31) Qian, Y.; Li, X. F.; Zhang, D. D.; Cai, D. Sen; Tian, H. Y.; Liu, W. Bin. Effects of Dietary Pantothenic Acid on Growth, Intestinal Function, Anti-Oxidative Status and Fatty Acids Synthesis of Juvenile Blunt Snout Bream Megalobrama Amblycephala. *PLoS One* 2015, 10 (3). https://doi.org/10.1371/journal.pone.0119518.
- (32) Leonardi, R.; Zhang, Y.-M.; Rock, C. O.; Jackowski, S. Coenzyme A: Back in Action. *Prog Lipid Res* **2005**, *44* (2), 125–153. https://doi.org/https://doi.org/10.1016/j.plipres.2005.04.001.
- (33) Hellmann, H.; Mooney, S. Vitamin B6: A Molecule for Human Health? *Molecules*. January 2010, pp 442–459. https://doi.org/10.3390/molecules15010442.
- (34) Lin, S.; Cronan, J. E. Closing in on Complete Pathways of Biotin Biosynthesis. *Mol. BioSyst.* **2011**, *7* (6), 1811–1821. https://doi.org/10.1039/C1MB05022B.
- (35) Bermingham, A.; Derrick, J. P. The Folic Acid Biosynthesis Pathway in Bacteria: Evaluation of Potential for Antibacterial Drug Discovery. *BioEssays*. 2002, pp 637–648. https://doi.org/10.1002/bies.10114.

- (36) Rowley, C. A.; Kendall, M. M. To B 12 or Not to B 12: Five Questions on the Role of Cobalamin in Host-Microbial Interactions. *PLoS Pathog* **2019**, *15* (1). https://doi.org/10.1371/journal.ppat.1007479.
- (37) Nikaido, H. Molecular Basis of Bacterial Outer Membrane Permeability Revisited. *Microbiology and Molecular Biology Reviews* **2003**, *67* (4), 593–656. https://doi.org/10.1128/mmbr.67.4.593-656.2003.
- (38) Rees, D. C.; Johnson, E.; Lewinson, O. ABC Transporters: The Power to Change. *Nature Reviews Molecular Cell Biology*. March 2009, pp 218–227. https://doi.org/10.1038/nrm2646.
- (39) ter Beek, J.; Guskov, A.; Slotboom, D. J. Structural Diversity of ABC Transporters. *Journal of General Physiology* **2014**, *143* (4), 419–435. https://doi.org/10.1085/jgp.201411164.
- (40) Rempel, S.; Stanek, W.; Slotboom, D.; ARjatscls, S. ECF-Type ATP-Binding Cassette Transporters. **2019**. https://doi.org/10.1146/annurev-biochem-013118.
- (41) Oldham, M. L.; Davidson, A. L.; Chen, J. Structural Insights into ABC Transporter Mechanism. *Current Opinion in Structural Biology*. December 2008, pp 726–733. https://doi.org/10.1016/j.sbi.2008.09.007.
- (42) Van Der Heide, T.; Poolman, B. *ABC Transporters: One, Two or Four Extracytoplasmic Substrate-Binding Sites?*; 2002; Vol. 3. https://www.embopress.org.
- (43) Rempel, S.; Stanek, W.; Slotboom, D.; ARjatscls, S. ECF-Type ATP-Binding Cassette Transporters. **2025**, *16*, 8. https://doi.org/10.1146/annurev-biochem-013118.
- (44) Setyawati, I. Energy-Coupling Factor Transporters: Exploration of the Mechanism of Vitamin Uptake and Inhibitory Potential of Novel Binders, University of Groningen, 2021. https://doi.org/10.33612/diss.172815141.
- (45) Wang, T.; Fu, G.; Pan, X.; Wu, J.; Gong, X.; Wang, J.; Shi, Y. Structure of a Bacterial Energy-Coupling Factor Transporter. *Nature* 2013, 497 (7448), 272–276. https://doi.org/10.1038/nature12045.
- (46) Zhang, P.; Wang, J.; Shi, Y. Structure and Mechanism of the S Component of a Bacterial ECF Transporter. *Nature* 2010, 468 (7324), 717–720. https://doi.org/10.1038/nature09488.
- (47) Erkens, G. B.; Berntsson, R. P. A.; Fulyani, F.; Majsnerowska, M.; Vujiĉić-Žagar, A.; Ter Beek, J.; Poolman, B.; Slotboom, D. J. The Structural Basis of Modularity in ECF-Type ABC Transporters. *Nat Struct Mol Biol* **2011**, *18* (7), 755–760. https://doi.org/10.1038/nsmb.2073.
- (48) Brooks, L. R. K.; Mias, G. I. Streptococcus Pneumoniae's Virulence and Host Immunity: Aging, Diagnostics, and Prevention. *Frontiers in Immunology*. Frontiers Media S.A. June 22, 2018. https://doi.org/10.3389/fimmu.2018.01366.

- (49) Zhang, M.; Bao, Z.; Zhao, Q.; Guo, H.; Xu, K.; Wang, C.; Zhang, P. Structure of a Pantothenate Transporter and Implications for ECF Module Sharing and Energy Coupling of Group II ECF Transporters. *Proc Natl Acad Sci U S A* 2014, *111* (52), 18560–18565. https://doi.org/10.1073/pnas.1412246112.
- (50) Diamanti, E.; Souza, P. C. T.; Setyawati, I.; Bousis, S.; Gómez, L. M.; Swier, L. J. Y. M.; Shams, A.; Tsarenko, A.; Stanek, W. K.; Jäger, M.; Marrink, S. J.; Slotboom, D. J.; Hirsch, A. K. H. Identification of Inhibitors Targeting the Energy-Coupling Factor (ECF) Transporters. *Commun Biol* 2023, 6 (1). https://doi.org/10.1038/s42003-023-05555-x.
- (51) Exapicheidou, I. A.; Shams, A.; Ibrahim, H.; Tsarenko, A.; Backenköhler, M.; Hamed, M. M.; Diamanti, E.; Volkamer, A.; Slotboom, D. J.; Hirsch, A. K. H. Hit Optimization by Dynamic Combinatorial Chemistry on Streptococcus Pneumoniae Energy-Coupling Factor Transporter ECF-PanT. *Chemical Communications* 2024, 60 (7), 870–873. https://doi.org/10.1039/d3cc04738e.
- (52) Zhang, M.; Bao, Z.; Zhao, Q.; Guo, H.; Xu, K.; Wang, C.; Zhang, P. Structure of a Pantothenate Transporter and Implications for ECF Module Sharing and Energy Coupling of Group II ECF Transporters. *Proc Natl Acad Sci U S A* 2014, 111 (52), 18560–18565. https://doi.org/10.1073/pnas.1412246112.
- (53) Zhang, M.; Bao, Z.; Zhao, Q.; Guo, H.; Xu, K.; Wang, C.; Zhang, P. Structure of a Pantothenate Transporter and Implications for ECF Module Sharing and Energy Coupling of Group II ECF Transporters. *Proc Natl Acad Sci U S A* 2014, 111 (52), 18560–18565. https://doi.org/10.1073/pnas.1412246112.
- (54) Slotboom, D. J. Structural and Mechanistic Insights into Prokaryotic Energy-Coupling Factor Transporters. *Nat Rev Microbiol* **2014**, *12* (2), 79–87. https://doi.org/10.1038/nrmicro3175.
- (55) Shams, A.; Bousis, S.; Diamanti, E.; Elgaher, W. A. M.; Zeimetz, L.; Haupenthal, J.; Slotboom, D. J.; Hirsch, A. K. H. Expression and Characterization of Pantothenate Energy-Coupling Factor Transporters as an Anti-Infective Drug Target. *Protein Science* **2024**, *33* (11). https://doi.org/10.1002/pro.5195.
- (56) Rodionov, D. A.; Hebbeln, P.; Eudes, A.; Ter Beek, J.; Rodionova, I. A.; Erkens, G. B.; Slotboom, D. J.; Gelfand, M. S.; Osterman, A. L.; Hanson, A. D.; Eitinger, T. A Novel Class of Modular Transporters for Vitamins in Prokaryotes. *J Bacteriol* **2009**, *91* (1), 42–51. https://doi.org/10.1128/JB.01208-08.
- (57) Lee, E. R.; Blount, K. F.; Breaker, R. R. Roseoflavin Is a Natural Antibacterial Compound That Binds to FMN Riboswitches and Regulates Gene Expression. *RNA Biology*. Taylor and Francis Inc. 2009. https://doi.org/10.4161/rna.6.2.7727.

- (58) Bousis, S.; Winkler, S.; Haupenthal, J.; Fulco, F.; Diamanti, E.; H, A. K. An Efficient Way to Screen Inhibitors of Energy-Coupling Factor 2 (ECF) Transporters in a Bacterial Uptake Assay 3. *Int. J. Mol. Sci* **2021**, *22*. https://doi.org/10.3390/xxxxx.
- (59) Drlica, K.; Zhao, X. DNA Gyrase, Topoisomerase IV, and the 4-Quinolones; 1997; Vol. 61.
- (60) Vivek Podder, A.; Patel, P.; Sadiq Affiliations, N. M. *Levofloxacin*. https://www.ncbi.nlm.nih.gov/books/NBK545180/?report=printable.
- (61) Pandey, N.; Cascella, M. Beta-Lactam Antibiotics. https://www.ncbi.nlm.nih.gov/books/NBK545311/.
- (62) Zhanel, G. G.; Wiebe, R.; Dilay, L.; Thomson, K.; Rubinstein, E.; Hoban, D. J.; Noreddin, A. M.; Karlowsky, J. A. Comparative Review of the Carbapenems. *Drugs* 2007, 67 (7), 1027–1052. https://doi.org/10.2165/00003495-200767070-00006.
- (63) Novelli, A.; Del Giacomo, P.; Rossolini, G. M.; Tumbarello, M. Meropenem/Vaborbactam: A next Generation β-Lactam β-Lactamase Inhibitor Combination. Expert Review of Anti-Infective Therapy. Taylor and Francis Ltd July 2, 2020, pp 643–655. https://doi.org/10.1080/14787210.2020.1756775.
- (64) Swier, L. J. Y. M.; Guskov, A.; Slotboom, D. J. Structural Insight in the Toppling Mechanism of an Energy-Coupling Factor Transporter. *Nat Commun* **2016**, 7. https://doi.org/10.1038/ncomms11072.
- (65) Kiefer, A. F.; Bousis, S.; Hamed, M. M.; Diamanti, E.; Haupenthal, J.; Hirsch, A. K. H. Structure-Guided Optimization of Small-Molecule Folate Uptake Inhibitors Targeting the Energy-Coupling Factor Transporters. *J Med Chem* 2022, 65 (13), 8869–8880. https://doi.org/10.1021/acs.jmedchem.1c02114.
- (66) Leonardi, R.; Jackowski, S. Biosynthesis of Pantothenic Acid and Coenzyme A. *EcoSal Plus* **2007**, *2* (2). https://doi.org/10.1128/ecosalplus.3.6.3.4.
- (67) Spry, C.; Kirk, K.; Saliba, K. J. Coenzyme A Biosynthesis: An Antimicrobial Drug Target. *FEMS Microbiology Reviews*. January 2008, pp 56–106. https://doi.org/10.1111/j.1574-6976.2007.00093.x.
- (68) Willocx, D.; Bizzarri, L.; Alhayek, A.; Kannan, D.; Bravo, P.; Illarionov, B.; Rox, K.; Lohse, J.; Fischer, M.; Kany, A. M.; Hahne, H.; Rottmann, M.; Witschel, M.; Odom John, A.; Hamed, M. M.; Diamanti, E.; Hirsch, A. K. H. Targeting Plasmodium Falciparum IspD in the Methyl-d-Erythritol Phosphate Pathway: Urea-Based Compounds with Nanomolar Potency on Target and Low-Micromolar Whole-Cell Activity. *J Med Chem* 2024. https://doi.org/10.1021/acs.jmedchem.4c00212.
- (69) Willocx, D.; Diamanti, E.; Hirsch, A. K. H. Targeting IspD for Anti-Infective and Herbicide Development: Exploring Its Role, Mechanism, and Structural Insights.

- *Journal of Medicinal Chemistry*. American Chemical Society January 23, 2025, pp 886–901. https://doi.org/10.1021/acs.jmedchem.4c01146.
- (70) Witschel, M.; Röhl, F.; Niggeweg, R.; Newton, T. In Search of New Herbicidal Inhibitors of the Non-Mevalonate Pathway. *Pest Management Science*. May 2013, pp 559–563. https://doi.org/10.1002/ps.3479.
- (71) Gierse, R. M.; Redeem, E.; Diamanti, E.; Wrenger, C.; Groves, M. R.; Hirsch, A. K. H. DXS as a Target for Structure-Based Drug Design. *Future Medicinal Chemistry*. Future Medicine Ltd. July 1, 2017, pp 1277–1294. https://doi.org/10.4155/fmc-2016-0239.
- (72) Johnston, M. L.; Freel Meyers, C. L. Revealing Donor Substrate-Dependent Mechanistic Control on DXPS, an Enzyme in Bacterial Central Metabolism. *Biochemistry* 2021, 60 (12), 929–939. https://doi.org/10.1021/acs.biochem.1c00019.
- (73) Masini, T.; Pilger, J.; Kroezen, B. S.; Illarionov, B.; Lottmann, P.; Fischer, M.; Griesinger, C.; Hirsch, A. K. H. De Novo Fragment-Based Design of Inhibitors of DXS Guided by Spin-Diffusion-Based NMR Spectroscopy. *Chem Sci* **2014**, *5* (9), 3543–3551. https://doi.org/10.1039/c4sc00588k.

## 7 Appendix

## 7.1 Side projects

Several side projects with different tasks were undertaken, but only those involving new methods will be discussed herein.

## 7.1.1 IspD project

"Optimization of crystallography Conditions for *Escherichia coli* IspD Enzyme." Manuscript in preparation.

A part of the project involved the adaptation and optimization of an MS-based assay for the IspD project, which was later taken over by Lorenzo Bizzarri and published in a recent study <sup>68</sup>.

#### Introduction

IspD, or 2-*C*-methyl-D-erythritol 4-phosphate cytidylyltransferase, is the third enzyme in the methylerythritol phosphate (MEP) pathway, a crucial biosynthetic route for isoprenoid precursor formation in bacteria and plants. This pathway is absent in mammals, making it an attractive target for the development of selective antimicrobial agents<sup>69</sup>. IspD catalyzes the cytidylation of 2-*C*-methyl-D-erythritol 4-phosphate (MEP) to form 4-diphosphocytidyl-2-*C*-methyl-D-erythritol (CDP-ME), a key step in the pathway that ultimately leads to the biosynthesis of essential terpenoids<sup>69,70</sup>.

Under the research focus of Prof. Dr. Anna Hirsch's group, efforts are directed toward the structural and functional characterization of different homologues of IspD *e.g. Acinetobacter baumannii* (*Ab*), *Mycobacterium tuberculosis* (*Mt*), *Pseudomonas aeruginosa*, *and Escherichia coli* (*Ec*) IspD to facilitate the rational design of potent inhibitors. Crystallographic studies have been pivotal in elucidating the active—site architecture and conformational changes upon ligand binding and provide valuable information on binding modes, allowing for iterative optimization of lead compounds. These structural insights are complemented by an IspD mass spectrometry (MS)-based assay, which enables high-throughput screening and kinetic evaluation of small-molecule inhibitors.

By leveraging these techniques, the identification and optimization of selective inhibitors with high affinity and specificity are facilitated, contributing to the development of novel anti-infectives targeting bacterial isoprenoid biosynthesis. These investigations aim to establish a robust framework for characterizing IspD and its inhibition, paving the way for future antimicrobial drug development against MEP pathway-dependent pathogens.

#### Methodology

## Ec-, Mt-, and AbIspD expression and purification

Different homologues of IspD were expressed in  $E.\ coli$  and the cell cultures were grown in LB medium overnight at 30 °C until an optical density (OD<sub>600</sub>) of 0.8; then, protein expression was induced by adding isopropyl  $\beta$ -D-thiogalactopyranoside (IPTG) to a final concentration of 0.1 mM. Expression was carried out overnight at 30 °C. Cells were pelleted by centrifugation, resuspended in lysis buffer (100 mM Tris pH 8.0, 800 mM NaCl, 10 mM imidazole, 5 mM  $\beta$ -mercaptoethanol) and Complete EDTA-free antiprotease (Roche Diagnostics, Meylan, France) (1 tablet Complete in 50 mL buffer), and 2  $\mu$ L of benzonase lysed by microfluidizer. Cellular debris were removed by centrifugation (30 min, 19,000 rpm, 4 °C). After centrifugation, the supernatant was applied on a HisTrap 5 ml previously equilibrated in the lysis buffer. The proteins were further purified by gel filtration on a HiLoad 16/60 Superdex-200 prep grade column equilibrated and

eluted with 10 mM Hepes pH 7.4, 150 mM NaCl for *E. coli* IspD, 10 mM Hepes pH 7.4, 150 mM NaCl for MtIspD, and 10 mM Tris pH 8, 800 mM NaCl for AbIspD. Fractions containing IpD were pooled, concentrated and stored at –80 °C.

## Crystallization Protocol for IspD Homologues Using the Gryphon System

The crystallization of three homologues of IspD was performed by concentrating each protein to 600  $\mu$ M in its respective purification buffer, with a final volume of 300  $\mu$ L. Crystallization trials were set up using the Gryphon system at the MINS group at HIPS, employing PECS (Protein Crystallization Screening) solutions. The plates were incubated at 18 °C, and crystal formation was monitored. For *E. coli* IspD, crystals were observed in well F12. For mounting, a solution was prepared by mixing 1.5  $\mu$ L of 15% Cryo BD with 8.5  $\mu$ L of the condition well solution (15%), and 1  $\mu$ L of this mixture was placed in the crystal well. Crystals were picked with a crystallization loop and stored in liquid nitrogen for further analysis. This approach enables the collection of high-quality crystals suitable for X-ray diffraction analysis, which will facilitate the structural characterization of IspD homologues.

#### **Crystallization condition optimization**

After identifying initial crystallization conditions for *E. coli* IspD, optimization was performed using a 24- well plate and testing various buffer compositions. The buffers used were 0.1 M Tris (pH 8.5), 32% (w/v) PEG 4000, and 0.8 M lithium chloride. The optimization focused on varying PEG concentrations (28%, 29%, 30%, 31%, 32%, and 33%) and testing different Tris pH values (7.5, 8.0, and 8.5), while maintaining a constant lithium chloride concentration at 0.8 M. The total volume in each well was 1 mL, and the plates were incubated at 18 °C. The method involved mixing the protein and the crystallization solution in a single drop, which was then placed on the well, using a technique known as

hanging drop vapor diffusion. This approach helped refine the conditions for crystal growth, improving the quality and reproducibility of the crystals.

## (Co)-crystallization of polyketomycin with E.coli IspD.

After determining the crystallization conditions for EcIspD, co-crystallization experiments were conducted with the polyketomycin compound. To identify optimal conditions for co-crystallization, we tested different concentrations of DMSO. Two conditions were used: one with 1% DMSO and the other with 5% DMSO. The protein solution (600  $\mu$ M) was incubated with polyketomycin (100 mM) for 4 hours. The crystallization plate, prepared as in previous steps, had each condition pipetted into the corresponding wells as the reservoir solution. After the 4-hour incubation, the protein-compound mixture was centrifuged at 1400 rpm for 10 minutes at 4 °C. For the crystallization setup, 4  $\mu$ L drops were prepared on specific slides at protein to reservoir solution ratios of 1:1, 1:2, and 1:3 (1  $\mu$ L protein with 3  $\mu$ L of reservoir, 2  $\mu$ L protein with 2  $\mu$ L of reservoir, and 3  $\mu$ L protein with 1  $\mu$ L of reservoir). The hanging drop method was used by placing these drops upside down above the reservoir wells. The plates were then incubated for several days, and crystals were mounted as described in the previous procedure for further measurements. This co-crystallization approach allows for the structural investigation of the protein-ligand complex, providing insights into the interaction between EcIspD and polyketomycin.

### 7.1.2 DXPS Project

"Adaptation and optimization of a coupled assay for diverse DXS enzyme homologues." Establishing protocol and writing the manuscript in preparation.

#### Introduction

The enzyme 1-deoxy-D-xylulose-5-phosphate synthase (DXPS) is the first enzyme in the methylerythritol 4-phosphate (MEP) pathway and acts as a rate-limiting step in the biosynthesis of isoprenoids in plants, bacteria, and protozoa. The enzyme DXPS is a crucial bacterial metabolic enzyme that catalyzes the formation of DXP from pyruvate and D-glyceraldehyde 3-phosphate (D-GAP). DXPS is essential in bacteria but absent in humans, making it a potential antibacterial target<sup>71</sup>. Recent studies have focused on understanding the structural and mechanistic properties of these enzymes, especially DXR, to support structure-based drug design and investigate their biotechnological applications<sup>71</sup>. The enzyme exhibits unique structural and mechanistic features, including a large active site and random sequential mechanism and displays catalytic promiscuity and relaxed substrate specificity<sup>72</sup>.

## Methodology

A different homologue of the DXPS enzyme such as *Mycobacterium tuberculosis* or MtDXS, *Plasmodium falciparum* DXS or PfDXS, and *Deinococcus radiodurans* DXS or DrDXS were investigated. The proteins were expressed and purified, and their binding affinity was assessed using various assays, including SPR, TSA, and a coupled assay. The DXPS-IspC coupled assay, or photometric assay for kinetic analysis of DXPS, was previously outlined by Masini et al. (2014). Optimization of this assay for different homologues has been carried out and is still ongoing<sup>73</sup>.

#### 7.2 Conference Contributions

**Topic:** "Evaluation of inhibitors against Energy-coupling factor (ECF) transporters using a bacterial uptake assay"

## 7.2.1 Poster presentations:

<u>Atanaz Shams</u>, Spyridon Bousis, Eleonora Diamanti, Mostafa Hamed, Ioulia Antonia Exapicheidou, Walid A. M. Elgaher, Jörg Haupenthal, Dirk. J. Slotboom, Anna K. H. Hirsch

- DPhG Annual Meeting 2022, "From Behring to Biotechnology moving Pharmaceutical Sciences towards One Health"
- HIPS symposium 2022
- Annual Meeting of the DZIF- 2023
- Gordon Research Conference- Mechanisms of Membrane Transport 2023

## 7.2.2 Oral presentation:

<u>Atanaz Shams</u>, Spyridon Bousis, Eleonora Diamanti, Mostafa Hamed, Ioulia Antonia Exapicheidou, Walid A. M. Elgaher, Jörg Haupenthal, Dirk. J. Slotboom, Anna K. H. Hirsch

- Joint retreat of the ABC transporters groups from the Netherlands and Germany Prof. Dr. Slotboom-2023
- Research (DZIF) and the Helmholtz International Graduate School for Infection Research- Summer School on Variome German Center for Infection- 2024